Review

International Journal of Modern Physics E
Vol. 22, No. 6 (2013) 1330015 (119 pages)

DOI: 10.1142/S0218301313300154

World Scientific
www.worldscientific.com

STUDIES OF NUCLEON RESONANCE STRUCTURE IN EXCLUSIVE MESON ELECTROPRODUCTION

I. G. Aznauryan[1,2], A. Bashir[3], V. M. Braun[4], S. J. Brodsky[5,6], V. D. Burkert[2], L. Chang[7,8], Ch. Chen[7,9,10], B. El-Bennich[11,12], I. C. Cloët[7,13], P. L. Cole[14], R. G. Edwards[2], G. V. Fedotov[15,16], M. M. Giannini[17,18], R. W. Gothe[15,*], F. Gross[2,19], Huey-Wen Lin[20], P. Kroll[21,4], T.-S. H. Lee[7], W. Melnitchouk[2], V. I. Mokeev[2,16], M. T. Peña[22,23], G. Ramalho[22,25], C. D. Roberts[7,10], E. Santopinto[18], G. F. de Teramond[24], K. Tsushima[13,25] and D. J. Wilson[7,26]

[1] *Yerevan Physics Institute, Yerevan, Armenia*
[2] *Thomas Jefferson National Accelerator Facility, Newport News, Virginia 23606, USA*
[3] *Instituto de Física y Matemáticas, Universidad Michoacana de San Nicolás de Hidalgo, Edificio C-3, Ciudad Universitaria, Morelia, Michoacán 58040, México*
[4] *Institut für Theoretische Physik, Universität Regensburg, 93040 Regensburg, Germany*
[5] *Stanford National Accelerator Laboratory, Stanford University, Stanford, California 94025, USA*
[6] *CP3-Origins, Southern Denmark University, Odense, Denmark*
[7] *Physics Division, Argonne National Laboratory, Argonne Illinois 60439, USA and Department of Physics, Illinois Institute of Technology, Chicago, Illinois 60616, USA*
[8] *Forschungszentrum Jülich, D-52425 Jülich, Germany*
[9] *Institute for Theoretical Physics and Department of Modern Physics, University of Science and Technology of China, Hefei 230026, P. R. China*
[10] *Department of Physics, Illinois Institute of Technology, Chicago, Illinois 60616, USA*
[11] *Universidade Cruzeiro do Sul, Rua Galvão Bueno, 868, 01506-000 São Paulo, SP, Brazil*
[12] *Instituto de Física Teórica, Universidade Estadual Paulista, Rua Dr. Bento Teobaldo Ferraz, 271, 01140-070 São Paulo, SP, Brazil*
[13] *CSSM and CoEPP, School of Chemistry and Physics, University of Adelaide, Adelaide SA 5005, Australia*
[14] *Department of Physics, Pocatello, Idaho State University, Idaho, 83209, USA*
[15] *University of South Carolina, Columbia, South Carolina 29208, USA*
[16] *Skobeltsyn Institute Nuclear Physics at Moscow State University, 119899 Moscow, Russia*
[17] *Dipartimento di Fisica, Università di Genova, Italy*
[18] *Istituto Nazionale di Fisica Nucleare, Sezione di Genova, Italy*
[19] *College of William and Mary, Williamsburg, Virginia 23187, USA*
[20] *Department of Physics, University of Washington, Seattle, Washington 98195, USA*
[21] *Fachbereich Physik, Universität Wuppertal, 42097 Wuppertal, Germany*
[22] *CFTP, IST, Universidade Técnica de Lisboa, UTL, Portugal*
[23] *Departamento de Física, IST, Universidade Técnica de Lisboa, UTL, Portugal*
[24] *Universidad de Costa Rica, San José, Costa Rica*
[25] *International Institute of Physics, Federal University of Rio Grande do Norte, Natal, RN 59078-400, Brazil*
[26] *Department of Physics, Old Dominion University, Norfolk, Virginia 23529, USA*
[*] *rwgothe@gmail.com*

[*]Corresponding author.

Received 4 April 2013
Accepted 9 April 2013
Published 27 June 2013

Studies of the structure of excited baryons are key factors to the N^* program at Jefferson Lab (JLab). Within the first year of data taking with the Hall B CLAS12 detector following the 12 GeV upgrade, a dedicated experiment will aim to extract the N^* electrocouplings at high photon virtualities Q^2. This experiment will allow exploration of the structure of N^* resonances at the highest photon virtualities ever achieved, with a kinematic reach up to $Q^2 = 12$ GeV^2. This high-Q^2 reach will make it possible to probe the excited nucleon structures at distance scales ranging from where effective degrees of freedom, such as constituent quarks, are dominant through the transition to where nearly massless bare-quark degrees of freedom are relevant. In this document, we present a detailed description of the physics that can be addressed through N^* structure studies in exclusive meson electroproduction. The discussion includes recent advances in reaction theory for extracting N^* electrocouplings from meson electroproduction off protons, along with Quantum Chromodynamics (QCD)-based approaches to the theoretical interpretation of these fundamental quantities. This program will afford access to the dynamics of the nonperturbative strong interaction responsible for resonance formation, and will be crucial in understanding the nature of confinement and dynamical chiral symmetry breaking in baryons, and how excited nucleons emerge from QCD.

Keywords: Electromagnetic form-factors; baryon resonances; meson production; lattice QCD calculations; quark models; dispersion relations; nonperturbative QCD; confinement; dynamical chiral symmetry breaking; CLAS; Jefferson lab.

PACS Number(s): 13.40.Gp, 14.20.Gk, 13.60.Le, 12.38.Gc, 12.39.-x, 11.55.Fv

Contents

1. The Case for Nucleon Resonance Structure Studies at High Photon Virtualities

1.1. *Background*

It has been known since the 1970s that the nucleon is a bound state of three valence quarks surrounded by an infinite sea of gluons and quark–antiquark pairs. In the underlying theory that describes the quark–gluon interactions, quantum chromodynamics (QCD), the quarks exist in three states ("colors") that transform into each other under a local SU(3) gauge transformation which is an *exact* local gauge symmetry of nature. Only colorless states are observed as free particles in nature; they are composed of either (i) quark–antiquark pairs (with canceling colors) in a sea of gluons (known as mesons) or (ii) three valence quarks (each with a different color combining to produce a colorless state) in a sea of gluons and quark–antiquark pairs (known as baryons, including the N^* states discussed in this review). An immediate implication of this understanding is that when energy is dumped into the nucleon ground states, they are excited, and can lose their energies only by emitting colorless states, mostly mesons. Many excited states or nucleon resonances, referred to generically as N^*s, have been observed. The spectrum of these excited states is summarized in Fig. 1. The studies of this resonance spectrum represent a rapidly evolving area and the recent updates can be found in Refs. 1–3.

QCD has the feature that the elementary couplings between quarks and gluons and the couplings of gluons to themselves become very small as the momentum carried by the quarks or gluons becomes very large. This feature, known as

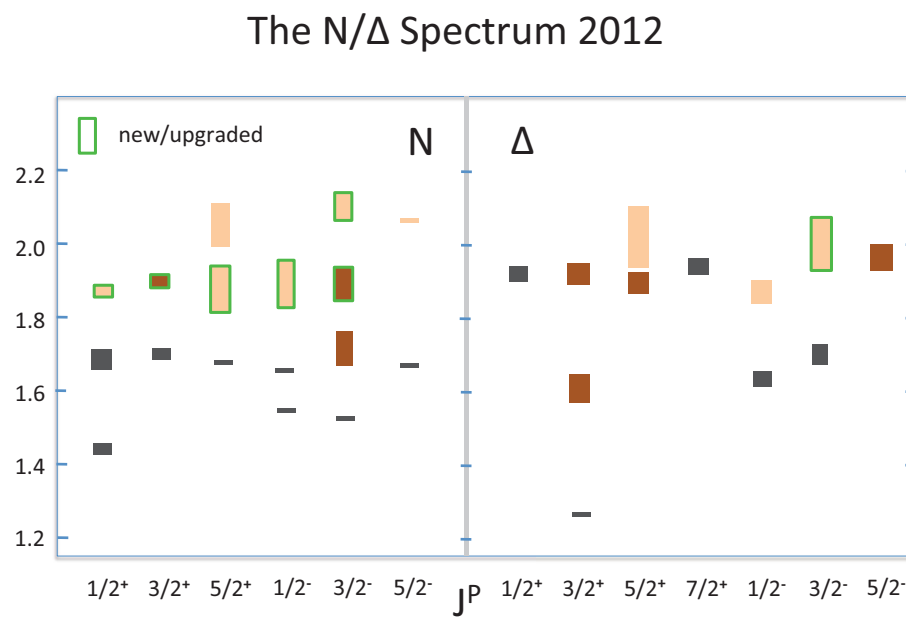

Fig. 1. (Color online) Nucleon resonance spectrum as known in 2012.[2–4] N^* states of spin-parity J^P are shown by boxes centred at the Breit–Wigner masses (vertical axis), while the box heights correspond to the N^* mass uncertainties. Resonance state ratings: black, dark brown, and light brown colors stand for four, three, and two star review of particle physics (RPP) status, respectively. Recent updates from the Bonn-Gatchina coupled-channel analysis[3] that included the new high precision meson photoproduction data including strangeness channels[1] are shown by the boxes framed in green.

asymptotic freedom, makes it possible to use perturbation theory to describe precisely the interactions of quarks and gluons at distances which are much smaller than the typical hadron size. Perturbative QCD (pQCD) has been very successful in explaining many high energy and/or short distance phenomena, and it is because of this success that QCD is believed to be the fundamental theory of the strong interactions. However, at the energies and distance scales found within the nucleon resonances, the quark–gluon running coupling becomes large. One consequence of this large coupling is that the quarks and gluons are *confined*; no matter how much energy is pumped into a nucleon, it is impossible to liberate either a colored quark or a colored gluon. Another feature of QCD in this region is that mass is spontaneously generated, and this effect is so large that it accounts for most (about 98%) of the mass of the nucleon and its excited states. Neither the mechanism of mass generation nor quark–gluon confinement can be understood by employing pQCD; a completely new understanding is needed. The need to understand QCD in this new, nonperturbative region is a fundamental problem that the study of N^* states seeks to address. This review examines various approaches that have been used to study this problem, describing current successes and the outlook for future progress.

1.2. *Excitation of nucleon resonances by photons and electrons*

The states in the excited nucleon spectrum are studied at Jefferson Lab (JLab) by scattering a beam of electrons or tagged photons from a nucleon target and observing the hadrons emitted in the final state, as illustrated in Fig. 2. Electrons interact with the target by exchanging a virtual photon, with a four-momentum squared $q^2 = -Q^2$, and for electron–nucleon scattering one has $Q^2 \geq 0$. As Q^2 increases, the virtual photon becomes capable of resolving the structures at smaller distances and the scattering is sensitive to the structure at shorter distance scales. The study of electroproduction of a final state X at high photon virtualities (high Q^2) reveals the inner structure of the resonance.

In May 2012, the 6-GeV program with the CEBAF large acceptance spectrometer (CLAS) in Hall B at JLab was successfully completed. Among the many, data runs with photons and electrons were several dedicated experiments focusing on the spectroscopy and structure of N^* states. CLAS was a unique instrument formed from a set of detectors and designed for the comprehensive exploration of exclusive meson electroproduction off nucleons. The CLAS detector afforded excellent opportunities to study the electroexcitation of nucleon resonances with great precision, and has contributed the lion's share of the world's data on meson photo- and electroproduction in the resonance excitation region.[5–11] For the first time, detailed information from sets of unpolarized cross-sections and different single- and double-polarization asymmetries have become available for many different meson electroproduction channels off protons and neutrons.

In order to extract resonance information from the electroproduction data, it must be analyzed and separated into the two contributions shown in Fig. 2. The contribution in Fig. 2(b) gives information about the $\gamma_v NN^*$ electrocouplings as they evolve with photon virtuality Q^2,[12–18] and how the N^* decays into any final state X, $N^* \to X$. Experimental studies of the structure of all prominent N^* states, in terms of the $\gamma_v NN^*$ electrocoupling evolution with Q^2, offer promising means of delineating the nature of the strong interaction in the nonperturbative regime of large quark–gluon running couplings. These studies are the necessary first steps in understanding how QCD generates most of the matter or mass in the real world, namely, mesons, baryons, and atomic nuclei.

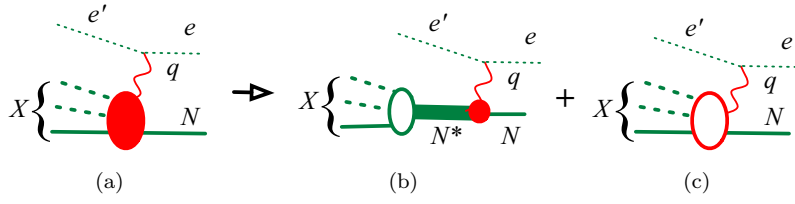

Fig. 2. (Color online) (a) Represents the scattering of an electron from a nucleon with the creation of a final state X. It is built from two contributions: (b) the excitation of several N^* intermediate states (only one shown in the figure) and (c) background contributions. Note that time flows from right to left in the diagrams.

To extract this information from the data, the process in Fig. 2(b) must be separated from the background contribution in Fig. 2(c). This is a major theoretical effort that has been approached in several different ways (see Sec. 2). The electroexcitation amplitudes for the low-lying resonances $P_{33}(1232)$, $P_{11}(1440)$, $D_{13}(1520)$, and $S_{11}(1535)$ were determined over a wide range of Q^2 in independent analyses of the π^+n, π^0p, ηp, and $\pi^+\pi^-p$ electroproduction channels.[9,19,20] Two of them, the $P_{11}(1440)$ and $D_{13}(1520)$ electrocouplings, have become available through independent analyses of single- and charged-double-pion electroproduction channels. The successful description of the measured observables in these exclusive channels resulting in the same $\gamma_v NN^*$ electrocoupling values confirms their reliable extraction from the experimental data. These results have recently been complemented by still preliminary electrocouplings of high-lying resonances with masses above 1.6 GeV (Ref. 21) in the $\pi^+\pi^-p$ electroproduction channel, which is particularly sensitive to high-mass resonances. An alternative resonance electrocoupling extraction in a combined multi-channel analysis of the $N\pi$, $N\eta$, and KY channels within the framework of the advanced excited baryon analysis center (EBAC) dynamic coupled channel (DCC) approach is in progress[22,23] (see Sec. 2.4).

1.3. *How can we isolate the quark degrees of freedom?*

The nonperturbative strong interaction is enormously challenging. Owing to the quark–gluon interaction, the elementary quarks and gauge-field gluons employed in the QCD Lagrangian are dressed by a cloud of gluons and quark–antiquark pairs coupled to gluon fields. In the regime of large quark–gluon running coupling this dressing generates effective objects — dressed quarks and dressed gluons. The dressing of the quarks gives rise to a momentum-dependent dynamical mass that reflects the structure of the dressed quarks, and these dressed *constituent* quarks become the effective degrees of freedom of normal nuclear matter. In the process of being dressed, the mass of the lightest quarks changes from a few MeV to an effective mass in the range of 250–400 MeV, and the theoretical *constituent quark models* treat these as real physical particles. In the evolution of the strong interaction from the pQCD regime of almost point-like and weakly coupled quarks and gluons (distances $< 10^{-17}$ m) to the nonperturbative regime, where dressed quarks and gluons acquire dynamical mass and structure (distances $\approx 10^{-15}$ m), two major nonperturbative phenomena emerge: (a) quark–gluon confinement and (b) dynamical chiral symmetry breaking (DCSB). Quark–gluon confinement locks colored quarks and gluons inside the hadron interior. It should be understood that confinement is *not* merely the statement that QCD supports only color singlet asymptotic states. Instead, it is the statement that the QCD spectrum contains only color singlet states of small spatial extent, such that the individual colored constituents cannot be isolated empirically. The dynamical generation of a length scale that characterizes these bound states is a crucial piece in the puzzles posed by confinement and DCSB. It is believed that the DCSB mechanism is responsi-

ble for the generation of the large effective quark masses, and both of these new phenomena are completely outside of the scope of pQCD. More than 98% of the hadron mass is generated nonperturbatively through the DCSB processes, while the Higgs mechanism accounts for less than 2% of the light-quark baryon masses. The nonperturbative strong interaction is responsible for the formation of all individual N^* states as bound systems of quarks and gluons. The DCSB mechanism will be discussed in more detail in Secs. 1.4.2 and 4.

Extraction of the $\gamma_v NN^*$ electrocouplings[5,6,24,25] gives information on the dressed quark mass, structure, and nonperturbative interaction, which is critical in exploring the nature of quark–gluon confinement and DCSB in baryons. Figure 3 illustrates two of the contributions to these electrocouplings. In Fig. 3(b), the virtual photon interacts directly with the constituent quark, an interaction which is sensitive to the *quark current* and depends on the quark–mass function. This contribution is the quark "core" interaction. The general unitarity condition for full meson electroproduction amplitudes requires contributions from nonresonant meson electroproduction and hadronic scattering amplitudes to the $\gamma_v pN^*$ vertex, as depicted in Fig. 3(c). This contribution incorporates all possible intermediate meson–baryon states and subsequent meson–baryon scattering processes that eventually result in the N^* formation. This contribution is referred to as the meson–baryon cloud (or sometimes simply as the *pion* cloud since the pion usually makes the largest contribution to the meson–baryon loops). These two contributions can be separated from one another using, for example, coupled channel analyses.

It was found that the structure of nucleon resonances in the Q^2 range below about 1.5 GeV^2 is determined by contributions from both diagrams in Fig. 3. As an example, these contributions to the structure of the $P_{11}(1440)$ and $D_{13}(1520)$ states are shown in Fig. 4. The absolute values of the meson–baryon dressing amplitudes are maximal for $Q^2 < 1$ GeV^2, and decrease with Q^2. In the region of $Q^2 > 1$ GeV^2, there is a gradual transition to where the quark degrees of freedom dominate, as is demonstrated by a better description of the $P_{11}(1440)$ and $D_{13}(1520)$ electrocouplings obtained within the framework of quark models.

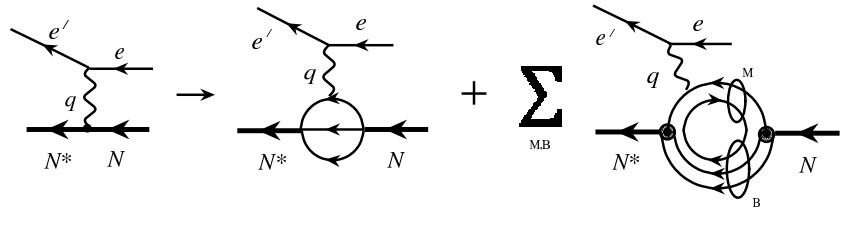

Fig. 3. (a) Represents the dressed $\gamma_v NN^*$ electrocoupling that determines the N^*-state contribution to the resonant part of meson electroproduction amplitudes. (b) The contribution of the three-quark core (with quarks denoted by thin lines). (c) Shows a contribution from the meson–baryon cloud. Here the baryons (B) are represented by their three-quark cores, the mesons (M) by their valence quark–antiquark structure, and the sum is over all meson and baryon states.

At photon virtualities of $Q^2 > 5$ GeV^2, the quark degrees of freedom are expected to dominate N^* structures.[16] This expectation is supported by the present analysis of the high-Q^2 behavior of the $\gamma_v pN^*$ electrocouplings[19] shown in Fig. 5, where the electrocoupling values scaled with Q^3 are plotted. The Q^3 scaling is predicted from constituent counting rules derived from pQCD, and this result implies that the meson cloud contributions are small. The indicated onset of scaling seen for $Q^2 > 3$ GeV^2 is likely related to the preferential interaction of the photon with dressed quarks, while interactions with the meson–baryon cloud results in strong deviations from this scaling behavior at smaller photon virtualities (greater distances).

Therefore, in the $\gamma_v pN^*$ electrocoupling studies for $Q^2 > 5$ GeV^2, the quark degrees of freedom, as revealed by the N^* structure, will be directly accessible from experiment with only small contributions from the meson–baryon cloud. This will mark the first time that this new and unexplored region in the electroexcitation of nucleon resonances will be investigated. A dedicated experiment on the N^* studies in exclusive meson electroproduction off protons with the CLAS12 detector (E12-09-003)[18] is scheduled to take place within the first year after the completion of

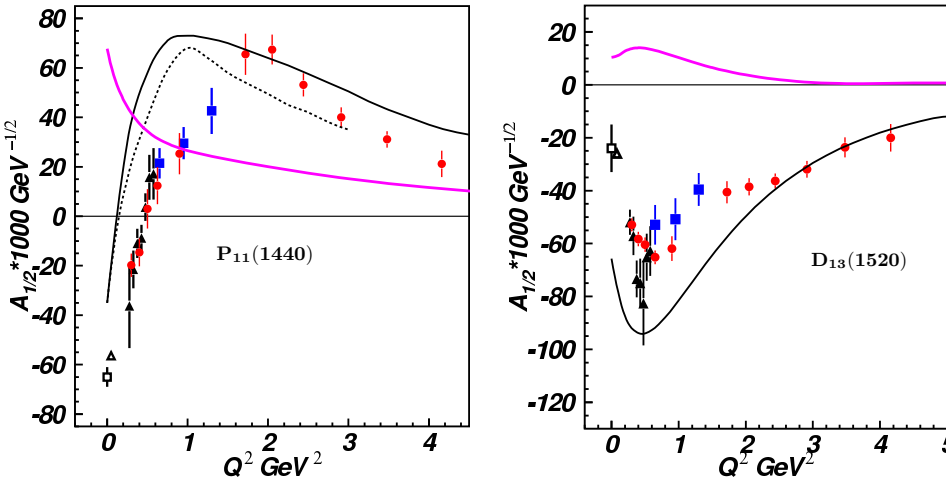

(a) (b)

Fig. 4. (Color online) (a) The $A_{1/2}$ electrocoupling of the $P_{11}(1440)$ excited state from the analyses of the $N\pi$ electroproduction data[19] (circles), $\pi^+\pi^- p$ electroproduction data[8] (triangles), and preliminary results from the $\pi^+\pi^- p$ electroproduction data at Q^2 from 0.5 to 1.5 GeV^2 (Ref. 7) (squares). The photocouplings are taken from RPP[4] (open square) and the CLAS data analysis[26] (open triangle). Predictions from relativistic light-front quark models[27,28] are shown by black solid and dashed lines, respectively. The absolute value of the meson–baryon cloud contribution as determined by the EBAC-DCC coupled-channel analysis[29] is shown by the magenta thick solid line. (b) The $A_{1/2}$ electrocoupling of the $D_{13}(1520)$ state. The data symbols are the same as in (a). The results of the hypercentral constituent quark model[30] and the absolute value of meson–baryon dressing amplitude[29] are presented by the black thin and magenta thick solid lines, respectively.

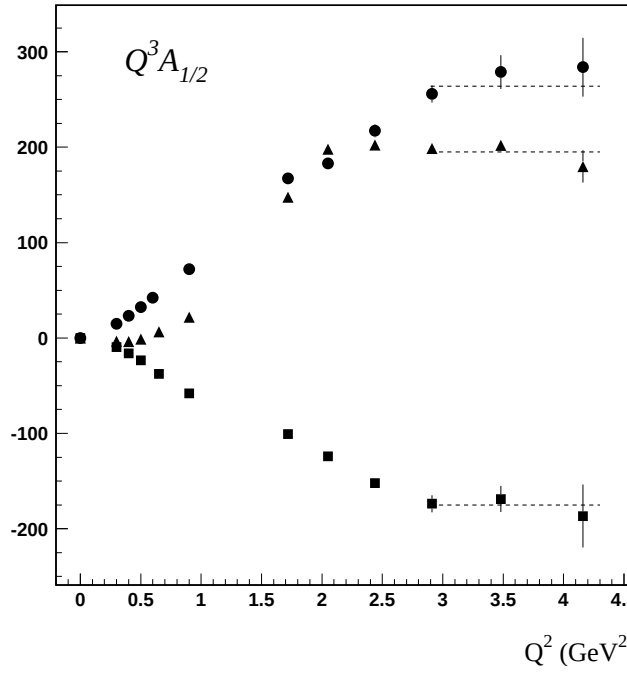

Fig. 5. The $A_{1/2}$ electrocouplings of $P_{11}(1440)$ (triangles), $D_{13}(1520)$ (squares) and $S_{11}(1535)$ (circles) scaled with Q^3 from the CLAS data analysis.[19]

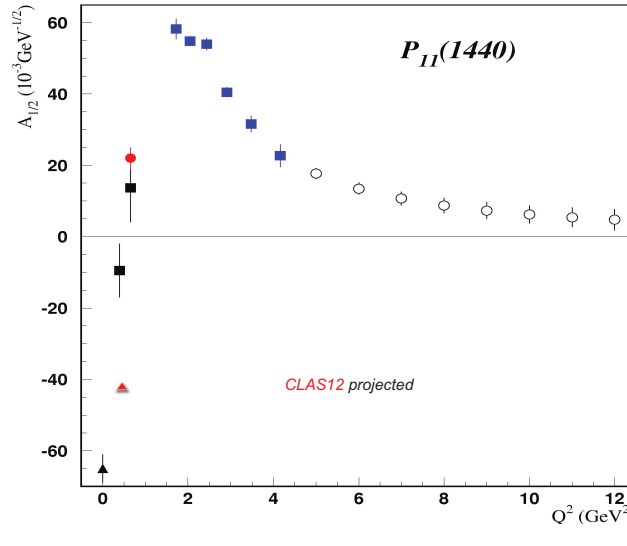

Fig. 6. (Color online) Available (filled symbols) and projected CLAS12[18] (open symbols) $A_{1/2}$ electrocouplings of the $P_{11}(1440)$ excited state.

the JLab 12-GeV Upgrade Project. By measuring the differential cross-sections off protons in the exclusive single-meson and double-pion electroproduction channels, complemented by single- and double-polarization asymmetries in single-meson electroproduction, this experiment seeks to obtain the world's only foreseen data on the electrocouplings of all prominent N^* states in the still unexplored domain of photon virtualities up to 12 GeV^2. As an example, the projected $A_{1/2}$ electrocoupling values of $P_{11}(1440)$ at photon virtualities from 5 GeV^2 to 12 GeV^2 are shown in Fig. 6. A similar quality of results is expected for the electrocouplings of all other prominent N^* states. The available reaction models for the extraction of the resonance electrocouplings have to be extended toward these high photon virtualities with the goal to reliably extract the $\gamma_v pN^*$ electrocouplings from the anticipated data on meson electroproduction off protons. In particular, the new reaction models must account for a gradual transition from meson–baryon to quark degrees of freedom in the nonresonant reaction mechanisms. The current status and prospects of the reaction model developments are discussed in Sec. 2.

1.4. *What can we learn?*

The analysis of the electroproduction data leads to the extraction of the amplitudes for the transition between the initial virtual photon–nucleon and the final N^* state (so-called $\gamma_v NN^*$ electrocoupling) that describe the physics, and that can be calculated theoretically. Among these amplitudes are $A_{1/2}(Q^2)$ and $A_{3/2}(Q^2)$, which describe the resonance electroexcitation for two different helicities of the initial transverse photon and nucleon, as well as $S_{1/2}(Q^2)$ for the description of the resonance electroexcitation by longitudinal photons of zero helicity. In a case of an N^* state of 1/2-spin, there is an alternative and equivalent way of describing resonance electroexcitation in terms of the form factors $F_1^{N^*}(Q^2)$ and $F_2^{N^*}(Q^2)$ that correspond to the helicity-conserving and helicity-flipping parts of the scattering in the infinite momentum frame. The confrontation of the theoretical predictions for these amplitudes with their experimental measurements is the basis for further understanding of nonperturbative QCD.

A strong collaboration between experimentalists and theorists has been established to achieve the challenging objectives in pursuing N^* studies at high photon virtualities. Three topical workshops[31–33] have been organized by Hall B, the Theory Center at JLab, and the University of South Carolina to foster these efforts and create opportunities to facilitate and stimulate further growth in this field. This overview is prepared based on the presentations and discussions at these dedicated workshops with the goal to develop:

(i) reaction models for the extraction of the $\gamma_v pN^*$ electrocouplings from the data on single-meson and double-pion electroproduction off protons at photon virtualities from 5 GeV^2 to 12 GeV^2, by incorporating the transition from meson–baryon to quark degrees of freedom into the reaction mechanisms;

(ii) approaches for the theoretical interpretation of $\gamma_v pN^*$ electrocouplings, which are capable of exploring how N^* states are generated nonperturbatively by strong interactions, and how these processes emerge from QCD.

Current theoretical approaches fall into two broad categories: (i) those that tackle the QCD equations of motion directly and (ii) those that use models inspired by our knowledge of QCD. It is important to realize that even those approaches that attempt to solve QCD directly can only do so approximately, with further improvements in these calculations expected over time. Furthermore, the demanding theoretical effort that is required might not be undertaken without the data obtained from electroproduction experiments. It is the interplay between theory and experiment that leads to progress. Until exact calculations exist, approaches that model QCD have an important role to play. They can give insight into different aspects of the problem and show us what to expect.

In this review, six approaches are discussed. Those that attempt to solve QCD directly are (i) lattice QCD (LQCD) (Sec. 3), (ii) QCD applications of the Dyson–Schwinger equation (DSEQCD) (Sec. 4), and (iii) light-cone sum rules (Sec. 5). Those that model various aspects of QCD or employ phenomenological constraints are (i) studies of quark–hadron duality (Sec. 6), (ii) light-front holographic QCD (anti-de Sitter space (AdS)/QCD) (Sec. 7), and (iii) constituent quark models (Sec. 8). Conclusions are given in Sec. 9.

1.4.1. *Lattice QCD (LQCD)*

QCD can be solved numerically on a four-dimensional lattice of space-time points. In order for the numerical solutions to converge, the physical Minkowski space is mapped into a Euclidean space in which physical time is replaced by imaginary time ($t \to i\tau$). The accuracy of the solutions obtained from LQCD are limited by the statistical accuracy of the numerical methods (so that, like experimental data, lattice "data" comes with error bars), and also by other approximations that derive from the fact that the lattice approximates continuous and infinite space-time by a discrete and finite lattice of space-time points. In addition, when finding N^* states on the lattice, operators that project an initial "white" source onto the quantum numbers of the N^* are constructed, and as the number of such independent operators is increased, the predictions for the states tends to become more reliable. Finally, current lattice methods require very long times to calculate results for the very small masses of the *up* and *down* quarks from which normal nuclear states are constructed (the masses are usually expressed in terms of the mass of the pion on the lattice, which is typically much larger than the physical mass of about 140 MeV). In looking at lattice calculations, one must be careful to note the effective pion mass associated with the calculation, and to observe whether or not the calculation is *quenched* (approximate calculations which omit quark–antiquark loops) or *unquenched* (calculations that include such loops and hence correspond to real QCD). All of these approximations are continually being improved.

Recent advances have shown the promising potential of LQCD in describing the resonance $\gamma_v NN^*$ electrocouplings from QCD. Proof-of-principle results on the Q^2-evolution of the $F_1^{P_{11}}(Q^2)$ and $F_2^{P_{11}}(Q^2)$ form-factors for the transition from the ground state proton to the excited $P_{11}(1440)$ state have recently become available, employing unquenched LQCD calculations,[34] see Fig. 24 from Sec. 3. The corresponding experimental values of the $F_1^{P_{11}}(Q^2)$ and $F_2^{P_{11}}(Q^2)$ form-factors are computed from the CLAS results[19] on the $\gamma_v pP_{11}(1440)$ electrocouplings.

Despite the simplified basis of projection operators used in these computations, along with relatively large pion masses of ≈ 400 MeV, a reasonable description of the experimental data from CLAS[19,20] was still achieved. In the future, when the LQCD evaluation of $\gamma_v NN^*$ electrocouplings will become available, employing a realistic basis of projection operators in a volume of relevant size with the physical pion mass, we will be able to compare with the experimental electrocoupling results for all prominent N^* states. Such comparisons will allow us to test our understanding of how the full complexity of strongly interacting phenomena responsible for generating the ground and excited state hadrons can arise from QCD.

LQCD results[14] further predict the contributions for particular configurations in the resonance structure that should couple strongly to gluons. These N^* states with very large contributions coming from confined gluons are referred to as *baryon hybrids* and it is of great interest to find them. The observation of such hybrids, with *massive constituent* "valence" gluons, would eliminate the distinction between gluon fields as the sole carriers of the strong interaction and quarks as the sole sources of massive matter. The proposed search for hybrid N^*s[24] opens up yet another door in the N^* program with the CLAS and CLAS12 detectors. Based on the LQCD results,[14] the hybrid N^* masses are expected to be heavier than 1.9 GeV. Since hybrid N^*s have the same quantum numbers as regular N^*s, a measurement of the Q^2 evolution of the $\gamma_v pN^*$ electrocouplings (sensitive to the characteristic Q^2 behavior of constituent gluons) will be essential in order to distinguish hybrids from regular states. The high-Q^2 regime is of particular interest, since it is in this region where the contribution from quark and gluon degrees of freedom to the N^* structure is expected to dominate.

1.4.2. *Dyson–Schwinger equation of QCD*

The Dyson–Schwinger equations of QCD (DSEQCD) represent the tower of coupled integral equations which infers the dressed quark and gluon propagators as well as full vertex for interaction of dressed quarks and dressed gluons from the QCD Lagrangian. Having these basic ingredients of hadron structure derived from QCD, the hadron spectra, elastic meson and nucleon form-factors and transition $\gamma_v NN^*$ electrocouplings can be evaluated employing Poincare covariant kernel for dressed quark and gluon scattering amplitudes which is responsible for generation of mesons and baryons.

(a) (b) (c)

Fig. 7. (Color online) Graphical representation of the Dyson–Schwinger equation for the dressed quark propagator. (a) The (inverse) dressed quark propagator, (b) is the (inverse) of the bare-quark propagator, and (c) is the self energy, with the curly line representing the gluon, and the open circles representing the dressing of the gluon propagator and the full gqq-vertex function.

The DSEQCD, illustrated in Fig. 7, displays the quark propagator (from which the mass function is extracted) as the sum of the undressed propagator (or the propagator for a *current* quark) plus the self energy of the quark, as generated by QCD from the interaction of a quark with its own gluon field, which is described by the dressed gluon propagator and dressed quark–gluon vertex. If nonperturbative QCD is the infinite sum of all quark and gluon interactions, then the Dyson–Schwinger equation gives the dressed propagator exactly, provided the *exact* dressed gluon propagator and the *exact* quark–gluon vertex are inserted into the equation. In practice, it is necessary to make an *ansatz* for quark–gluon vertex employing certain truncation of full qqg-vertex. Furthermore, frequently the simplifying parametrizations are also employed in the treatment of dressed gluon propagators. Agreement of the results obtained from the two conceptually different frameworks of DSEQCD and LQCD with the experimental measurements of the $\gamma_v NN^*$ electrocouplings will offer compelling evidence for both (i) the validity of QCD in the nonperturbative regime and (ii) the use of the Dyson–Schwinger equations as a practical way to approximate QCD in the strong-coupling region solving the QCD equation of motion in continuous Euclidean space-time.

As an example, Fig. 8 shows the dressed quark masses as a function of momentum running over the quark propagator as calculated by DSEQCD[36,37] and LQCD[35] for different values of the bare-quark mass. The sharp increase from the mass of almost undressed current quarks ($p > 2$ GeV) to dressed constituent quarks ($p < 0.4$ GeV) clearly demonstrates that the dominant part of the dressed quark and consequently the hadron mass *in toto* is generated nonperturbatively by the strong interaction. The bulk of the dressed quark mass arises from a cloud of low-momentum gluons attaching themselves to the current-quark in the regime where the running quark–gluon coupling is large, and which is completely inaccessible by pQCD. The region where the dressed quark mass displays the fastest increase represents the transition domain from pQCD ($p > 2$ GeV) to confinement ($p < 0.4$ GeV). The solution of the DSEQCD gap equation (illustrated in Fig. 7)[38] shows that the propagator pole in the confinement regime leaves the real-momentum axis and the momentum squared p^2 of the dressed quark becomes substantially different from that for the dynamical mass squared $[M(p)]^2$. This means that the dressed quark in the confinement regime will never be on-shell, as is required for a free particle when it propagates through space-time. Therefore, dressed quarks have to

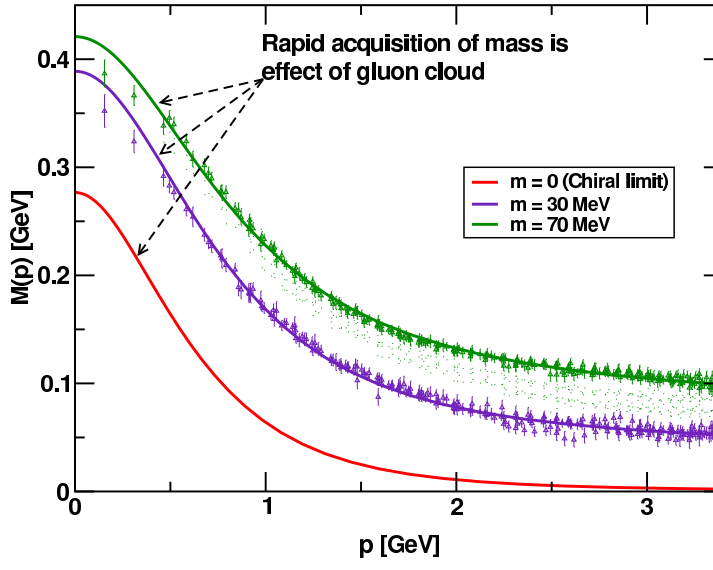

Fig. 8. (Color online) The mass function for a dressed quark evaluated within the framework of LQCD[35] (points with error bars) and DSEQCD[36,37] (solid lines) for two values of bare masses, 70 MeV and 30 MeV, are shown in green and magenta, respectively. The chiral limit of zero bare-quark mass, which is close to the bare masses of u and d quarks, is shown in red. Momenta $p < 0.4$ GeV correspond to confinement, while those at $p > 2$. GeV correspond to the regime which is close to pQCD. The areas that are accessible for mapping of the dressed quark mass function by the $\gamma_v NN^*$ electrocoupling studies with 6 GeV and 11 GeV electron beams are shown to the left of the blue solid and red dashed lines, respectively.

be strongly bound, locked inside the nucleon, and confinement becomes a property of the dressed quark and gluon propagators.

These dressing mechanisms are also responsible for the phenomenon of DCSB. If the bare-quark masses are zero, then QCD is chirally symmetric, meaning that the helicity of a quark (the projection of its spin in the direction of its motion, either $+1/2$ or $-1/2$) is unchanged by the scattering. This symmetry is dynamically broken by the QCD interactions, so that even if the quark masses were zero the dressed quark mass would be nonzero. Such a phenomena cannot be generated in pQCD: it is completely nonperturbative. It can be explained by the DSE shown in Fig. 7. This equation can generate a dynamical mass even if the bare-quark mass is zero (see also Fig. 8 for $m = 0$, the chiral limit). In the physical world, the bare-quark masses are only a few MeV, while the dressed quark masses are several hundreds of MeV, showing that more than 98% of dressed quark and hadron masses are generated nonperturbatively through DCSB processes.

The DSEQCD studies[13,38] suggest that the quark-core contribution (illustrated in Fig. 3(b)) to the electromagneticn (EM) transition amplitudes from the ground to excited nucleon states are determined primarily by the processes as depicted in Fig. 9. The momentum-dependent dressed quark mass affects all quark

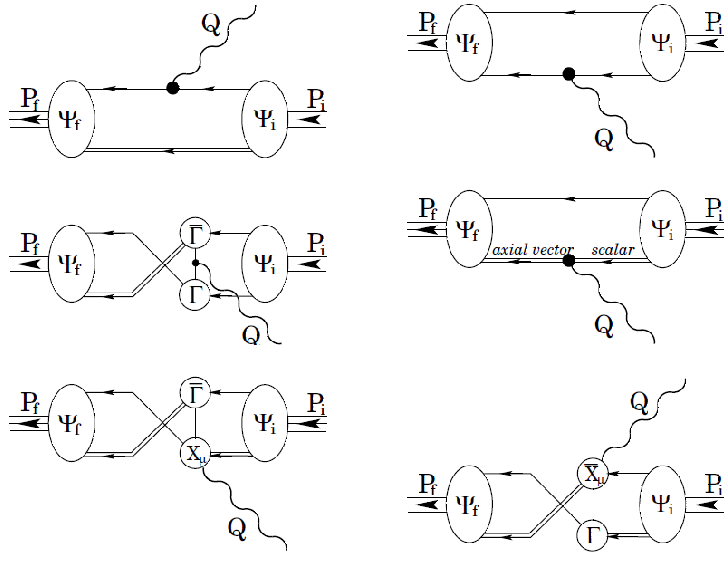

Fig. 9. The dressed quark interactions for the quark-core contribution to the EM transition amplitudes ($\gamma_v NN^*$ electrocouplings) from the ground nucleon state of four-momentum P_i to excited nucleon states of four-momentum P_f in the DSEQCD approach.[38] Solid and double-solid lines stand for dressed quark and the superposition of scalar and axial-vector diquark propagators, respectively. The Γ vertices describe the transition amplitudes between two-quark and diquark states, while the X-vertices represent the Schwinger interaction of the virtual photon with the transition current between the diquark and two-quark states. The ψ_i and ψ_f amplitudes describe the transitions between the intermediate diquark–quark states and the initial nucleon and final N^* states, respectively.

propagators and the virtual photon interaction with the dressed quark EM currents affords access to the dynamical quark structure. The transition currents between diquark and two-quark states elucidates the very details of the strong interaction between and among dressed quarks. The value of momentum that is carried away by a single quark can roughly be estimated by assuming equal sharing of the virtual photon momentum among all three dressed quarks. Under this assumption it is reasonably straightforward to see that the measurements of $\gamma_v NN^*$ electrocouplings at 5 GeV^2 $< Q^2 <$ 12 GeV^2 will be able to span nearly the entire range of quark momenta where the transition from confinement to pQCD occurs, as seen in Fig. 8. Therefore, the DSEQCD analyses of the $\gamma_v NN^*$ electrocouplings of all prominent N^* states expected from CLAS12 will offer a unique way to explore how quark–gluon confinement emerges from QCD. Strong constraints on the dressed quark mass function can be derived from the data on elastic nucleon form-factors and from $\gamma_v NN^*$ electrocouplings of different excited nucleon states. Consistent results obtained from the studies of elastic form-factors and $\gamma_v NN^*$ electrocouplings of all prominent excited proton states are of particular importance for reliable evaluation of this fundamental ingredient of nonperturbative strong interaction from the experimental data.

DSEQCD studies have revealed the sensitivity of $\gamma_v NN^*$ electrocouplings to diquark correlations in baryons. This qq-pair correlation is generated by a non-perturbative strong interaction, which is responsible for meson formation, and can be described by the finite sizes of quasi-particles formed of paired quarks. In the DSEQCD approach, depending on the parity of the N^* state, the two-quark assembly is described by either a superposition of scalar and axial-vector diquarks or a superposition of pseudoscalar and vector diquarks. It turns out that the relative contributions of the possible diquark components strongly depend on the quantum numbers of the N^* state. Furthermore, the amplitudes shown in Fig. 9, which describe the transitions between the intermediate diquark–quark state and the initial ground ψ_i or the final N^* state ψ_f, are strongly dependent on the quantum numbers of both the initial nucleon and the final N^* states. The information on the electrocouplings of as many N^* states as possible is needed for fully separating and identifying the mechanisms in the electroexcitation of nucleon resonances.

1.4.3. *Light-cone sum rules (LCSR)*

A particularly successful way to analyze the structure of a bound system of quarks is to look at the system in the *infinite momentum frame*, where the momentum of the system, P_z (assumed to be in the $\hat{z}$ direction), is very large. Since any successful theory must be Poincareé invariant, the physics cannot depend on the frame in which the interaction is observed, but *approximations* that may be valid in one frame may not be easy to implement or even understand in another frame. For example, in the infinite-momentum frame it is natural to assume that the $\hat{z}$ component of the momenta of the constituents particles, $(k_i)_z$, are also large (because they must be carried along with the bound state), and to ignore (at least as a first approximation) the transverse components $(\mathbf{k}_i)_\perp$. In this case, the $\hat{z}$ component of the momenta of each constituent quark is written in terms of its momentum fraction x_i, so that $(k_i)_z = x_i P_z$. As $P_z \to \infty$, the mass of the particle becomes less and less important, and the particle moves closer and closer to the *light-cone* swept out by a light beam. For this reason, analyses in the infinite-momentum frame are described in terms of light-cone coordinates, and it turns out that this becomes a completely general, frame independent formalism which has many theoretical advantages, as well as some non-intuitive properties.

As reviewed briefly in Sec. 5, the LCSR technique provides a way to relate the $\gamma_v NN^*$ electrocoupling amplitudes to integrals over matrix elements involving *distribution amplitudes* (DA) that depend only on the x_i (and are related to the bound state wave function integrated over the transverse momentum components). The DA can be expanded in a series of terms which can be calculated with the help of LQCD. This series has the nice feature that the first few few terms dominate the physics at $Q^2 \sim 2 - 10$ GeV^2, and that at very high Q^2 the results of pQCD emerge automatically. So far this method has been used to make predictions about the nucleon elastic form-factor ($\gamma_v NN$) and $N^*(1535)$ electroproduction ($\gamma_v NN^*$).

1.4.4. *Duality*

All of the methods discussed so far have used quarks and gluons (either bare or dressed) to describe the physics. This is a natural choice in that these are the degrees of freedom that appear in the QCD Lagrangian. However, the physics can also be discussed directly in terms of the colorless degrees of freedom one observes in nature: nucleons, N^*s, and mesons. Many years ago it was observed that the total cross-section for electrodisintegration of a nucleon, $\gamma_v + N \to$ *anything*, which depends on two variables, Q^2 and $\nu = P \cdot q/M$ (where P is the four-momentum of the nucleon and M its mass), shows nontrivial resonance structure, which appears as ridges at the values of the resonance masses $M^{*2} = (P+q)^2 = M^2 + 2M\nu - Q^2$. As Q^2 increases, these ridges were found to follow a smooth function which describes the high-energy behavior of the cross-section, extrapolated into the resonance region. This function is sometimes referred to as the *scaling* function, since it depends only on the variable $x_B = Q^2/(2M\nu)$, and is approximately independent of the scale Q^2. It is related to the distribution amplitudes mentioned above, and hence can be understood as a consequence of the underlying quark degrees of freedom in the target nucleon. At asymptotically large Q^2, in a given interval of x_B the cross-section is dominated by an ever increasing number of overlapping resonances, whose collective behavior is given by the scaling function.

At modest Q^2, however, where the resonances appear as distinct peaks in the cross-section (when plotted as a function of x_B for fixed Q^2), it has been discovered that the *average* of the cross-sections over an interval of x_B agrees with the average of the scaling function over the same interval. This feature, know as quark–hadron *duality*, suggests that the average behavior of the resonances is the same as the average behavior of the quarks, establishing a connection between hadronic degrees of freedom and quark degrees of freedom. As discussed in Sec. 6, there are indications that duality also works for exclusive processes, $\gamma_v + N \to X_i$ (where X_i is a particular final state, such as $X_i = N + \pi$, for example). These connections can provide constraints on the exclusive N^* production channels that can relate them to the underlying quark degrees of freedom.

1.4.5. *Light-front holographic QCD (AdS/QCD)*

A new method for the study of hadron physics is derived from the idea of mapping QCD, defined using light-front coordinates in four-dimensional Minkowski space-time, onto a five-dimensional AdS familiar from studies of gravity. This is *holographic* in the sense that it defines a correspondence between theories in a different number of space-time dimensions, much as a two-dimensional film can be made to produce a three-dimensional image. AdS/QCD has led to new insights into the color-confining, nonperturbative dynamics and the internal structure of relativistic light-hadron bound states. The formalism is relativistic and frame-independent. Hadrons are described as eigenstates of a light-front (LF) Hamiltonian with a specific color-confining potential. A single parameter κ sets the mass scale of the

hadrons. The hadronic spectroscopy of the LF holographic model gives a good description of the masses of the observed light-quark mesons and baryons. Elastic and transition form-factors are computed from the overlap of the LF wave functions. Many predictions of LF holography for baryon resonances can be tested at the 12-GeV JLab facility. An outline of this new method is given in Sec. 7.

1.4.6. *Constituent quark models*

Constituent quark models offer an alternative to the approaches discussed above. These models postulate that constituent (dressed) quarks are physical particles with a definite mass, and usually replace the difficult nonperturbative interactions between dressed quarks by a potential that includes a confining term that will not allow two quarks to be separated. The simplicity of these models makes the calculation of the resonance electrocouplings a comparatively straightforward problem. They are currently the only available phenomenological tool to investigate the electrocouplings over the full range of the baryon spectrum and the physical insight they provide make them very attractive. While some aspects of constituent quark models can be justified from QCD in the heavy quark limit, the challenge is to employ the information available from observable analyses within the quark models in order to understand the underlying physics of light quarks described by QCD.

Different approaches to the physical analyses of $\gamma_v NN^*$ electrocouplings at high photon virtualities within the framework of constituent quark models is discussed in Sec. 8. In some of these the covariant wave functions of an N^*, which normally would be calculated from a covariant wave equation using a QCD inspired kernel (the covariant version of a potential), are modeled directly. While this method simplifies the problem by bypassing the need to model the kernel and solve the equation, the consequence is that the masses of the resonances cannot be predicted and the wave functions of different resonances are not derived from a common dynamics. Nevertheless, these calculations do provide a simple prediction for the quark core interactions, depicted in Fig. 3(b), and provide useful insights into the Q^2 behavior of these core diagrams. Approaches of this type are described in Secs. 8.2 and 8.3. One of these uses the covariant spectator theory (ST) the other LF dynamics.

Section 8.4 summarizes a number of dynamical models that calculate the three-quark wave functions from model potentials. Most of these models assume a linear confining interaction and a short range one-gluon-exchange interaction with a Coulomb-like structure. The three-quark equations are solved using variational methods, and the parameters in the potentials fixed to the observed spectrum of N^* states. EM transitions between the states are then calculated.

1.5. *Reflections*

The studies of the EM transition amplitudes between the nucleon ground and its excited states in a wide range of photon virtualities elucidate relevant degrees of freedom in the N^* structure at different distances and eventually will allow us to

access the complexity of the nonperturbative strong interaction, which is responsible for the formation of various resonance states with different quantum numbers. With the 12-GeV upgrade of the JLab accelerator and the new CLAS12 detector, we have a unique opportunity to study the structure of the nucleon resonances at high Q^2 beginning the first year of running after completion of the JLab 12-GeV Upgrade Project. These studies will address some of the most fundamental issues of present-day hadron physics:

(i) How does nature achieve confinement?
(ii) How is confinement tied into dynamical chiral symmetry breaking, which describes the origin of most of the visible mass in the universe?
(iii) Can the fundamental QCD Lagrangian successfully describe the complex structure of all the N^* states?

These questions are very difficult to answer. As discussed above, study of the behavior of the resonances at high Q^2 provides a decisive advantage; in this region the meson cloud contributions become small and the quark core contributions we seek to study are exposed. With the massive N^* states that can be excited at high Q^2 it is also possible that we will see the widely anticipated, but not yet established, hybrid baryons in which massive confined gluons play a role equal to that of valence quarks. All of these efforts will be greatly enhanced by the new CLAS12 detector which will provide simultaneous data for a wide range of N^* states from major exclusive meson electroproduction channels, which theorists can use to untangle the competing contributions that enter each state in a different way.

A coordinated effort between experimental and theoretical physicists is required. This review summarizes where we are today and can be used, we hope, to bring other interested scientists up-to-date so that they may join this exciting effort. For further conclusions, see Sec. 9.

2. Analysis Approaches for Evaluation of Nucleon Resonance Electrocouplings from the CLAS Data: Status and Prospects

2.1. *Introduction*

The CLAS detector at JLab is a unique instrument, which has provided the lion's share of the world's data on meson photo- and electroproduction in the resonance excitation region. Cross-sections and polarization asymmetries collected with the CLAS detector have made it possible for the first time to determine electrocouplings of all prominent N^* states over a wide range of photon virtualities ($Q^2 < 5.0$ GeV^2) allowing for a comprehensive analysis of exclusive single-meson ($\pi^+ n$, $\pi^0 p$, ηp, and KY) reactions in electroproduction off protons. Furthermore, CLAS was able to precisely measure $\pi^+\pi^- p$ electroproduction differential cross-sections owing to the nearly full kinematic coverage of the detector for charged particles.

With the advent of the future CLAS12 detector, the Q^2 reach will be considerably extended for exploring the nature of confinement and DCSB in baryons for

Table 1. $N\pi$ and $N\pi\pi$ branching fractions for decays of excited proton states that have prominent contributions to the exclusive single- and/or charged-double-pion electroproduction channels. The values are taken from Ref. 4 or from the CLAS data analyses.[19,21] The asterisks * mark most suitable exclusive channel(s) for the studies of a particular N^* state.

N^*, Δ^* states	Branching fraction $N\pi$ (%)	Branching fraction $N\pi\pi$ (%)	Prominent in $N\pi$ exclusive channels	Prominent in the $\pi^+\pi^-p$ exclusive channel
$P_{33}(1232)$	100	0	*	
$P_{11}(1440)$	60	40	*	*
$D_{13}(1520)$	60	40	*	*
$S_{11}(1535)$	45	< 10	*	
$S_{31}(1620)$	< 25	75		*
$S_{11}(1650)$	75	< 15	*	
$F_{15}(1680)$	65	35	*	*
$D_{33}(1700)$	< 15	85		*
$P_{13}(1720)$	< 15	> 70		*
$F_{35}(1905)$	< 10	90		*
$F_{37}(1950)$	40	> 25	*	*

our N^* structure studies. Indeed, the CLAS12 detector will be the sole instrument worldwide that will allow for performing experiments to determine the $\gamma_v NN^*$ electrocouplings of prominent excited proton states as listed in Table 1. These will be the highest photon virtualities yet achieved for N^* studies with photon virtualities in the range between 5.0 GeV^2 and 10.0–12.0 GeV^2, where the upper Q^2 boundary depends on the mass of excited proton state. The primary objective of the dedicated experiment E12-09-003, *Nucleon Resonance Studies with CLAS12*,[18] is to determine the $\gamma_v NN^*$ electrocouplings from the exclusive meson electroproduction reactions, π^+n, π^0p, and $\pi^+\pi^-p$, off protons. The CLAS12 experiment E12-09-003[18] was approved for 40 days of running time and it is scheduled to start in the first year of running with the CLAS12 detector, that is right after the Hall B 12-GeV upgrade. This experiment represents the next step towards extending our current N^* program with the CLAS detector[5,6]; it will make use of the 11-GeV continuous electron beam that will be delivered to Hall B of JLab. We remark that the maximum energy of the electron beam to Hall B will be 11 GeV for the 12 GeV upgrade to Jefferson JLab.

The data from the π^+n, π^0p, and $\pi^+\pi^-p$ electroproduction channels will play a key role in the evaluation of $\gamma_v NN^*$ electrocouplings. The primary $N\pi$ and $\pi^+\pi^-p$ exclusive channels, combined, account for approximately 90% of the total cross-section for meson electroproduction in the resonance excitation region of $W < 2.0$ GeV. Both single- and charged-double-pion electroproduction channels are sensitive to N^* contributions, as can be seen in Table 1. Further, these two channels offer complementary information for cross checking the N^* parameters derived in the fits to the observables in the exclusive channel.

A necessary first step towards extracting the $\gamma_v NN^*$ electrocouplings, in a robust way, requires that we employ independent analyses of the single- and

charged-double-pion electroproduction data within the framework of several different phenomenological reaction models. A reliable separation of resonant and nonresonant contributions, moreover, is crucial for evaluating the $\gamma_v NN^*$ electrocouplings within each of the frameworks provided by these approaches. Independent analyses of major meson electroproduction channels offer a sensitive test as well as a quality check in separating the contributions of resonant and nonresonant mechanisms. Consistent extractions of the N^* electrocoupings among different channels are imperative, as well as Q^2-independent values of their hadronic decays and masses. The $\pi^+ n$, $\pi^0 p$, and $\pi^+\pi^- p$ exclusive electroproduction channels, for example, have entirely different nonresonant mechanisms. Clearly, the value of the $\gamma_v NN^*$ electrocouplings must be analysis independent and must remain the same in all exclusive channels, since resonance electroexcitation amplitudes do not depend on the final states that will populate the different exclusive reaction channels. Therefore, consistency in ascertaining the values of the $\gamma_v NN^*$ electrocouplings from a large body of observables, as measured in $\pi^+ n$, $\pi^0 p$, and $\pi^+\pi^- p$ electroproduction reactions, will give good measure of the reliability of the extraction of these fundamental quantities. In the next section, we shall review the current status and prospects for developing several phenomenological reaction models with the primary objective of determining $\gamma_v NN^*$ electrocouplings from independent analyses of the single- and charge-double-pion electroproduction data ($\pi^+ n$, $\pi^0 p$, and $\pi^+\pi^- p$).

2.2. *Approaches for independent analyses of the CLAS data on single- and charged-double-pion electroproduction off protons*

Several phenomenological reaction models[19–21,39–41] were developed by the CLAS Collaboration for evaluating the $\gamma_v NN^*$ electrocouplings in independent analyses of the data on $\pi^+ n$, $\pi^0 p$, and $\pi^+\pi^- p$ electroproduction off protons. These models were successfully applied to single-pion electroproduction for $Q^2 < 5.0$ GeV^2 and $W < 1.7$ GeV. The $\gamma_v NN^*$ electrocouplings were extracted from the CLAS $\pi^+\pi^- p$ electroproduction data for the kinematical ranges of $Q^2 < 1.5$ GeV^2 and $W < 1.8$ GeV.[5,21,24] The CLAS data on single-pion exclusive electroproduction were also analyzed within the framework of the MAID[25] and the SAID[42,43] approaches. These reaction models have allowed us to access resonant amplitudes by fitting all available observables in each channel independently and within the framework of different reaction models. Consequently, the $\gamma_v NN^*$ electrocouplings, along with the respective $N\pi$ and $N\pi\pi$ hadronic decay widths, were determined by employing a Breit–Wigner parametrization of the resonant amplitudes.

2.2.1. *CLAS collaboration approaches for resonance electrocoupling extraction from the data on single-pion electroproduction off protons*

Analyses of the rich CLAS data samples have extended our knowledge considerably of single-meson electroproduction reactions off protons, i.e., the $\pi^+ n$ and $\pi^0 p$ channels. A total of nearly 120,000 data points have been collected on reactions arising

from unpolarized differential cross-sections, longitudinally-polarized beam asymmetries as well as from longitudinal-target and beam-target asymmetries with a nearly complete coverage in the phase space for exclusive reactions.[19] The data were analyzed within the framework of two conceptually different approaches, namely: (a) the unitary isobar model (UIM) and (b) a model employing dispersion relations.[39,40] All well-established N^* states in the mass range of $M_{N^*} < 1.8$ GeV were incorporated into the $N\pi$ channel analyses.

The UIM follows the approach detailed in Ref. 25. The $N\pi$ electroproduction amplitudes are described as a superposition of N^* electroexcitations in the s-channel and nonresonant Born terms. A Breit–Wigner ansatz, with energy-dependent hadronic decay widths,[44] is employed for the resonant amplitudes. Nonresonant amplitudes are described by a gauge-invariant superposition of nucleon s- and u-channel exchanges and in the t-channel by π, ρ, and ω exchanges. The latter are reggeized; this allows for a better description of the data in the second- and the third-resonance regions, whereas for $W < 1.4$ GeV, the role of Regge-trajectory exchanges becomes insignificant. The Regge-pole amplitudes were constructed using the prescription delineated in Refs. 45 and 46 allowing us to preserve gauge invariance of the nonresonant amplitudes. The final-state interactions are treated as πN rescattering in the K-matrix approximation.[39]

In another approach, dispersion relations relate the real and imaginary parts of the invariant amplitudes, which describe $N\pi$ electroproduction in a model-independent way.[39] For the 18 independent invariant amplitudes describing the $\gamma_v N \to N\pi$ transition EM current, dispersion relations (17 unsubtracted and one subtracted) at fixed t are employed. This analysis has shown that the imaginary parts of amplitudes are dominated by resonant contributions for $W > 1.3$ GeV. That is to say, in this kinematical region, they are described solely by resonant contributions. For smaller W values, both the resonant and nonresonant contributions to the imaginary part of the amplitudes are taken into account based on an analysis of πN elastic scattering and by making use of the Watson theorem and the requisite dispersion relations.

For either of these approaches, the Q^2 evolution of the nonresonant amplitudes is determined by the behavior of the hadron EM form-factors, which are probed at different photon virtualities. The s- and u-channel nucleon exchange amplitudes depend on the proton and neutron EM form-factors, respectively. The t-channel π, ρ, ω exchanges depend on pion EM form-factors and $\rho(\omega) \to \pi\gamma$ transition form-factors. The exact parametrization of these EM form-factors as a function of Q^2 that are employed in the analyses of the CLAS single-pion electroproduction data can be found in Ref. 19. These analyses have demonstrated that for photon virtualities $Q^2 > 0.9$ GeV^2, the reggeization of the Born amplitudes becomes insignificant in the resonance region for $W < 1.9$ GeV. Consequently, at these photon virtualities, the background of UIM was constructed from the nucleon exchanges in the s- and u-channels and in the t-channel through π, ρ and ω exchanges. In the approach based on dispersion relations, we additionally take into account the Q^2 evolution

of the subtraction function $f_{\rm sub}(Q^2,t)$. The subtraction function was determined using a linear parametrization over the Mandelstam variable t and through fitting two parameters to the data in each bin of Q^2 (Ref. 19). Employing information on the Q^2 evolution of hadron EM form factors from other experiments or from our fits to the CLAS data, we are able to predict the Q^2 evolution of the nonresonant contributions to single-pion electroproduction in the region of Q^2, where the meson–baryon degrees of freedom remain relevant.

These two approaches provide a good description of the $N\pi$ exclusive channel observables in the entire range covered by the CLAS measurements: $W < 1.7$ GeV and $Q^2 < 5.0$ GeV^2, resulting in χ^2/d.p. < 2.0 for $Q^2 < 1.0$ GeV^2 and χ^2/d.p. < 3.0 at Q^2 from 1.5 GeV^2 to 4.5 GeV^2 (Ref. 19). Exclusive structure functions $\sigma_T + \varepsilon\sigma_L$, σ_{TT}, σ_{LT}, and $\sigma_{LT'}$ were derived from the measured CLAS cross-sections and polarization asymmetries. An example of the description of the structure function moments is shown in Fig. 10. The results from these two approaches further provide information for setting the systematical uncertainties associated with the models. A consistent description of a large body of observables in the $N\pi$ exclusive channels, obtained within the respective frameworks of two conceptually different approaches, lends credibility to a correct evaluation of the resonance contributions.

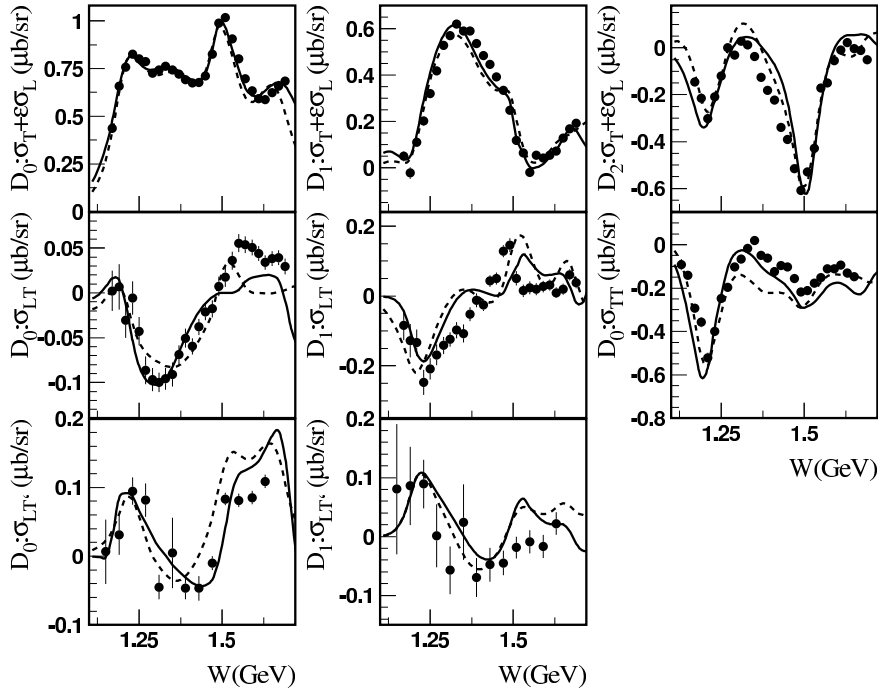

Fig. 10. Results for the Legendre moments of the $ep \to en\pi^+$ structure functions in comparison with experimental data[47] for $Q^2 = 2.44$ GeV^2. The solid (dashed) curves correspond to the results obtained using DR (UIM) approach.

2.2.2. *Evaluation of $\gamma_v NN^*$ resonance electrocouplings from the data on charged-double-pion electroproduction off protons*

The $\pi^+\pi^- p$ electroproduction data measured with the CLAS detector[7,8] provide information on nine independent one-fold differential and fully-integrated cross-sections in a mass range of $W < 2.0$ GeV and for photon virtualities in the range of $0.25 < Q^2 < 1.5$ GeV^2. Examples of the available $\pi^+\pi^- p$ one-fold differential cross-section data for specific bins in W and Q^2 are shown in Figs. 11 and 12. Analysis of these data have allowed us to establish which mechanisms contribute to the measured cross-sections. The peaks in the invariant mass distributions provide evidence for the presence of the channels arising from $\gamma_v p \to$ Meson+Baryon $\to \pi^+\pi^- p$ having an unstable baryon or meson in the intermediate state. Pronounced dependences in angular distributions further allow us to establish the relevant t-, u-, and s-channel exchanges. The mechanisms without pronounced kinematical dependences are identified through examination in various differential cross-sections, with their presence emerging from correlation patterns. The phenomenological reaction model JM[20,21,41,48] was developed in collaboration between Hall B at JLab and the Skobeltsyn Nuclear Physics Institute in Moscow State University. The primary objective of this work is to determine the $\gamma_v NN^*$ electrocouplings, and corresponding $\pi\Delta$ and ρp partial hadronic decay widths from fitting all measured observables in the $\pi^+\pi^- p$ electroproduction channel.

The amplitudes of the $\gamma_v p \to \pi^+\pi^- p$ reaction are described in the JM model as a superposition of the $\pi^-\Delta^{++}$, $\pi^+\Delta^0$, ρp, $\pi^+ D^0_{13}(1520)$, $\pi^+ F^0_{15}(1685)$, and $\pi^- P^{++}_{33}(1600)$ sub-channels with subsequent decays of unstable hadrons to the final $\pi^+\pi^- p$ state, and additional direct 2π-production mechanisms, where the final $\pi^+\pi^- p$ state comes about without going through the intermediate process of forming unstable hadron states.

The JM model incorporates contributions from all well-established N^* states listed in Table 1 to the $\pi\Delta$ and ρp sub-channels only. We also have included the $3/2^+(1720)$ candidate state, whose existence is suggested in the analysis[7] of the CLAS $\pi^+\pi^- p$ electroproduction data. In the current version of the JM model version (2012),[20] the resonant amplitudes are described by a unitarized Breit–Wigner ansatz as proposed in Ref. 49; it was modified to make it fully consistent with the parametrization of individual N^* state contributions by a relativistic Breit–Wigner ansatz with energy-dependent hadronic decay widths[50] employed in the JM model unitarity.[20] Quantum number conservation in strong interactions allows the transitions between $D_{13}(1520)/D_{13}(1700)$, $S_{11}(1535)/S_{11}(1650)$, and $3/2^+(1720)/P_{13}(1720)$ pairs of N^* states incorporated into the JM model. We found that use of the unitarized Breit–Wigner ansatz has a minor influence on the $\gamma_v NN^*$ electrocouplings, but it may substantially affect the N^* hadronic decay widths determined from fits to the CLAS data.

Nonresonant contributions to the $\pi\Delta$ sub-channels incorporate a minimal set of current-conserving Born terms.[41,50] They consist of t-channel pion exchange,

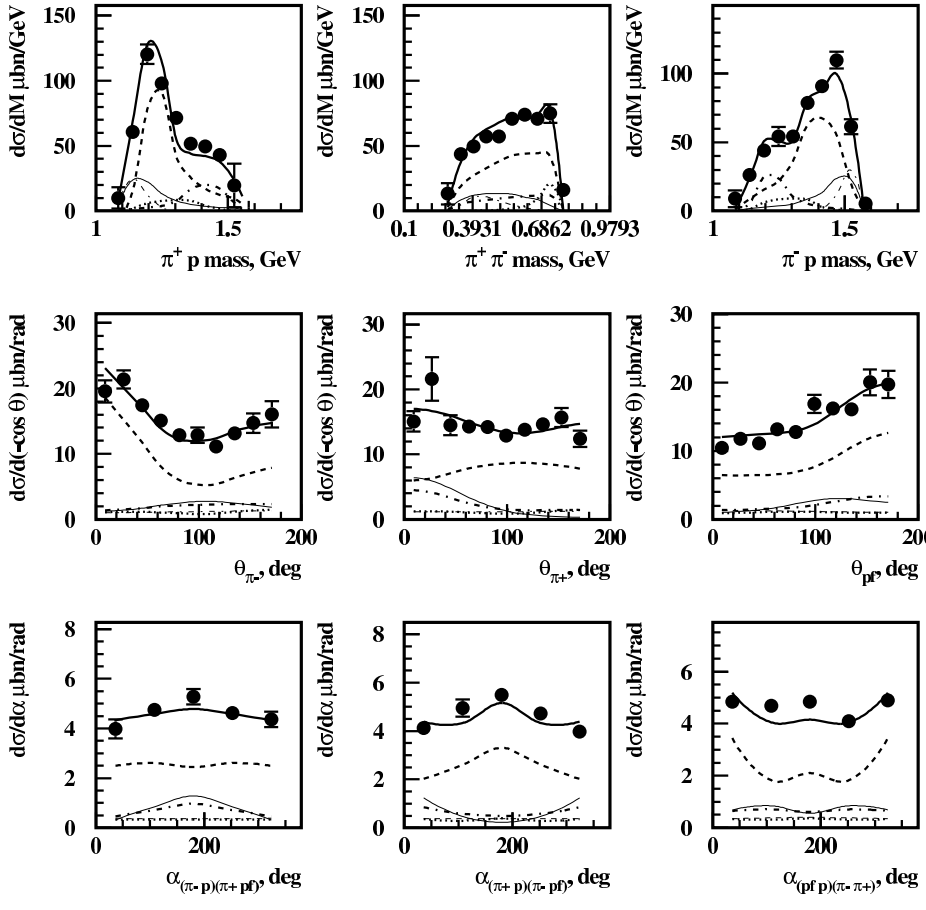

Fig. 11. Fits to the CLAS $ep \to e'\pi^+\pi^- p$ data[7] within the framework of JM model[21,41] at $W = 1.71$ GeV and $Q^2 = 0.65$ GeV^2. Full model results are shown by thick solid lines together with the contributions from $\pi^-\Delta^{++}$ (dashed thick lines), ρp (dotted thick lines), $\pi^+\Delta^0$ (dash-dotted thick lines), $\pi^+ D^0_{13}(1520)$ (thin solid lines), and $\pi^+ F^0_{15}(1685)$ (dash-dotted thin lines) isobar channels. The contributions from other mechanisms described in Sec. 2.2.2 are comparable with the data error bars and they are not shown in the plot.

s-channel nucleon exchange, u-channel Δ exchange, and contact terms. Non-resonant Born terms were reggeized and current conservation was preserved as proposed in Refs. 45 and 46. The initial- and final-state interactions in $\pi\Delta$ electroproduction are treated in an absorptive approximation, with the absorptive coefficients estimated from the data from πN scattering.[50] Nonresonant contributions to the $\pi\Delta$ sub-channels further include additional contact terms that have different Lorentz-invariant structures with respect to the contact terms in the sets of Born terms. These extra contact terms effectively account for nonresonant processes in the $\pi\Delta$ sub-channels beyond the Born terms, as well as for the final-state interaction effects that are beyond those taken into account by absorptive approx-

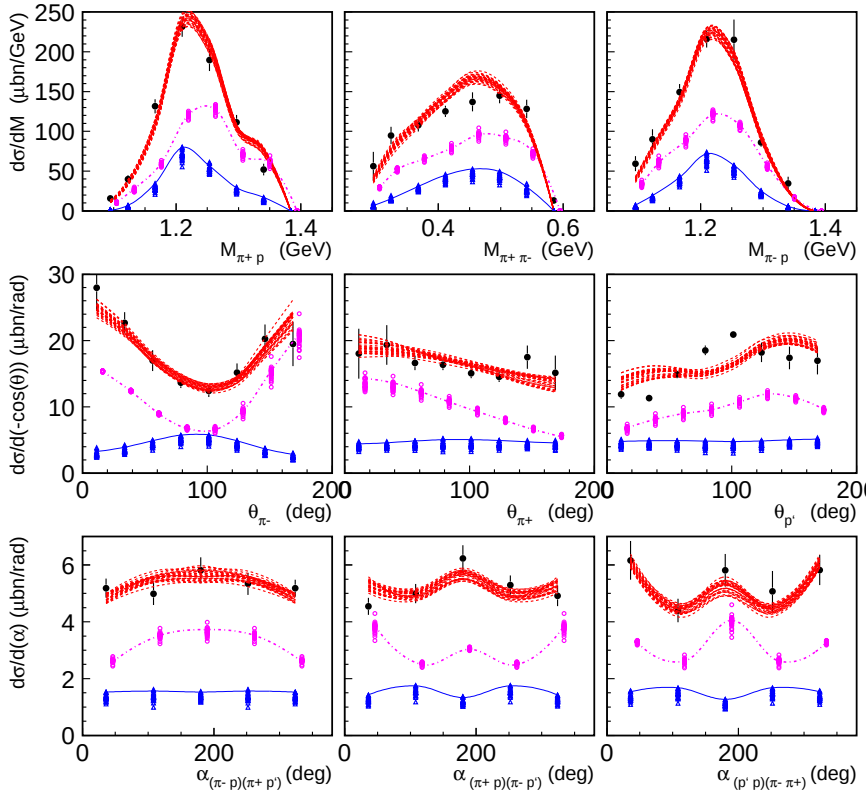

Fig. 12. (Color online) Resonant (blue triangles) and nonresonant (green open circles) contributions to the differential cross-sections (red lines) obtained from the CLAS data,[8] fit within the framework of the JM model at $W = 1.51$ GeV, $Q^2 = 0.38$ GeV^2. The solid blue and dotted-dashed green lines stand for the resonant and nonresonant contributions, respectively, which were computed for minimal χ^2/d.p. achieved in the data fit. The points for resonant and nonresonant contributions are shifted on each panel for better visibility. Dashed lines show selected fits.

imation. Parametrizations of the extra contact terms in the $\pi\Delta$ sub-channels are given in Ref. 41.

Nonresonant amplitudes in the ρp sub-channel are described within the framework of a diffractive approximation, which also takes into account the effects caused by ρ-line shrinkage.[51] The latter effects play a significant role in the N^* excitation region, and in particular, in near-threshold and sub-threshold ρ-meson production for $W < 1.8$ GeV. Even in this kinematical regime the ρp sub-channel may affect the one-fold differential cross-sections due to the contributions from nucleon resonances that decay into the ρp final states. Therefore, a reliable and credible treatment of nonresonant contributions in the ρp sub-channel becomes important for ascertaining the electrocouplings and corresponding hadronic parameters of these resonances. The analysis of the CLAS data[7,8] has revealed the presence of the ρp sub-channel contributions for $W > 1.5$ GeV.

The $\pi^+ D^0_{13}(1520)$, $\pi^+ F^0_{15}(1685)$, and $\pi^- P^{++}_{33}(1600)$ sub-channels are described in the JM model by nonresonant contributions only. The amplitudes of the $\pi^+ D^0_{13}(1520)$ sub-channel were derived from the nonresonant Born terms in the $\pi\Delta$ sub-channels by implementing an additional γ_5-matrix that accounts for the opposite parities of the Δ and $D_{13}(1520)$.[52] The magnitudes of the $\pi^+ D^0_{13}(1520)$ production amplitudes were independently fit to the data for each bin in W and Q^2. The contributions from the $\pi^+ D^0_{13}(1520)$ sub-channel should be taken into account for $W > 1.5$ GeV.

The $\pi^+ F^0_{15}(1685)$ and $\pi^- P^{++}_{33}(1600)$ sub-channel contributions are seen in the data[7] at $W > 1.6$ GeV. These contributions are almost negligible at smaller W. The effective contact terms were employed in the JM model for parametrization of these sub-channel amplitudes.[48,52] Magnitudes of the $\pi^+ F^0_{15}(1685)$ and $\pi^- P^{++}_{33}(1600)$ sub-channel amplitudes were fit to the data for each bin in W and Q^2.

A general unitarity condition for $\pi^+\pi^- p$ electroproduction amplitudes requires the presence of so-called direct-2π-production mechanisms, where the final $\pi^+\pi^- p$ state is created without going through the intermediate step of forming unstable hadron states.[53] These intermediate stage processes are beyond those aforementioned contributions from two-body sub-channels. Direct 2π production amplitudes were established for the first time in the analysis of the CLAS $\pi^+\pi^- p$ electroproduction data.[41] They are described in the JM model by a sequence of two exchanges in t and/or u channels by unspecified particles. The amplitudes of the 2π-production mechanisms are parametrized by an Lorentz-invariant contraction between spin-tensors of the initial and final-state particles, while two exponential propagators describe the above-mentioned exchanges by unspecified particles. The magnitudes of these amplitudes are fit to the data for each bin in W and Q^2. Recent studies of the correlations between the final-hadron angular distributions have allowed us to establish the phases of the 2π direct-production amplitudes.[54] The contributions from the 2π direct-production mechanisms are maximal and substantial ($\approx 30\%$) for $W < 1.5$ GeV and they decrease with increasing W, contributing less than 10% for $W > 1.7$ GeV. However, even in this kinematical regime, 2π direct-production mechanisms can be seen in the $\pi^+\pi^- p$ electroproduction cross-sections due to an interference of the amplitudes from two-body sub-channels.

The JM model provides a reasonable description of the $\pi^+\pi^- p$ differential cross-sections for $W < 1.8$ GeV and $Q^2 < 1.5$ GeV^2 with a χ^2/d.p. < 3.0, accounting only for statistical uncertainties in the experimental data. As a typical example, the nine one-fold differential cross-sections for $W = 1.71$ GeV and $Q^2 = 0.65$ GeV^2, with fits, are shown in Fig. 11, together with the contributions from each of the individual mechanisms incorporated into the JM description. Each contributing mechanism has a distinctive shape for the cross-section as is depicted by the observables in Fig. 11. Furthermore, any contributing mechanism will be manifested by substantially different shapes in the cross-sections for the observables, all of which are highly correlated through the underlying-reaction dynamics. The fit takes into

account all of the nine one-fold differential cross-sections simultaneously and allows for identifying the essential mechanisms contributing to $\pi^+\pi^- p$ electroproduction off protons. Such a global fit serves towards understanding the underlying mechanisms and thereby affording access to the dynamics.

This successful fit to the CLAS $\pi^+\pi^- p$ electroproduction data has further allowed us to determine the resonant parts of cross-sections. An example is shown in Fig. 12. The uncertainties associated with the resonant part are comparable with those of the experimental data. It therefore provides strong evidence for an unambiguous separation of resonant/nonresonant contributions. A credible means for separating resonances from background was achieved by fitting CLAS data within the framework of the JM model and it is of particular importance in the extraction of the $\gamma_v NN^*$ electrocouplings, as well as for evaluating each of the excited states decay widths into the $\pi\Delta$ and ρp channels. A special fitting procedure for the extraction of resonance electrocouplings with the full and partial $\pi\Delta$ and ρp hadronic decay widths was developed, thereby allowing us to obtain uncertainties of resonance parameters and which account for both experimental data uncertainties and for the systematical uncertainties from the JM reaction model.[20]

2.3. *Resonance electrocouplings from the CLAS pion electroproduction data*

Several analyses of CLAS data were carried out on single- and charged-double-pion electroproduction off protons within the framework of fixed-t dispersion

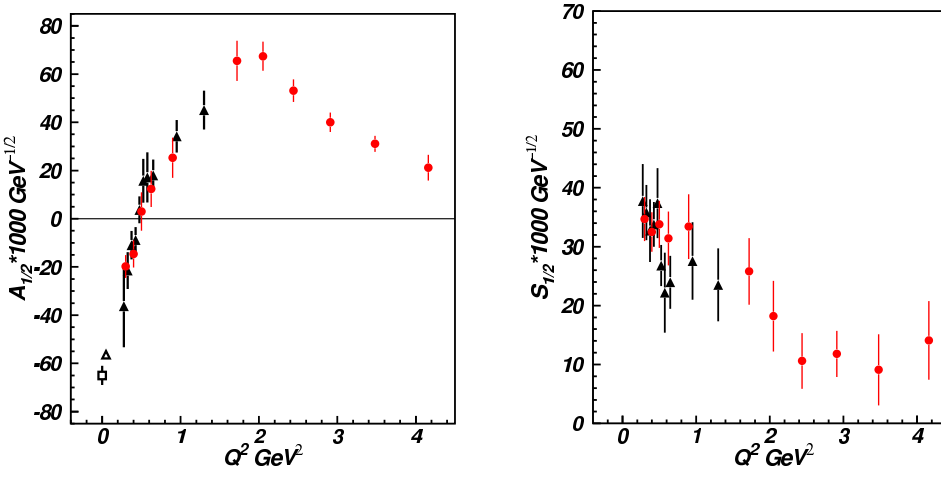

(a) (b)

Fig. 13. (Color online) $A_{1/2}$ (a) and $S_{1/2}$ (b) electrocouplings of the $P_{11}(1440)$ resonance determined in independent analyses of the CLAS data on $N\pi$ (circles),[19] and $\pi^+\pi^- p$ (triangles)[21] electroproduction off protons. Squares and triangles at $Q^2 = 0$ GeV^2 correspond to Ref. 4 and the CLAS $N\pi$[26] photoproduction results, respectively.

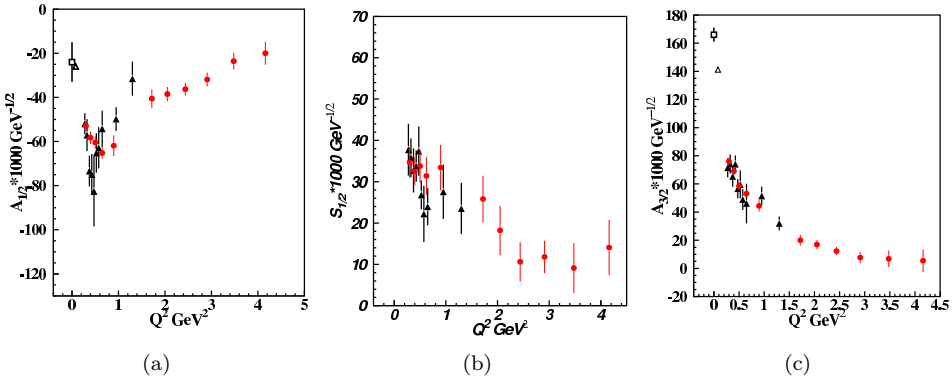

(a) (b) (c)

Fig. 14. (Color online) $A_{1/2}$ (a), $S_{1/2}$ (b), and $A_{3/2}$ (c) electrocouplings of the $D_{13}(1520)$ resonance determined in independent analyses of the CLAS data on $N\pi$ (circles),[19] and $\pi^+\pi^-p$ (triangles)[21] electroproduction off protons. Squares and triangles at $Q^2 = 0$ GeV^2 correspond to Ref. 4 and the CLAS $N\pi$[26] photoproduction results, respectively.

relations, the UIM model, and the JM model as described in Secs. 2.2.1 and 2.2.2, which have provided, for the first time, information on electrocouplings of the $P_{11}(1440)$, $D_{13}(1520)$, and $F_{15}(1685)$ resonances from independent analyses of π^+n, π^0p, and $\pi^+\pi^-p$ electroproduction channels.[19–21] The electrocouplings of the $P_{11}(1440)$ and $D_{13}(1520)$ resonances determined from these channels are shown in Figs. 13 and 14. They are consistent within uncertainties. The longitudinal $S_{1/2}$ electrocouplings of the $D_{13}(1520)$, $S_{11}(1535)$, $S_{31}(1620)$, $S_{11}(1650)$, $F_{15}(1685)$, $D_{33}(1700)$, and $P_{13}(1720)$ excited proton states have become available from the CLAS data for the first time as well.[19,21]

Consistent results on $\gamma_v NN^*$ electrocouplings from the $P_{11}(1440)$, $D_{13}(1520)$, and $F_{15}(1685)$ resonances that were determined from independent analyses of the major meson electroproduction channels, π^+n, π^0p, and $\pi^+\pi^-p$, demonstrate that the extraction of these fundamental quantities are reliable as these different electroproduction channels have quite different backgrounds. Furthermore, this consistency also strongly suggests that the reaction models described in Secs. 2.2.1 and 2.2.2 will provide a reliable evaluation of the $\gamma_v NN^*$ electrocouplings for analyzing either single- or charged-double-pion electroproduction data. It therefore makes it possible to determine electrocouplings for all resonances that decay preferentially to the $N\pi$ and/or $N\pi\pi$ final states.

The studies of $N\pi$ exclusive channels are the primary source of information on electrocouplings of the N^* states with masses below 1.6 GeV.[19] The reaction kinematics restrict the $P_{33}(1232)$ state to only the $N\pi$ exclusive channels. The $P_{11}(1440)$ and $D_{13}(1520)$ resonances have contributions to both single- and double-pion electroproduction channels, which are sufficient for the extraction of their respective electrocouplings. Analysis of the $\pi^+\pi^-p$ electroproduction off protons allows us to check the results of $N\pi$ exclusive channels for the resonances that have substantial decays to both the $N\pi$ and $N\pi\pi$ channels.

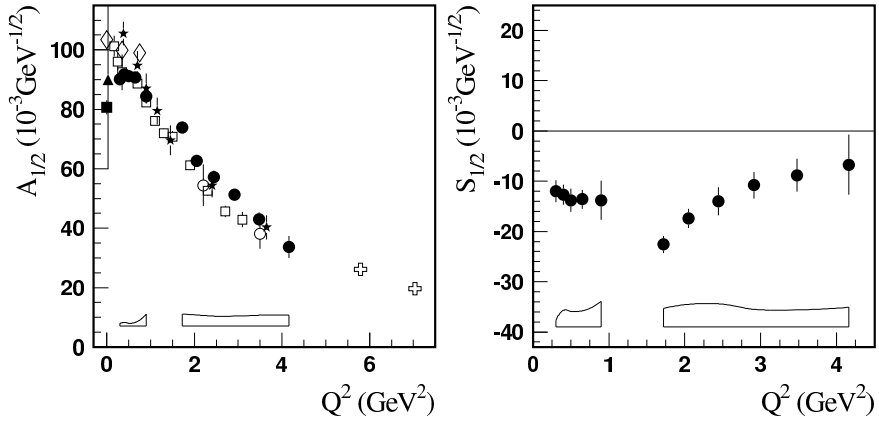

Fig. 15. Transverse electrocoupling $A_{1/2}$ of the $\gamma^* p \to S_{11}(1535)$ transition. The full circles are the electrocouplings extracted from $N\pi$ electroproduction data.[19] The electrocouplings extracted from $N\eta$ electroproduction data are: the stars,[55] the open boxes,[9] the open circles,[56] the crosses,[57] and the rhombuses.[39,40] The full box and triangle at $Q^2 = 0$ correspond to Ref. 4 and the CLAS $N\pi$[26] photoproduction results, respectively.

For the $S_{11}(1535)$ resonance, the hadronic decays to the $N\pi\pi$ final state is unlikely (see Table 1). Therefore, the studies of this very pronounced $N\pi$-electroproduction resonance become problematic in the charged-double-pion electroproduction off protons. On the other hand, the $S_{11}(1535)$ resonance has a large branching ratio to the πN and ηN channels. Since 1999, this resonance has been extensively studied at Jefferson Lab over a wide range of Q^2 up to 4.5 GeV^2 and 7 GeV^2 for the channels $N\pi$ and $N\eta$, respectively in the electroproduction off protons (see Fig. 15). For $N\eta$ electroproduction, the $S_{11}(1535)$ strongly dominates the cross-section for $W < 1.6$ GeV and is extracted from the data in a nearly model-independent way using a Breit–Wigner form for the resonance contribution.[9,55–57] These analyses assume that the longitudinal contribution is small enough to have a negligible effect on the extraction of the transverse amplitude. This assumption is confirmed by the analyses of the CLAS $N\pi$ electroproduction data.[19] Accurate results were obtained in both reactions for the transverse electrocoupling $A_{1/2}$; they show a consistent Q^2 slope and allowed for the determination of the branching ratios to the $N\pi$ and $N\eta$ channels.[19] Transverse $A_{1/2}$ electrocouplings of the $S_{11}(1535)$ extracted in independent analyses of $N\pi$ and $N\eta$ electroproduction channels are in a reasonable agreement, after taking the systematical uncertainties of the analysis[19] into consideration. Expanding the proposal, nucleon resonance studies with CLAS12,[18] by further incorporating $N\eta$ electroproduction at high Q^2 would considerably enhance our capabilities for extracting self-consistent and reliable results for the $S_{11}(1535)$ electrocouplings in independent analyses of the $N\pi$ and $N\eta$ electroproduction channels.

The charged-double-pion electroproduction channel is of particular importance for evaluation of high-lying resonance electrocouplings, since most N^* states with

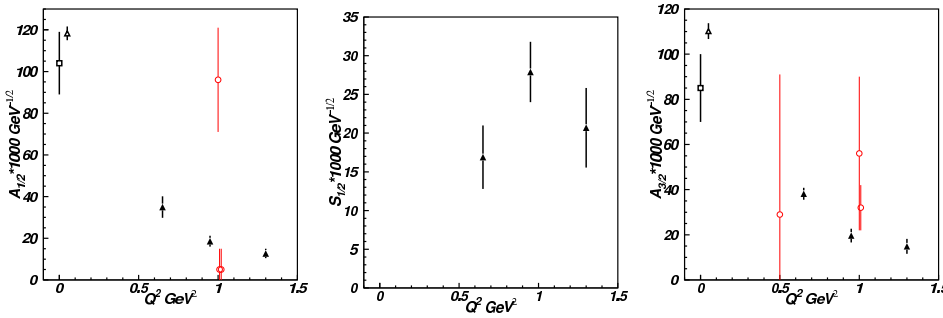

(a) (b) (c)

Fig. 16. (Color online) Electrocouplings of $D_{33}(1700)$ resonance $A_{1/2}$ (a), $S_{1/2}$ (b) and $A_{3/2}$ (c) determined in analyses the CLAS $\pi^+\pi^- p$ electroproduction data[41] and world data on $N\pi$ electroproduction off protons.[58]

masses above 1.6 GeV decay preferentially by two pion emission (Table 1). Preliminary results on the electrocouplings of the $S_{31}(1620)$, $S_{11}(1650)$, $F_{15}(1685)$, $D_{33}(1700)$, and $P_{13}(1720)$ resonances were obtained from an analysis of the CLAS $\pi^+\pi^- p$ electroproduction data[7] within the framework of the JM model.[21] As an example, electrocouplings of the $D_{33}(1700)$ resonance were determined from analysis of the CLAS $\pi^+\pi^- p$ electroproduction data and are shown in Fig. 16 in comparison with the previous world's data taken from Ref. 58. The $D_{33}(1700)$ resonance decays preferentially to $N\pi\pi$ final states with the branching fraction exceeding 80%. Consequently, electrocouplings of this resonance determined from the $N\pi$ electroproduction channels have large uncertainties due to insufficient sensitivity of these exclusive channels contributing to the $D_{33}(1700)$ resonance. The CLAS results have considerably improved our knowledge on electrocouplings of the $S_{31}(1620)$, $S_{11}(1650)$, $F_{15}(1685)$, $D_{33}(1700)$, and $P_{13}(1720)$ resonances. They have provided accurate information on the Q^2 evolution of the transverse electrocouplings, while longitudinal electrocouplings of these states were determined, again, for the first time.

Most of the N^* states with masses above 1.6 GeV decay preferentially through channels with two pions in the final state, thus making it difficult to explore these states in single-pion electroproduction channels. The CLAS KY electroproduction data[10,11] may potentially provide independent information on the electrocouplings of these states. At the time of this writing, however, reliable information on KY hadronic decays from N^*s are not yet available. The N^* hyperon decays can be obtained from fits to the CLAS KY electroproduction data,[10,11] which should be carried out independently in different bins of Q^2 by utilizing the Q^2-independent behavior of resonance hadronic decays. The development of reaction models for the extraction of $\gamma_v NN^*$ electrocouplings from the KY electroproduction channels is urgently needed. Furthermore, complementary studies of the KY decay mode can be carried out with future data from the Japan Proton Accelerator Research

Complex (J-PARC) and through J/Ψ decays to various $\bar{N}N^*$ channels at the Beijing Electron Positron Collider (BEPC).

Most of the well-established resonances have substantial decays to either the $N\pi$ or $N\pi\pi$ final states. Therefore, studies of $N\pi$ and $\pi^+\pi^-p$ electroproduction off protons will allow us to determine the electrocouplings of all prominent excited proton states and such studies will mark the first step in the evaluation of resonance electrocouplings in the unexplored regime of photon virtualities ranging from 5 to 12 GeV^2.

2.4. *Status and prospect of excited baryon analysis center (EBAC)*

2.4.1. *The case for a multi-channel global analyses*

Interactions among different hadronic final states are termed final-state interactions (FSI). In exclusive meson electroproduction, for example, FSI represent a key issue both in terms of the extraction as well as in the physical interpretation of the nucleon resonance parameters. In the reaction models for analyses of different exclusive meson electroproduction channels, as detailed above, FSI are treated phenomenologically for each specific reaction. Analyses of exclusive hadroproduction have allowed us to explicitly establish the relevant mechanisms for hadron interactions among the various final states for different exclusive photo- and electroproduction channels in terms of the meson–baryon degrees of freedom. The information on meson electroproduction amplitudes comes mostly from CLAS experiments. These results on meson–baryon hadron interaction amplitudes open up additional opportunities for the extraction of resonances, their photo- and electrocouplings, as well as their associated hadronic decay parameters. These parameters can be constrained through a global analysis of all exclusive meson electroproduction data from different photo- and electroproduction channels as analyzed within the framework of coupled-channel approaches.[59–61]

These approaches have allowed us to explicitly take into account the hadronic FSI among the exclusive meson electroproduction channels and to build up reaction amplitudes consistent with the restrictions imposed by a general unitarity condition. Another profound consequence of unitarity is reflected by the relations among the nonresonant meson production mechanisms and the contributions from meson–baryon dressing amplitudes (i.e., the meson–baryon cloud) to the resonance electrocouplings along with their hadronic decay parameters. Use of coupled-channel approaches have allowed us to determine such contributions in the fitting to the experimental data. Therefore, global analyses of all exclusive meson photo- and electroproduction data within the framework of coupled-channel approaches will reveal information on the resonance structure in terms of quark–core and meson–baryon cloud contributions at different distance scales.

The $N\pi$ and $\pi^+\pi^-p$ electroproduction channels are strongly coupled through FSI. The data from experiments with hadronic probes have shown that the $\pi N \rightarrow$

$\pi\pi N$ reactions are the second biggest exclusive contributors to inclusive πN interactions. Therefore, data on the mechanisms contributing to single- and charged-double-pion electroproduction off protons are needed for the development of global multi-channel analyses for the extraction of $\gamma_v NN^*$ electrocouplings within the framework of coupled-channel approaches. A consistent description of hadronic interactions between the πN and $\pi\pi N$ asymptotic states is critical for the reliable extraction of $\gamma_v NN^*$ electrocouplings within the framework of coupled-channel approaches.

2.5. *Dynamical coupled channel model*

In this section, we report on the development and results of the EBAC-dynamical-coupled-channel-model (DCC) approach spanning the period from January 2006 through March 2012. This analysis project has three primary components:

(i) perform a DCC analysis on the world data on meson production reactions from the nucleon to determine the meson–baryon partial-wave amplitudes,
(ii) extract the N^* parameters from the determined partial-wave amplitudes,
(iii) investigate the interpretations of the extracted N^* properties in terms of the available hadron models and LQCD.

The EBAC is conducting DCC analyses of JLab data and other relevant data in order to extract N^* parameters and to investigate the reaction mechanisms for mapping out the important components of the N^* structure as a function of distance or Q^2. This work is predicated upon the dynamical model for the $\Delta(1232)$ resonance,[62] which was developed by the Argonne National Laboratory-Osaka University (ANL-Osaka) collaboration.[63] In the EBAC extension to the ANL-Osaka formulation,[62] the reaction amplitudes $T_{\alpha,\beta}(p,p';E)$ for each partial wave are calculated from the following coupled-channels integral equations:

$$T_{\alpha,\beta}(p,p';E) = V_{\alpha,\beta}(p,p') + \sum_{\gamma} \int_0^{\infty} q^2 dq V_{\alpha,\gamma}(p,q) G_{\gamma}(q,E) T_{\gamma,\beta}(q,p',E)\,, \quad (1)$$

$$V_{\alpha,\beta} = v_{\alpha,\beta} + \sum_{N^*} \frac{\Gamma^{\dagger}_{N^*,\alpha}\Gamma_{N^*,\beta}}{E - M^*}\,, \quad (2)$$

where α, β, $\gamma = \gamma N$, πN, ηN, KY, ωN, and $\pi\pi N$ which has $\pi\Delta$, ρN, σN resonant components, $v_{\alpha,\beta}$ are meson-exchange interactions deduced from the phenomenological Lagrangian, $\Gamma_{N^*,\beta}$ describes the excitation of the nucleon to a bare N^* state with a mass M^*, and $G_{\gamma}(q,E)$ is a meson–baryon propagator. The DCC model, defined by Eqs. (1) and (2), respects unitarity for both two- and three-body reactions.

This DCC model was used initially in fitting πN reactions from elastic scattering to extract parameters associated with the strong-interaction parts of $V_{\alpha,\beta}$ in Eq. (2) and corresponding EM components of $V_{\alpha,\beta}$ came from fits to the $\gamma p \to \pi^0 p, \pi^+ n$,

and $p(e, e'\pi^{0,+})N$ data in the invariant mass range of $W \leq 2$ GeV. To simplify the analysis during the developmental stage (2006–2010), the KY and ωN channels were not included in these fits.

The resulting six-channel model was then tested by comparing the predicted πN, $\gamma N \to \pi\pi N$ production cross-sections with data. In parallel to analyzing the data, a procedure to analytically continue Eqs. (1) and (2) to the complex-energy plane was developed to allow for extracting the positions and residues of several nucleon resonances. In the following, we present a sample of some of our results in these efforts.

2.5.1. *Results for single-pion production reactions*

In fitting the πN elastic-scattering channel, we found that one or two bare N^* states were needed for each partial wave. The coupling strengths of the $N^* \to MB$ vertex interactions $\Gamma_{N^*,MB}$ with $MB = \pi N$, ηN, $\pi\Delta$, ρN, σN were then determined in the χ^2-fits to the data and these results can be found in Ref. 64.

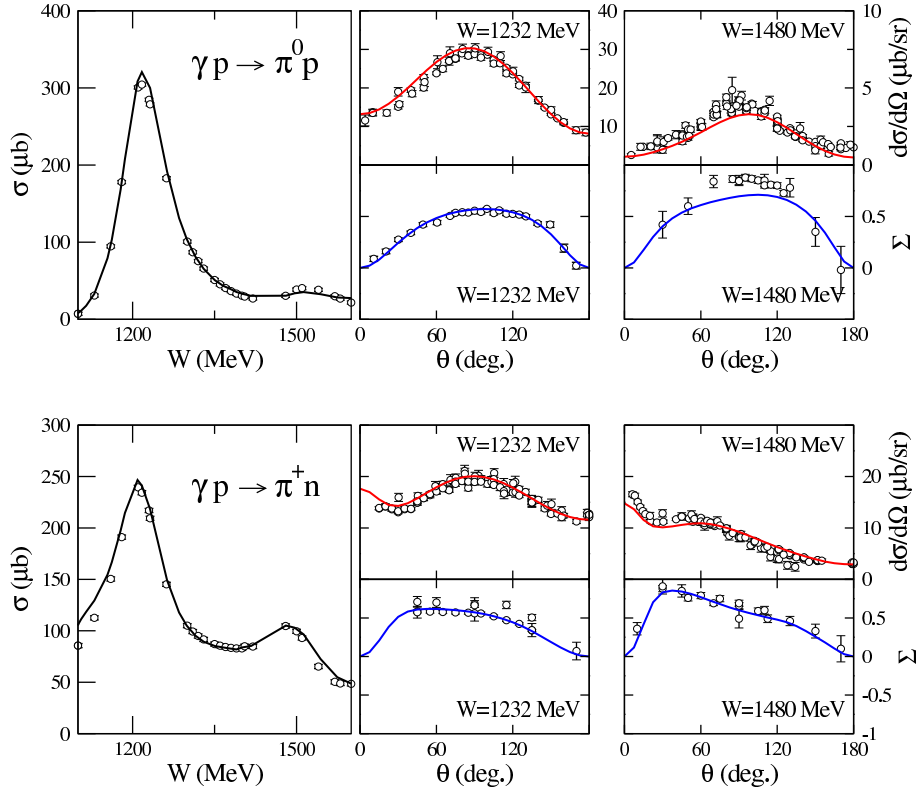

Fig. 17. (Color online) The DCC results[29] of total cross-sections (σ), differential cross-sections ($d\sigma/d\Omega$), and photon asymmetry (Σ) of $\gamma p \to \pi^0 p$ (upper parts), $\gamma p \to \pi^+ n$ (lower parts).

Our next step was to determine the bare $\gamma N \to N^*$ interaction $\Gamma_{N^*,\gamma N}$ by fitting the data from $\gamma p \to \pi^0 p$ and $\gamma p \to \pi^+ n$ reactions.

Because we did not adjust any parameter which had already been fixed in earlier fits to the πN elastic scattering, we found[29] that our fits to the data were sound only up to invariant masses not exceeding $W = 1.6$ GeV. Figure 17 shows our results for total cross-sections (σ), differential cross-sections ($d\sigma/d\Omega$), and the photon asymmetry (Σ). The Q^2 dependence of the $\Gamma_{N^*,\gamma N}$ vertex functions were then determined[65] by fitting the $p(e,e'\pi^0)p$ and $p(e,e'\pi^+)n$ data up to $W = 1.6$ GeV and $Q^2 = 1.5$ (GeV/c)^2.

2.5.2. *Results for two-pion production reactions*

As delineated above, the DCC model was constructed from fitting single-pion data. We then tested the efficacy of this model by examining to what extent the model could describe the $\pi N \to \pi\pi N$ and the $\gamma N \to \pi\pi N$ data. Interestingly, at the near-threshold region of $W \leq 1.4$ GeV, we found[66,67] that the predicted total cross-sections are in excellent agreement with the data. At higher W, the predicted $\pi N \to \pi\pi N$ cross-sections describe the major features of the available data reasonably well, as shown in Fig. 18. Here, we further see the important role that the effects from coupled channels play. The predicted $\gamma p \to \pi^+\pi^- p$, $\pi^0\pi^0 p$ cross-sections, however,

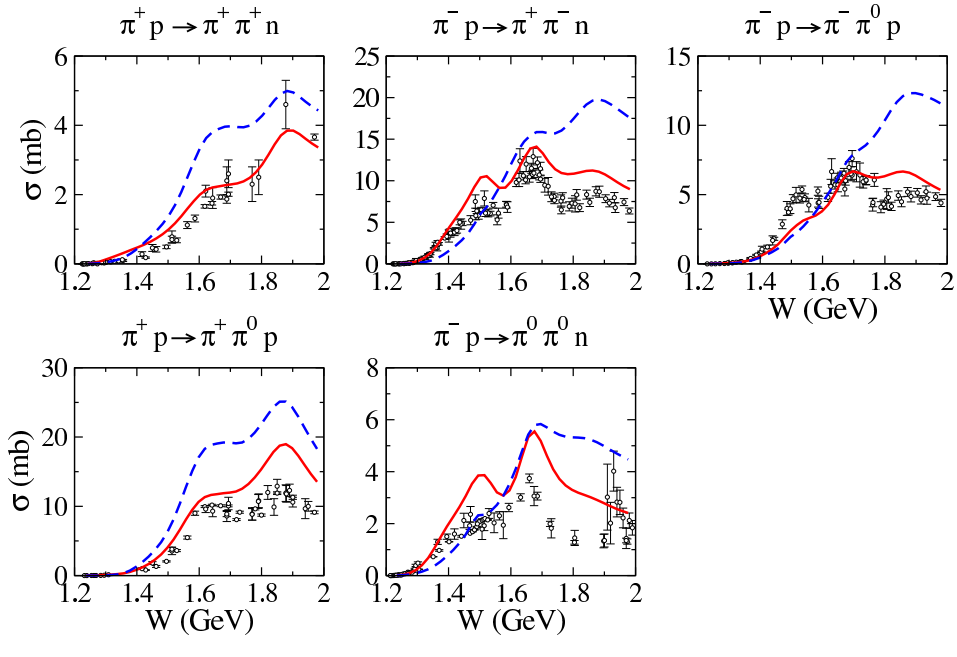

Fig. 18. (Color online) The predicted[66] total cross-sections of the $\pi N \to \pi\pi N$ are compared with data. The dashed curves come from switching off the coupled-channel effects in the DCC model of Ref. 62.

exceed the data by about a factor of two, while the fits describe, more or less, the overall shapes of the two-particle invariant-mass distributions.

2.5.3. *Resonance extractions*

We define resonances as the eigenstates of the Hamiltonian with the outgoing waves being the respective decay channels as is described in Refs. 23 and 69. One can then show that the nucleon resonance positions are the poles M_R of meson–baryon scattering amplitudes as calculated from Eqs. (1) and (2) on the Riemann surface in the complex-E plane. The coupling of meson–baryon states with the resonances can be determined by the residues $R_{N^*,MB}$ at the pole positions. Our procedures for determining M_R and $R_{N^*,MB}$ are further explained in our recent work (see, Refs. 23 and 68–70).

With our method of analytic continuation into the complex plane,[23,69] we are able to analyze the dynamical origins of the nucleon resonances within the framework of the EBAC DCC model.[62] This was done by examining how the resonance positions move as each of the coupled-channel couplings are systematically switched off. For example, as illustrated in Fig. 19 for the P_{11} states, this exercise revealed that two poles in the Roper region and the next-higher pole are associated with the same bare state on the Riemann surface.

2.5.4. *Prospects and path forward*

During the developmental stage of the DCC analysis by the EBAC collaboration in 2006–2010, the DCC model parameters were determined by separately analyzing the following data sets: $\pi N \to \pi N$,[64] $\gamma N \to \pi N$,[29] $N(e,e'\pi)N$,[65] $\pi N \to \pi\pi N$,[66]

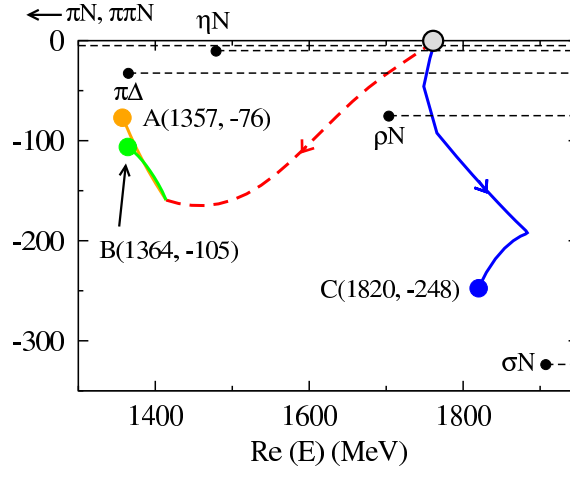

Fig. 19. (Color online) The trajectories of the evolution of three nucleon resonances in P_{11} from the same bare N^* state. The results are from Ref. 68.

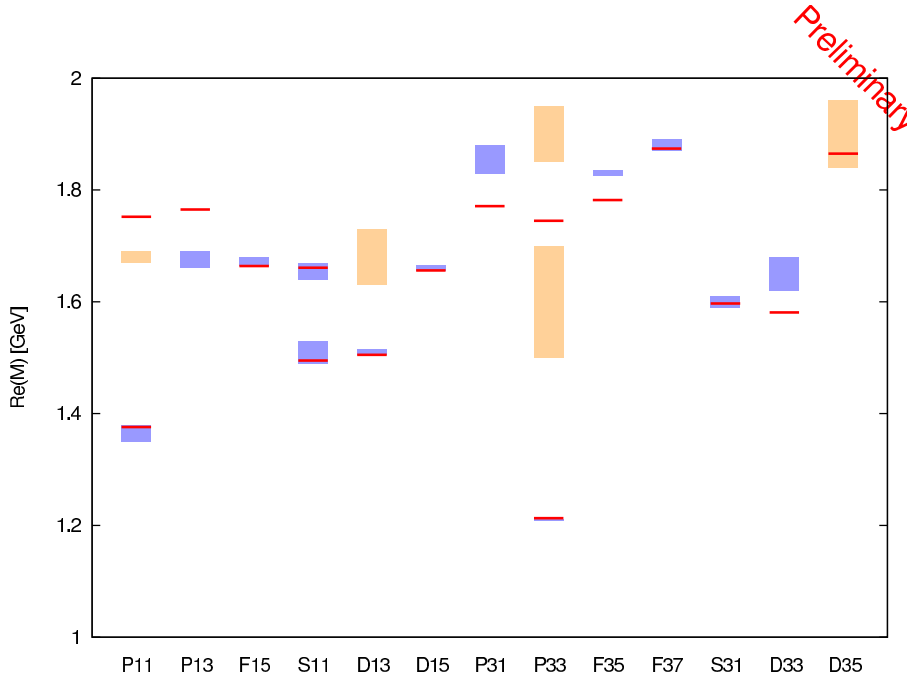

Fig. 20. (Color online) Preliminary results (red bars) of the determined N^* spectrum are compared with four-star (blue bands) and three-star (brown bands) states listed by the Particle Data Group.

and $\gamma N \to \pi\pi N$.[67] The very extensive data on $K\Lambda$ and $K\Sigma$ production, however, were not included in this analysis. To afford the highest-precision extraction of nucleon resonances, it behooves us to perform a combined and simultaneous coupled-channels analysis with all meson production reactions included.

In the summer of 2010, we initiated a comprehensive eight-channel combined analysis of the world's data that include strange mesons in the final state, i.e., $\pi N, \gamma N \to \pi N, \eta N, K\Lambda, K\Sigma$. The EBAC collaboration came to an end on March 31, 2012 and, in its place, the ANL-Osaka collaboration has taken over this DCC analysis task. Preliminary results of the full eight-channel combined analysis of the excited nucleon spectrum are shown in Fig. 20. We expect to have completed the analysis by early 2013. The ANL-Osaka analysis will then proceed to extract the $\gamma N \to N^*$ form-factors from the anticipated Jefferson Lab data on meson electroproduction, extending the momentum reach to much higher Q^2. Further, we will explore the interpretations of the extracted resonance parameters in terms of the available hadron models, such as the Dyson–Schwinger equation model, constituent quark model, and LQCD. Making these connections with these hadron models is needed to complete the DCC project with conclusive results, as is discussed in Refs. 62, 63, 68 and 71.

2.6. *Future developments*

The CLAS collaboration has provided a wealth of data, much of which is still being analyzed. These rich data sets have impacted and expanded the N^* program, through which reaction models can now be tuned to extract the $\gamma_v NN^*$ electrocouplings for CLAS12 experiments with $Q^2 > 5.0$ GeV^2, thereby enabling deeper N^* studies.[15] Preliminary CLAS data on charged-double-pion electroproduction for photon virtualities in the range of $2.0 < Q^2 < 5.0$ GeV^2 have recently become available.[72] They span the entire N^* excitation region for $W < 2.0$ GeV and the statistics allow for 115 bins in W and Q^2. The data consist of nine one-fold differential cross-sections as shown in Figs. 11 and 12. The extension of the JM approach to higher Q^2 values up to 5.0 GeV^2 covering the entire N^* excitation region is in progress and will be completed within two years after the publication of this document.

After the completion of this data analysis, electrocouplings of the $P_{11}(1440)$ and $D_{13}(1520)$ resonances will become available from both the $N\pi$ and $\pi^+\pi^- p$ electroproduction channels for $0.2 < Q^2 < 5.0$ GeV^2. We will then have reliable information on the electrocouplings for these two states over a full range of distances that correspond to transitioning, wherein the quark degrees of freedom in the resonance structure dominate. The studies of the N^* meson–baryon dressing as described in Refs. 29 and 73 strongly suggest a nearly negligible contribution from the meson–baryon cloud to the $A_{1/2}$ electrocouplings of the $D_{13}(1520)$ resonance for $Q^2 > 1.5$ GeV^2. Therefore, theoretical interpretations of already available and future CLAS results on $A_{1/2}$ electrocouplings of the $D_{13}(1520)$ resonance are of particular interest for approaches that are capable of describing the quark content of resonances based on QCD.

Analysis of the CLAS $\pi^+\pi^- p$ electroproduction data[72] within the framework of the JM approach will deliver the first information on electrocouplings of most of the high-lying excited proton states ($M > 1.6$ GeV) for $2.0 < Q^2 < 5.0$ GeV^2. This information will allow us to considerably extend our knowledge on how strong interactions generate excited proton states having different quantum numbers.

There will also be analyses of the available and future CLAS results on electrocouplings of all prominent N^* states for $Q^2 > 2.0$ GeV^2 within the framework of the LCSR approach as outlined in Sec. 5 that will constrain the quark-distribution amplitudes of the various N^* states. Access to the quark-distribution amplitudes in the N^* structure is of particular importance, since these amplitudes can be evaluated from QCD employing lattice calculations.

Information on the Q^2 evolution of nonresonant mechanisms as obtained from analyses of the CLAS data on single- and charged-double-pion electroproduction at $Q^2 < 5.0$ GeV^2 will serve as the starting point for the development of reaction models that will make it possible to determine the $\gamma_v NN^*$ electrocouplings from fitting the anticipated CLAS12 data for Q^2 from 5.0 to 12.0 GeV^2.

A consistent description of a large body of observables in the $N\pi$ exclusive channels achieved within the framework of two conceptually different approaches as outlined in Sec. 2.2.1 and with the success of the JM model in describing of $\pi^+\pi^- p$ electroproduction off protons all serve to demonstrate that the meson–baryon degrees of freedom play a significant role at photon virtualities of $Q^2 < 5.0$ GeV^2. Further development to the reaction models is needed in analyzing these exclusive channels for the anticipated CLAS12 data, where the quark degrees of freedom are expected to dominate. The reaction models for the description of $\pi^+ n$, $\pi^0 p$, and $\pi^+\pi^- p$ electroproduction off protons for $Q^2 > 5.0$ GeV^2 should explicitly account for contributions from these quark degrees of freedom. At present, however, there is no overarching theory of hadron interactions that will offer any "off-the-shelf" approach at these particular distance scales, where the quark degrees of freedom dominate, but are still well inside the regime of the nonperturbative strong interaction. Given the state of hadronic theory, we are pursuing a phenomenological way for evaluating the nonresonant mechanisms for the higher-Q^2 regime. We will explore the possibilities of implementing different models that employ quark degrees of freedom by explicitly comparing the predictions from these models directly to the data. First, we will start from models that employ handbag diagrams for parametrizing nonresonant single-pion electroproduction and we will then extend this work for a proper description of $\pi^+\pi^- p$ electroproduction off protons.

For the kinematics accessible at the Jefferson Lab energy upgrade, one reaches the region where a description of the processes of interest in terms of quark degrees of freedom applies. In this case, the calculation of cross-sections and other observables can be performed within the handbag approach, which is based on QCD factorization of the scattering amplitudes in hard subprocesses, pion electroproduction off quarks, and the generalized parton distributions (GPDs) for $p \to p$ or $p \to \Delta$ transitions.

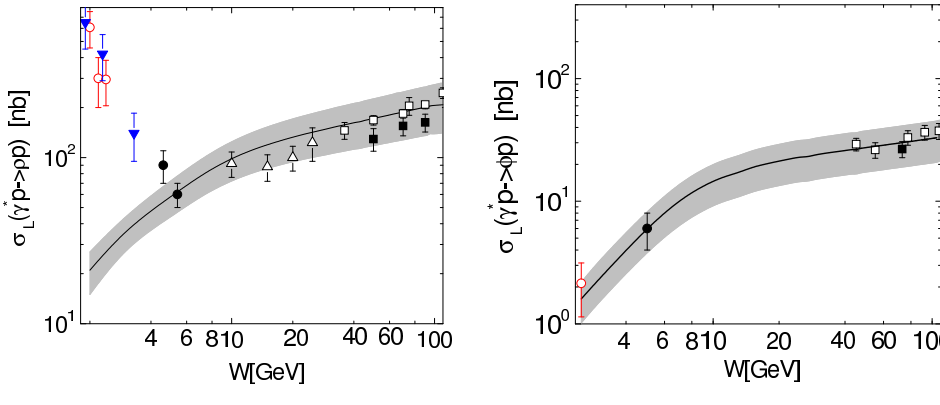

(a) (b)

Fig. 21. (Color online) Predictions of the longitudinal cross-section of ρ^0 (a) and ϕ (b) production versus W at $Q^2 = 4\,\text{GeV}^2$. For references to data see Refs. 74–76 and references therein.

In recent years, the data on the electroproduction of vector and pseudoscalar mesons have been analyzed extensively. In particular, as described in Refs. 74–76, a systematic analysis of these processes in the kinematical region of large Q^2 (> 3 GeV^2) and W larger than about 4 GeV but having small Bjorken-x (i.e., small skewness) has led to a set of GPDs ($H, E, \tilde{H}, H_T, \ldots$) that respect all theoretical constraints — polynomiality, positivity, parton distributions, and nucleon form-factors. These GPDs are also in reasonable agreement with moments calculated within LQCD[77] and with the data on deeply virtual Compton scattering in the aforementioned kinematical region.[78] On the other hand, applications in the kinematical region accessible presently from the 6-GeV JLab data as characterized by rather large values of Bjorken-x and small W, in general, do not lead to agreement with experiment. Predictions for ρ^0 electroproduction, for instance, fails by an order of magnitude, whereas for ϕ electroproduction it works quite well, as can be seen in Fig. 21. For the JLab energy upgrade, one can expect fair agreement between experiment and predictions for meson electroproduction evaluated from these set of GPDs.[a]

To describe the electroproduction of nucleon resonances in meson–baryon intermediate states in the $\pi^+\pi^- p$ exclusive electroproduction, one needs the $p \to N^*$ transition GPDs. In principle, these GPDs are new unknown functions. Therefore, straightforward predictions for reactions like $\gamma^* p \to \pi N^*$ are not possible at present. In the large N_c limit, however, one can at least relate the $p \to \Delta^+$ GPDs to the flavor diagonal $p \to p$ ones since the nucleon and the Δ are eigenstates of the same object, the chiral soliton.[79,80] The proton–proton GPDs always occur in the isovector combination $F^{(3)} = F^u - F^d$ where F is a proton–proton GPD. With the help of flavor symmetry one can further relate the $p \to \Delta^+$ GPDs to all other octet-decuplet transitions. Using these theoretical considerations, the observables for $\gamma^* p \to \pi N^*$ can be estimated. However, one should be aware, that the quality of the large N_c and SU(3)$_F$ relations are unknown; corrections of the order of 20% to 30% are to be expected. One should also bear in mind that pions electroproduced by transversely-polarized virtual photons must further be taken into account as has been shown in Refs. 75 and 76. Within the handbag approach, the contributions from such photons are related to the transversity (helicity-flip) GPDs. Despite this complication, an estimate of hard exclusive resonance production seems feasible.

A well-developed program on resonance studies at high photon virtualities[18] will allow us to determine electrocouplings of several high-lying N^* states with dominant $N\pi\pi$ decays (see Table 1) from the data on charged-double-pion electroproduction channel. However, reliable extraction of these electrocouplings for these states should be supported by independent analyses of other exclusive electroproduction channels having different nonresonant mechanisms. The ηp and $K\Lambda$ electroproduction channels may well improve our knowledge on electrocouplings

[a]Tables of predictions for electroproduction of various mesons in this kinematical region can be obtained from the authors of Ref. 76 upon request.

of the isospin 1/2 $P_{13}(1720)$ state due to isospin filtering in these exclusive channels. The studies of $K\Sigma$ and $\eta\pi N$ electroproduction may further offer access to the electrocouplings of the $D_{33}(1700)$ and $F_{35}(1905)$ resonances. More detailed studies on the feasibility of incorporating these additional exclusive channels for evaluating the electrocouplings of high-lying resonances are, in any case, a clear and present need.

3. N^* Physics from Lattice QCD

3.1. *Introduction*

QCD, when combined with the electroweak interactions, underlies all of nuclear physics, from the spectrum and structure of hadrons to the most complex nuclear reactions. The underlying symmetries that are the basis of QCD were established long ago. Under very modest assumptions, these symmetries predict a rich and exotic spectrum of QCD bound states, few of which have been observed experimentally. While QCD predicts that quarks and gluons are the basic building blocks of nuclear matter, the rich structure that is exhibited by matter suggests there are underlying collective degrees of freedom. Experiments at nuclear and high-energy physics laboratories around the world measure the properties of matter with the aim to determine its underlying structure. Several such new experiments worldwide are under construction, such as the 12-GeV upgrade at JLab's electron accelerator, its existing the experimental halls, as well as the new Hall D.

To provide a theoretical determination and interpretation of the spectrum, *ab initio* computations within LQCD have been used. Historically, the calculation of the masses of the lowest-lying states, for both baryons and mesons, has been a benchmark calculation of this discretized, finite-volume computational approach, where the aim is well-understood control over the various systematic errors that enter into a calculation; for a recent review, see Ref. 81. However, there is now increasing effort aimed at calculating the excited states of the theory, with several groups presenting investigations of the low-lying excited baryon spectrum, using a variety of discretizations, numbers of quark flavors, interpolating operators, and fitting methodologies.[82–85] Some aspects of these calculations remain unresolved and are the subject of intense effort, notably the ordering of the Roper resonance in the low-lying nucleon spectrum.

The Hadron Spectrum Collaboration, involving the Lattice Group at JLab, Carnegie Mellon University, University of Maryland, University of Washington, and Trinity College (Dublin), is now several years into its program to compute the high-lying excited-state spectrum of QCD, as well as their (excited-state) EM transition form-factors up to $Q^2 \sim 10$ GeV^2. This program has been utilizing "anisotropic" lattices, with finer temporal than spatial resolution, enabling the hadron correlation functions to be observed at short temporal distances and hence many energy levels to be extracted.[86,87] Recent advances suggest that there is a rich spectrum of mesons and baryons, beyond what is seen experimentally. In fact, the HSC's

calculation of excited spectra, as well as recent successes with GPUs, were featured in *Selected FY10 Accomplishments in Nuclear Theory in the FY12 Congressional Budget Request.*

3.2. *Spectrum*

The development of new operator constructions that follow from continuum symmetry constructions has allowed, for the first time, the reliable identification of the spin and masses of the single-particle spectrum at a statistical precision at or below about 1%. In particular, the excited spectrum of isovector as well as isoscalar mesons[90–92] shows a pattern of states, some of which are familiar from the $q\bar{q}$ constituent quark model, with up to total spin $J = 4$ and arranged into corresponding multiplets. In addition, there are indications of a rich spectrum of exotic J^{PC} states, as well as a pattern of states interpretable as nonexotic hybrids.[93] The pattern of these multiplets of states, as well as their relative separation in energy, suggest a phenomenology of constituent quarks coupled with effective gluonic degrees of freedom. In particular, the pattern of these exotic and nonexotic hybrid states appears to be consistent with a bag-model description and inconsistent with a flux-tube model.[93]

Recently, this lattice program has been extended into the baryon spectrum, revealing for the first time, the excited-state single-particle spectrum of nucleons, deltas, lambdas, sigmas, xis, and omegas along with their total spin up to $J = 7/2$ in both positive and negative parity.[14,88,94] The results for the nucleon and delta channels at the lightest pion-mass ensemble are shown in Fig. 22. There was found a high multiplicity of levels spanning across J^P, which is consistent with $\mathrm{SU}(6) \otimes$

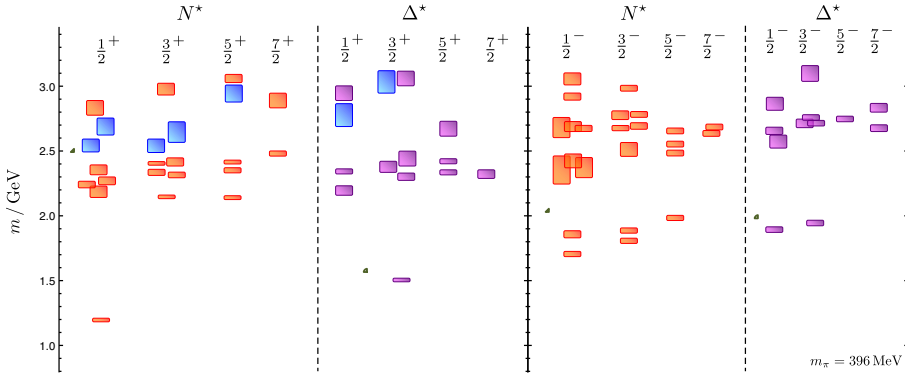

Fig. 22. (Color online) Results from Refs. 14 and 88 showing the spin-identified spectrum of nucleons and deltas from the lattices at $m_\pi = 396$ MeV. The spectrum of states within the rectangles are identifiable as admixtures of $\mathrm{SU}(6) \otimes O(3)$ representations and a counting of levels, along with the spectral overlaps of interpolating fields onto the states, that is consistent with the nonrelativistic qqq constituent quark model. In addition, there are additional states of hybrid character, shown in blue, that have relatively large overlap onto operators which sample gluonic excitations. The pattern of these positive-parity "hybrid" baryons is compatible with a color-octet gluonic excitation having $J^P = 1^+$.

$O(3)$ multiplet counting, and hence with that of the nonrelativistic qqq constituent quark model. In particular, the counting of levels in the low-lying negative-parity sectors are consistent with the nonrelativistic quark model and with the observed experimental states.[4] The spectrum observed in the first-excited positive-parity sector is also consistent in counting with the quark model, but the comparison with experiment is less clear, with the quark model predicting more states than are observed experimentally, spurring phenomenological investigations to explain the discrepancies (e.g., see Refs. 4 and 95–100).

It was found that there is significant mixing among each of the allowed multiplets, including the 20-plet that is present in the nonrelativistic qqq quark model but does not appear in quark–diquark models[97] (see in particular Ref. 101). These results lend credence to the assertion that there is no "freezing" of degrees of freedom with respect to those of the nonrelativistic quark model. These qualitative features of the calculated spectrum extend across all three of the quark–mass ensembles studied. Furthermore, no evidence was found for the emergence of parity-doubling in the spectrum.[102]

In addition, it was found that there are states, above the first positive parity band of states, which have large overlap onto interpolating fields which transform like chromomagnetic fields (color octet, $J^{\mathrm{PC}} = 1^{+-}$). The form of the operators suggest that within a hybrid baryon the three quarks are arranged in a color octet with the chromomagnetic gluonic excitation making the state an overall color singlet. The low-lying hybrid states overlap strongly onto the "nonrelativistic" subset of the hybrid interpolators, those constructed using only upper components of Dirac spinors. We can interpret this as suggesting that the quarks within the lightest hybrid baryons are dominantly in S-waves. In light of this it seems unlikely that the Roper is dominantly of hybrid character as has been speculated in the past.

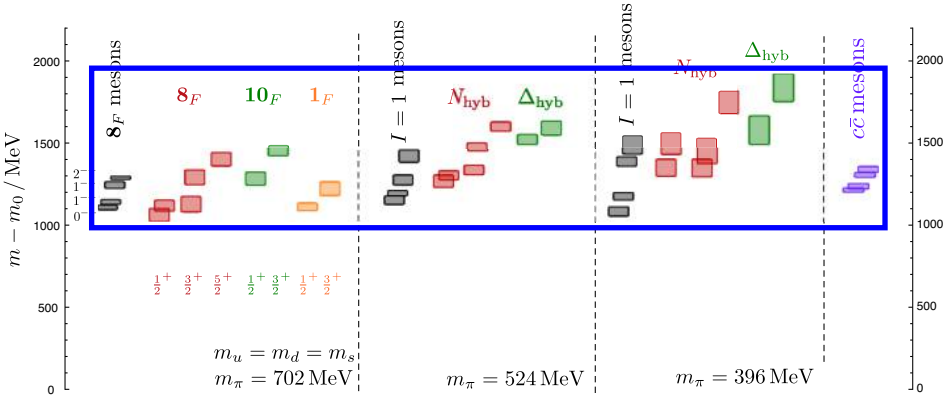

Fig. 23. (Color online) Results from Refs. 14, 88 and 89 showing the spectrum of hybrid mesons and baryons for three light quark masses. Mass scale is $m - m_\rho$ for light quark mesons, $m - m_{J/\Psi}$, and $m - m_N$ for baryons to approximately subtract the effect of differing numbers of quarks.

In Fig. 23, we present the spectrum of light and charm quark mesons and light quark baryons identified as "hybrid" in origin. To isolate the energy scale associated with the chromomagnetic gluonic excitation, the energies splittings from a constituent quark mass scale are shown. The structure of the operators that interpolate the hybrid states from the vacuum, along with the observation that the energy scale of gluonic excitations appears to be common for mesons and baryons, provides evidence that the gluonic excitation sector in QCD may turn out to be relatively simple. We suggest that a chromomagnetic excitation ($J^{\rm PC} = 1^{+-}$) is lightest with an energy scale in the region of 1.3 GeV.

It was argued that the extracted N and Δ spectrum can be interpreted in terms of single-hadron states, and based on investigations in the meson sector[91] and initial investigations of the baryon sector at a larger volume,[88] little evidence was found for multi-hadron states. To study multi-particle states, and hence the resonant nature of excited states, operator constructions with a larger number of fermion fields are needed. Such constructions are in progress,[103,104] and it is believed that the addition of these operators will lead to a denser spectrum of states. With suitable understanding of the discrete energy spectrum of the system, the Lüscher formalism[105] and its inelastic extensions (for example, see Ref. 106) can be used to extract the energy dependent phase shift for a resonant system, such as has been performed for the $I = 1\rho$ system.[107] The energy of the resonant state is determined from the energy dependence of the phase shift. It is this resonant energy that is suitable for chiral extrapolations. Suitably large lattice volumes and smaller pion masses are needed to adequately control the systematic uncertainties in these calculations.

3.3. *Electromagnetic transition form-factors*

The measurement of the excited-to-ground state radiative transition form-factors in the baryon sector provides a probe into the internal structure of hadrons. Analytically, these transition form-factors can be expressed in terms of matrix elements between states $\langle N(p_f)|V_\mu(q)|N^*(p_i)\rangle$ where V_μ is a vector (or possibly axial-vector) current with some four-momentum $q = p_f - p_i$ between the final (p_f) and initial (p_i) states. This matrix element can be related to the usual form-factors $F_1^*(q^2)$ and $F_2^*(q^2)$. However, the exact meaning as to the initial state $|N^*\rangle$ is the source of some ambiguity since in general it is a resonance. In particular, how is the EM decay disentangled from that of some $N\pi$ hadronic contribution?

Finite-volume LQCD calculations are formulated in Euclidean space, and as such, one does not directly observe the imaginary part of the pole of a resonant state. However, the information is encoded in the volume and energy dependence of excited levels in the spectrum. Lüscher's formalism[105] and its many generalizations show how to relate the infinite-volume energy-dependent phase shifts in resonant scattering to the energy dependence of levels determined in a continuous but finite-volume box in Euclidean space. In addition, infinite-volume matrix elements can

be related to those in finite-volume[108] up to a factor which can be determined from the derivative of the phase shift.

For the determination of transition form-factors, what all this means in practice is that one must determine the excited-state transition matrix element from each excited level in the resonant region of a state, down to the ground state. The excited levels and the ground state might each have some nonzero momentum, arising in some Q^2 dependence. In finite volume, the transition form-factors are both Q^2 and energy dependent, the latter coming from the discrete energies of the states within the resonant region. The infinite-volume form-factors are related to these finite-volume form-factors via the derivative of the phase shift as well as another kinematic function. Sitting close to the resonant energy, in the large volume limit the form-factors become independent of the energy as expected.

The determination of transition form-factors for highly excited states was first done in the charmonium sector with quenched QCD.[109,110] Crucial to these calculations was the use of a large basis of nonlocal operators to form the optimal projection onto each excited level. In a quenched theory, the excited charmonium states are stable and have no hadronic decays, thus there is no correction factor.

The determination of the EM transitions in light-quark baryons will eventually require the determination of the transition matrix elements from multiple excited levels in the resonance regime, the latter determined through the spectrum calculations in the previous section. However, as a first step, the Q^2 dependence of transition form-factors between the ground and first-excited state can be investigated within a limited basis. These first calculations of the $F_{1,2}^{pR}(Q^2)$ excited transition levels, in Refs. 111 and 34 already have shown many interesting features.

The first calculations of the $P_{11} \to \gamma N$ transition form-factors were performed a few years ago using the quenched approximation.[111] Since then, these calculations have been extended to full QCD with two light quarks and one strange quark ($N_f = 2 + 1$) using the same anisotropic lattice ensembles as for the spectrum calculations. Preliminary results[34] of the Q^2 dependence of the first-excited nucleon

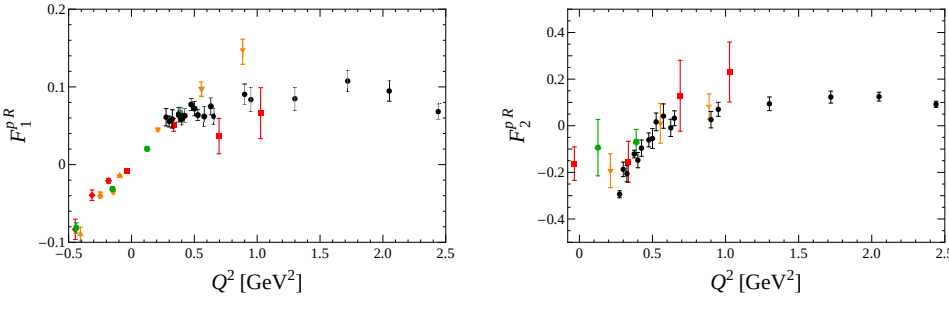

(a) (b)

Fig. 24. Proton-Roper transition form-factor $F_1^{pR}(Q^2)$ (a) and $F_2^{pR}(Q^2)$ (b) on the $N_f = 2 + 1$ anisotropic lattices with $M_\pi \approx 390$, 450, 875 MeV whose volumes are 3, 2.5, 2.5 fm, respectively.

(the Roper) to the ground-state proton, $F_{1,2}^{pR}$, are shown in Fig. 24. These results focus on the low Q^2 region. At the unphysical pion masses used, some points are in the time-like region. What is significant in these calculations with full-QCD lattice ensembles is that the sign of F_2 at low Q^2 has flipped compared to the quenched result, which had relatively mild Q^2 dependence at similar pion masses. These results suggest that at low Q^2 the pion-cloud dynamics are significant in full QCD.

The results so far are very encouraging, and the prospects are quite good for extending these calculations. The use of the larger operator basis employed in the spectrum calculations, supplemented with multi-particle operators, and including the correction factors from the resonant structure contained in phase shifts, should allow for the determination of multiple excited-level transition form-factors up to about $Q^2 \approx 3$ GeV^2.

3.4. *Form-factors at* $Q^2 \approx 6$ GeV^2

The traditional steps in a lattice form-factor calculation involve choosing suitable creation and annihilation operators with the quantum numbers of interest, and typically where the quark fields are spatially smeared so as to optimize overlap with the state of interest, often the ground state. These smearing parameters are typically chosen to optimize the overlap of a hadron at rest or at low momentum. As the momentum is increased, the overlap of the boosted operator with the desired state in flight becomes small and statistically noisy. One method to achieve high Q^2 is to decrease the quark smearing, which has the effect of increasing overlap onto many excited states. By choosing a suitably large basis of smearing, one can

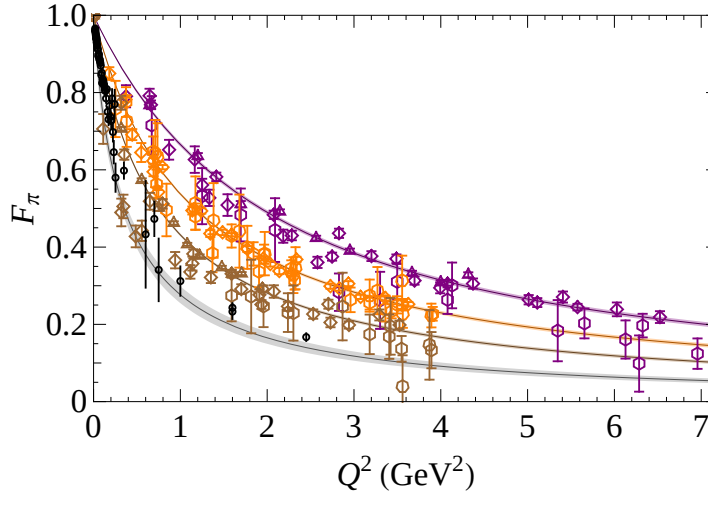

Fig. 25. Pion form-factor utilizing an extended basis of smearing functions to increase the range of Q^2 with multiple pion masses at 580, 875, 1350 MeV. The experimental points are shown as (black) circles while the lowest gray band is the extrapolation to the physical pion mass using lattice points from Ref. 112.

then project onto the desired excited state at high(er) momentum. This technique can extend the range of Q^2 in form-factor calculations until lattice discretization effects become dominant. An earlier version of this technique (with smaller basis) was used for a quenched calculation of the Roper transition form-factor reaching about 6 GeV^2.[111,113] Figure 25 shows an example from $N_f = 2 + 1$ at 580, 875, 1350 MeV pion masses using extended basis to extract pion form-factors with Q^2 reaching nearly 7 GeV^2 (Ref. 112) for the highest-mass ensemble. The extrapolated form-factor at the physical pion mass shows reasonable agreement with JLab precision measurements. Future attempts will focus on decreasing the pion masses and exploring Q^2-dependence of pion form-factors for yet higher Q^2.

As before, these form-factor calculations need to be extended to use a larger operator basis of single and multi-particle operators to overlap with the levels within the resonant region of the excited state, say the Roper. These operator constructions are suitable for projecting onto excited states with high momentum, as demonstrated in Ref. 103. Future work will apply these techniques to form-factor calculations.

3.5. *Form-factors at high $Q^2 \gg 10$ GeV^2*

At very high Q^2, lattice discretization effects can become quite large. A costly method to control these effects is to go to much smaller lattice spacing, basically $a \sim 1/Q$. An alternative method that was been devised long ago is to use renormalization-group techniques,[114] and in particular, step-scaling techniques introduced by the ALPHA collaboration. The step-scaling method was initially applied to compute the QCD running coupling and quark masses. The technique was later extended to handle heavy-quark masses with a relativistic action.[115,116] The physical insight is that the heavy-quark mass dependence of ratios of observables is expected to be milder than the observable itself. For form-factors, the role of the large heavy-quark mass scale is now played by the large momentum scale Q. Basically, the idea is to construct ratios of observables (form-factors) such that the overall Q^2 dependence is mild, and that suitable products of these ratios, evaluated at different lattice sizes and spacings, can be extrapolated to equivalent results at large volume and fine lattice spacing. The desired form-factor is extracted from the ratios.

The technique, only briefly sketched here, is being used now in a USQCD LQCD proposal by Renner[117] to compute the pion form-factor at large Q^2, and the technique is briefly discussed in Ref. 112. In principle, the same technique can be used to compute excited-state transition form factors, and although feasibility has yet to be established, it seems worth further investigation.

3.6. *Outlook*

There has been considerable recent progress in the determination of the highly excited spectrum of QCD using lattice techniques. While at unphysically large pion

masses and small lattice volumes, already some qualitative pictures of the spectrum of mesons and baryons is obtained. With the inclusion of multi-hadron operators, the outlook is quite promising for the determination of the excited spectrum of QCD. Anisotropic lattice configurations with several volumes are available now for pion masses down 230 MeV. Thus, it seems quite feasible to discern the resonant structure for at least a few low-lying states of mesons and baryons, of course within some systematic uncertainties, in the two-year timeframe. One of the more open questions is how to properly handle multi-channel decays which becomes more prevalent for higher-lying states. Some theoretical work has already been done using coupled-channel methods, but more work is needed and welcomed.

With the spectrum in hand, it is fairly straightforward to determine EM transition form-factors for the lowest few levels of N^*, and up to some moderate Q^2 of a few GeV^2, in the two year time-frame. Baryon form-factors will probably continue to drop purely disconnected terms from the current insertion. Meson transition form-factors, namely an exotic to nonexotic meson will be the first target in the short time-frame (less than two years), with the aim to determine photo-couplings. It might well be possible that with the new baryon operator techniques developed, the transition form factors can be extracted to $Q^2 \approx 6\ \mathrm{GeV}^2$. Going to an isotropic lattice with a small lattice spacing, it seems feasible to reach higher Q^2, say $10\ \mathrm{GeV}^2$, and this could be available in less than five years. To reach $Q^2 \gg 10\ \mathrm{GeV}^2$ will probably require step-scaling techniques. The high-Q^2 limit is of considerable interest since it allows for direct comparisons with perturbative methods.

4. Illuminating the Matter of Light-Quark Hadrons

4.1. *Heart of the problem*

QCD is the strong-interaction part of the Standard Model of Particle Physics. Solving this theory presents a fundamental problem that is unique in the history of science. Never before have we been confronted by a theory whose elementary excitations are not those degrees of freedom readily accessible through experiment; i.e., whose elementary excitations are *confined*. Moreover, there are numerous reasons to believe that QCD generates forces which are so strong that less than 2% of a nucleon's mass can be attributed to the so-called current-quark masses that appear in QCD's Lagrangian; viz., forces capable of generating mass *from nothing* (see Sec. 4.3). This is the phenomenon known as DCSB. Elucidating the observable predictions that follow from QCD is basic to drawing the map that explains how the Universe is constructed.

The need to determine the essential nature of light-quark confinement and DCSB, and to understand nucleon structure and spectroscopy in terms of QCD's elementary degrees of freedom, are two of the basic motivations for an upgraded JLab facility. In addressing these questions, one is confronted with the challenge of elucidating the role of quarks and gluons in hadrons and nuclei. Neither confinement nor DCSB is apparent in QCD's Lagrangian and yet they play the dominant

role in determining the observable characteristics of real-world QCD. The physics of hadronic matter is ruled by *emergent phenomena*, such as these, which can only be elucidated and understood through the use of nonperturbative methods in quantum field theory. This is both the greatest novelty and the greatest challenge within the standard model. Essentially new ways and means must be found in order to explain precisely via mathematics the observable content of QCD.

Bridging the gap between QCD and the observed properties of hadrons is a key problem in modern science. The international effort focused on the physics of excited nucleons is at the heart of this program. It addresses the questions: Which hadron states and resonances are produced by QCD, and how are they constituted? The N^* program therefore stands alongside the search for hybrid and exotic mesons and baryons as an integral part of the search for an understanding of the strongly interacting piece of the standard model.

4.2. *Confinement*

Regarding confinement, little is known and much is misapprehended. It is therefore important to state clearly that the static potential measured in numerical simulations of quenched LQCD is not related in any known way to the question of light-quark confinement. It is a basic feature of QCD that light-quark creation and annihilation effects are fundamentally nonperturbative; and hence it is impossible in principle to compute a potential between two light quarks.[118,119] Thus, in discussing the physics of light-quarks, linearly rising potentials, flux-tube models, etc., have no connection with nor justification via QCD.

A perspective on confinement drawn in quantum field theory was laid out in Ref. 121 and exemplified in Sec. 2 of Ref. 37. It draws upon a long list of sources; e.g., Refs. 122–125, and, expressed simply, relates confinement to the analytic properties of QCD's Schwinger functions, which are often called Euclidean-space Green functions or propagators and vertices. For example, one reads from the reconstruction theorem[126,127] that the only Schwinger functions which can be associated with expectation values in the Hilbert space of observables; namely, the set of measurable expectation values, are those that satisfy the axiom of reflection positivity. This is an extremely tight constraint whose full implications have not yet been elucidated.

There is a deep mathematical background to this perspective. However, for a two-point function; i.e., a propagator, it means that a detectable particle is associated with the propagator only if there exists a nonnegative spectral density in terms of which the propagator can be expressed. No function with an inflexion point can be written in this way. This is readily illustrated and Fig. 26 serves that purpose. The simple pole of an observable particle produces a propagator that is a monotonically-decreasing convex function, whereas the evolution depicted in Fig. 26(b) is manifest in the propagator as the appearance of an inflexion point at $P^2 > 0$. To complete the illustration, consider $\Delta(k^2)$, which is the single scalar function that describes the dressing of a Landau-gauge gluon propagator. Three

possibilities are exposed in Fig. 26(c). The inflexion point possessed by $M(p^2)$, visible in Fig. 8, entails, too, that the dressed quark is confined.

With the view that confinement is related to the analytic properties of QCD's Schwinger functions, the question of light-quark confinement may be translated into the challenge of charting the IR behavior of QCD's universal β-function. (The behavior of the β-function on the perturbative domain is well known.) This is a well-posed problem whose solution is a primary goal of hadron physics; e.g., Refs. 128–130. It is the β-function that is responsible for the behavior evident in Figs. 26 and 8, and thereby the scale-dependence of the structure and interactions of dressed gluons and quarks. One of the more interesting of contemporary questions is whether it is possible to reconstruct the β-function, or at least constrain it tightly, given empirical information on the gluon and quark mass functions.

Experiment-theory feedback within the N^*-programme shows promise for providing the latter.[5,13,15] This is illustrated through Fig. 27, which depicts the running-gluon-mass, analogous to $M(p)$ in Fig. 8, and the running-coupling determined by analyzing a range of properties of light-quark ground-state, radially-excited and exotic scalar-, vector- and flavored-pseudoscalar-mesons in the rainbow-ladder truncation, which is leading order in a symmetry-preserving DSE truncation scheme.[131] Consonant with modern DSE- and LQCD results,[120] these functions

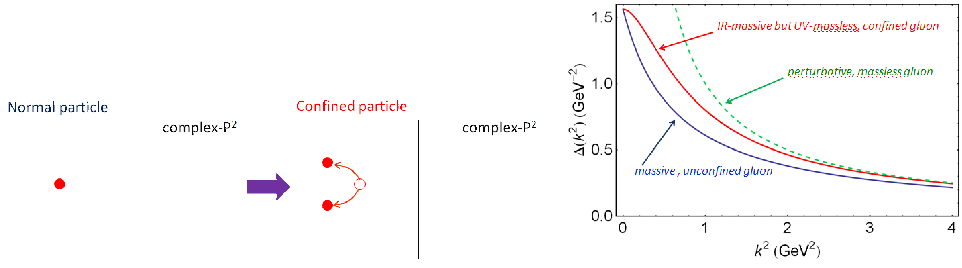

Fig. 26. (Color online) (a) An observable particle is associated with a pole at timelike-P^2, which becomes a branch point if, e.g., the particle is dressed by photons. (b) When the dressing interaction is confining, the real-axis mass-pole splits, moving into pairs of complex conjugate singularities. No mass-shell can be associated with a particle whose propagator exhibits such singularity structure. The imaginary part of the smallest magnitude singularity is a mass-scale, μ_σ, whose inverse, $d_\sigma = 1/\mu_\sigma$ is a measure of the dressed parton's fragmentation length. (c) $\Delta(k^2)$, the function that describes dressing of a Landau-gauge gluon propagator, plotted for three distinct cases. A bare gluon is described by $\Delta(k^2) = 1/k^2$ (the dashed line), which is convex on $k^2 \in (0, \infty)$. Such a propagator has a representation in terms of a non-negative spectral density. In some theories, interactions generate a mass in the transverse part of the gauge-boson propagator, so that $\Delta(k^2) = 1/(k^2 + m_g^2)$, which can also be represented in terms of a non-negative spectral density. In QCD, however, self-interactions generate a momentum-dependent mass for the gluon, which is large at infrared (IR) momenta but vanishes in the ultraviolet (UV).[120] This is illustrated by the curve labeled "IR-massive but UV-massless." With the generation of a mass-*function*, $\Delta(k^2)$ exhibits an inflexion point and hence cannot be expressed in terms of a non-negative spectral density.[37]

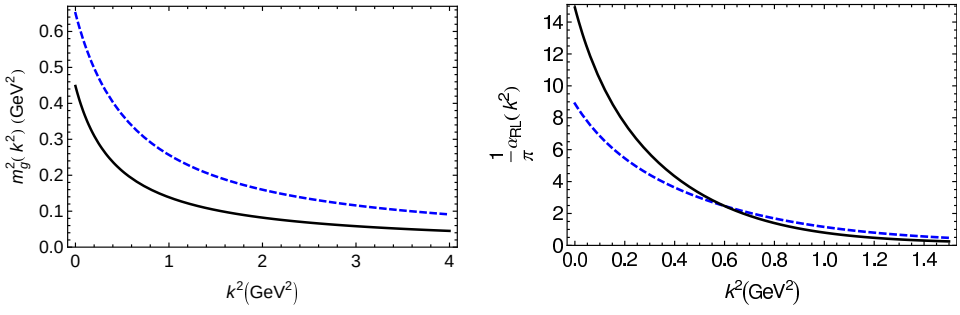

(a) (b)

Fig. 27. (Color online) (a) Rainbow-ladder gluon running-mass; and (b) rainbow-ladder effective running-coupling, both determined in a DSE analysis of properties of light-quark mesons. The dashed curves illustrate forms for these quantities that provide the more realistic picture.[128,142] (Figures drawn from Ref. 128.)

derive from a gluon propagator that is a bounded, regular function of space-like momenta, which achieves its maximum value on this domain at $k^2 = 0$,[130,132,133] and a dressed quark–gluon vertex that does not possess any structure which can qualitatively alter this behavior.[134,135] In fact, the dressed gluon mass drawn here produces a gluon propagator much like the curve labeled "IR-massive but UV-massless" in Fig. 26(c).

Notably, the value of $M_g = m_g(0) \sim 0.7$ GeV is typical[132,133]; and the IR value of the coupling, $\alpha_{\rm RL}(M_g^2)/\pi = 2.2$, is interesting because a context is readily provided. With nonperturbatively-massless gauge bosons, the coupling below which DCSB breaking is impossible via the gap equations in QED and QCD is $\alpha_c/\pi \approx 1/3$.[136–138] In a symmetry-preserving regularization of a vector × vector contact-interaction used in rainbow-ladder truncation, $\alpha_c/\pi \approx 0.4$; and a description of hadron phenomena requires $\alpha/\pi \approx 1$.[139] With nonperturbatively massive gluons and quarks, whose masses and couplings run, the IR strength required to describe hadron phenomena in rainbow-ladder truncation is unsurprisingly a little larger. Moreover, whilst a direct comparison between $\alpha_{\rm RL}$ and a coupling, $\alpha_{\rm QLat}$, inferred from quenched-lattice results is not sensible, it is nonetheless curious that $\alpha_{\rm QLat}(0) \lesssim \alpha_{\rm RL}(0)$.[130] It is thus noteworthy that with a more sophisticated, nonperturbative DSE truncation,[140,141] some of the IR strength in the gap equation's kernel is shifted from the gluon propagator into the dressed quark–gluon vertex. This cannot materially affect the net IR strength required to explain observables but does reduce the amount attributed to the effective coupling (see, e.g., Ref. 141, wherein $\alpha(M_g^2) = 0.23\pi$ explains important features of the meson spectrum).

4.3. *Dynamical chiral symmetry breaking*

Whilst the nature of confinement is still debated, Fig. 8 shows that DCSB is a fact. This figure displays the current-quark of perturbative QCD evolving into a

constituent-quark as its momentum becomes smaller. Indeed, QCD's dressed quark behaves as a constituent-like-quark or a current-quark, or something in between, depending on the momentum with which its structure is probed.

DCSB is the most important mass generating mechanism for visible matter in the Universe. This may be illustrated through a consideration of the nucleon. The nucleon's σ-term is a Poincaré- and renormalization-group-invariant measure of the contribution to the nucleon's mass from the fermion mass term in QCD's Lagrangian:[143]

$$\sigma_N \stackrel{K^2=0}{=} \frac{1}{2}(m_u + m_d)\langle N(P+K)|J(K)|N(P)\rangle \approx 0.06\ m_N\,, \tag{3}$$

where $J(K)$ is the dressed scalar vertex derived from the source $[\bar{u}(x)u(x) + \bar{d}(x)d(x)]$ and m_N is the nucleon's mass. Some have imagined that the nonvalence s-quarks produce a non-negligible contribution but it is straightforward to estimate[119,144]

$$\sigma_N^s = 0.02 - 0.04\ m_N\,. \tag{4}$$

Based on the strength of DCSB for heavier quarks,[143] one can argue that they do not contribute a measurable σ-term. It is thus plain that more than 90% of the nucleon's mass finds its origin in something other than the quarks' current-masses.

The source is the physics which produces DCSB. As we have already mentioned, Fig. 8 shows that even in the chiral limit, when $\sigma_N \equiv 0 \equiv \sigma_N^s$, the massless quark–parton of pQCD appears as a massive dressed quark to a low-momentum probe, carrying a mass-scale of approximately $(1/3)m_N$. A similar effect is experienced by the gluon–partons: they are perturbatively massless but are dressed via self-interactions, so that they carry an IR mass-scale of roughly $(2/3)m_N$, see Fig. 27. In such circumstances, even the simplest symmetry-preserving Poincaré-covariant computation of the nucleon's mass will produce $m_N^0 \approx 3\ M_Q^0$, where $M_Q^0 \approx 0.35\,\mathrm{GeV}$ is a mass-scale associated with the IR behavior of the chiral-limit dressed quark mass-function. The details of real-world QCD fix the strength of the running coupling at all momentum scales. That strength can, however, be varied in models; and this is how we know that if the interaction strength is reduced, the nucleon mass tracks directly the reduction in M_Q^0 (see Fig. 28 and Sec. 4.4). Thus, the nucleon's mass is a visible measure of the strength of DCSB in QCD. These observations are a contemporary statement of the notions first expressed in Ref. 145.

It is worth noting, in addition that DCSB is an amplifier of explicit chiral symmetry breaking. This is why the result in Eq. (3) is ten times larger than the ratio $\hat{m}/m_N$, where $\hat{m}$ is the renormalization-group-invariant current-mass of the nucleon's valence-quarks. The result in Eq. (4) is not anomalous: the nucleon contains no valence strangeness. Following this reason, one can view DCSB as being responsible for roughly 98% of the proton's mass, so that the Higgs mechanism is (almost) irrelevant to light-quark physics.

The behavior illustrated in Figs. 26 and 27 has a marked influence on hadron elastic form-factors. This is established, e.g., via comparisons between Refs. 147–151

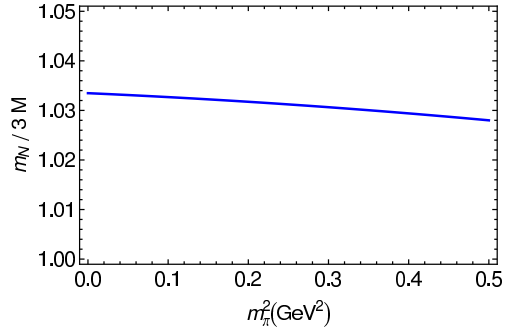

Fig. 28. (Color online) Evolution with current-quark mass of the ratio $m_N/[3M]$, which varies by less than 1% on the domain depicted. The calculation is described in Ref. 146. The current-quark mass is expressed through the computed value of m_π^2: $m_\pi^2 = 0.49$ GeV^2 marks the s-quark current-mass.

and Refs. 139, 152 and 153. Owing to the greater sensitivity of excited states to the long-range part of the interaction in QCD,[128,142,154] we expect this influence to be even larger in the Q^2-dependence of nucleon-to-resonance electrocouplings, the extraction of which, via meson electroproduction off protons, is an important part of the current CLAS program and studies planned with the CLAS12 detector.[5,6,15,16,18,24] In combination with well-constrained QCD-based theory, such data can potentially, therefore, be used to chart the evolution of the mass function on $0.3 \lesssim p \lesssim 1.2$, which is a domain that bridges the gap between nonperturbative and pQCD. This can plausibly assist in unfolding the relationship between confinement and DCSB.

In closing this subsection, we re-emphasize that the appearance of running masses for gluons and quarks is a quantum field theoretical effect, unrealizable in quantum mechanics. It entails, moreover, that: quarks are not Dirac particles; and the coupling between quarks and gluons involves structures that cannot be computed in perturbation theory. Recent progress with the two-body problem in quantum field theory[140] has enabled these facts to be established.[155] One may now plausibly argue that the theory is in a position to produce the first reliable symmetry-preserving, Poincaré-invariant prediction of the light-quark hadron spectrum.[141]

4.4. *Mesons and baryons: Unified treatment*

Owing to the importance of DCSB, it is only within a symmetry-preserving, Poincaré-invariant framework that full capitalization on the results of the N^*-program is possible. One must be able to correlate the properties of meson and baryon ground- and excited-states within a single, symmetry-preserving framework, where symmetry-preserving includes the consequence that all relevant Ward–Takahashi identities are satisfied. This is not to say that constituent-quark-like models are worthless. As will be seen in this article, they are of continuing value

because there is nothing better that is yet providing a bigger picture. Nevertheless, such models have no connection with quantum field theory and therefore not with QCD; and they are not "symmetry-preserving" and hence cannot veraciously connect meson and baryon properties.

An alternative is being pursued within quantum field theory via the Faddeev equation. This analogue of the Bethe–Salpeter equation sums all possible interactions that can occur between three dressed quarks. A tractable equation[157] is founded on the observation that an interaction which describes color-singlet mesons also generates nonpointlike quark–quark (diquark) correlations in the color-antitriplet channel.[158] The dominant correlations for ground state octet and decuplet baryons are scalar (0^+) and axial-vector (1^+) diquarks because, e.g., the associated mass-scales are smaller than the baryons' masses and their parity matches that of these baryons. On the other hand, pseudoscalar (0^-) and vector (1^-) diquarks dominate in the parity-partners of those ground states.[38,146] This approach treats mesons and baryons on the same footing and, in particular, enables the impact of DCSB to be expressed in the prediction of baryon properties.

Incorporating lessons learnt from meson studies,[159] a unified spectrum of u, d, s-quark hadrons was obtained using symmetry-preserving regularization of a vector × vector contact interaction.[38,146] These studies simultaneously correlate the masses of meson and baryon ground- and excited-states within a single framework; and in comparison with relevant quantities, they produce $\overline{\text{rms}} \lesssim 15\%$, where $\overline{\text{rms}}$ is the root-mean-square-relative-error/degrees-of-freedom. As indicated by Fig. 29,

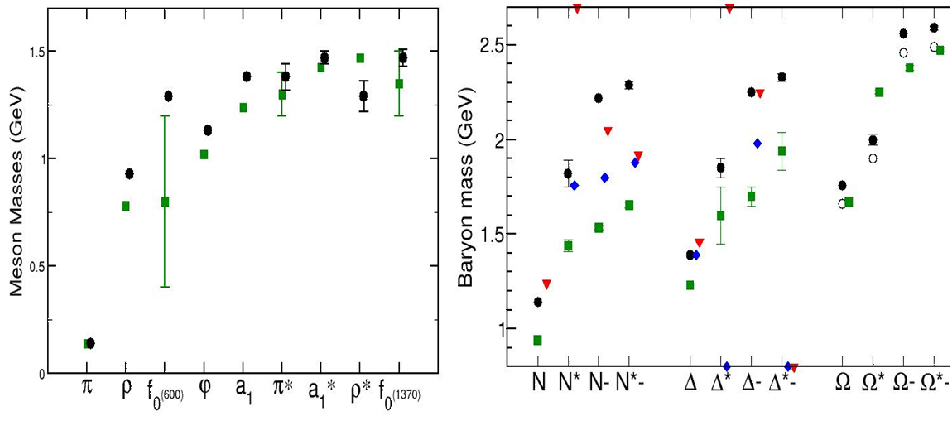

Fig. 29. (Color online) Comparison between DSE-computed hadron masses (filled circles) and bare baryon masses from the EBAC,[68] (filled diamonds) and Jülich,[156] (filled triangles); and experiment,[4] (filled-squares). For the coupled-channels models a symbol at the lower extremity indicates that no associated state is found in the analysis, whilst a symbol at the upper extremity indicates that the analysis reports a dynamically-generated resonance with no corresponding bare-baryon state. In connection with Ω-baryons, the (open-circles) represent a shift downward in the computed results by 100 MeV. This is an estimate of the effect produced by pseudoscalar-meson loop corrections in Δ-like systems at a s-quark current-mass.

Table 2. Bare masses (GeV) determined in an Argonne-Osaka coupled-channels analysis of single- and double-pion electroproduction reactions compared with DSE results for the mass of each baryon's dressed quark core. The notation is as follows: P_{11} corresponds to the $N(1440)$; S_{11} to the $N(1535)$ and the second state in this partial wave; P_{33} to the Δ and the next state in this partial wave; and D_{33} to the parity partner of the Δ. The rms $-$ |rel. error| $= 9.4 \pm 5.7\%$.

	P_{11}	S_{11}	S_{11}	P_{33}	P_{33}	D_{33}
ANL-Osaka	1.83	2.04	2.61	1.28	2.16	2.17
DSE	1.83	2.30	2.35	1.39	1.84	2.33
|Rel. Err.|	0	11.3%	11.1%	7.9%	17.4%	8.6%

they uniformly overestimate the Particle Data Group[4] (PDG) values of meson and baryon masses. Given that the truncation employed omits deliberately the effects of a meson–cloud in the Faddeev kernel, this is a good outcome, since inclusion of such contributions acts to reduce the computed masses.

Following this line of reasoning, a striking result is agreement between the DSE-computed baryon masses[146] and the bare masses employed in modern coupled-channels models of pion-nucleon reactions,[68,156] see Fig. 29. The Roper resonance is very interesting. The DSE studies[38,146] produce a radial excitation of the nucleon at 1.82 ± 0.07 GeV. This state is predominantly a radial excitation of the quark–diquark system, with the diquark correlations in their ground state. Its predicted mass lies precisely at the value determined in the analysis of Ref. 68. This is significant because for almost 50 years the Roper resonance has defied understanding.

Discovered in 1963/64,[160] the Roper appears to be an exact copy of the proton except that its mass is 50% greater. The mass was the problem: hitherto it could not be explained by any symmetry-preserving QCD-based tool. That has now changed. Combined, see Fig. 19, Refs. 38, 68 and 146 demonstrate that the Roper resonance is indeed the proton's first radial excitation, and that its mass is far lighter than normal for such an excitation because the Roper obscures its dressed quark-core with a dense cloud of pions and other mesons. Such feedback between QCD-based theory and reaction models is critical now and for the foreseeable future, especially since analyses of CLAS data on nucleon-resonance electrocouplings suggest strongly that this structure is typical; i.e., most low-lying N^*-states can best be understood as an internal quark-core dressed additionally by a meson cloud.[20] This is highlighted further by a comparison between the DSE results and the bare masses obtained in the most complete Argonne-Osaka coupled-channels analysis to date, see Table 2.[b]

Additional analysis within the framework of Refs. 38 and 146 suggests a fascinating new possibility for the Roper, which is evident in Table 3. The nucleon

[b]With the closing of EBAC at JLab in March 2012, a collaboration between scientists at Argonne National Laboratory and the University of Osaka has accepted the coupled-channels challenge posed by extant and forthcoming CLAS data on the electromagnetic transitions between ground and excited nucleon states.

ground state is dominated by the scalar diquark, with a significantly smaller but nevertheless important axial-vector diquark component. This feature persists in solutions obtained with more sophisticated Faddeev equation kernels (see, e.g., Table 2 in Ref. 149). From the perspective of the nucleon's parity partner and its radial excitation, the scalar diquark component of the ground-state nucleon actually appears to be unnaturally large. Expanding the study to include baryons containing one or more s-quarks, the picture is confirmed: the ground state N, Λ, Σ, Ξ are all characterized by $\sim 80\%$ scalar diquark content,[38] whereas their parity partners have a 50–50 mix of $J = 0, 1$ diquarks.

One can nevertheless understand the structure of the octet ground-states. As with so much else in hadron physics, the composition of these flavor octet states is intimately connected with DCSB. In a two-color version of QCD, scalar diquarks are Goldstone modes.[161,162] (This is a long-known result of Pauli–Gürsey symmetry.) A "memory" of this persists in the three-color theory, for example: in low masses of scalar diquark correlations; and in large values of their canonically normalized Bethe–Salpeter amplitudes and hence strong quark + quark − diquark coupling within the octet ground-states. (A qualitatively identical effect explains the large value of the πN coupling constant and its analogues involving other pseudoscalar-mesons and octet-baryons.) There is no commensurate enhancement mechanism associated with the axial-vector diquark correlations. Therefore the scalar diquark correlations dominate within octet ground-states.

Within the Faddeev equation treatment, the effect on the first radial excitations is dramatic: orthogonality of the ground- and excited-states forces the radial excitations to be constituted almost entirely from axial-vector diquark correlations. It is critical to check whether this outcome survives with Faddeev equation kernels built from a momentum-dependent interaction.

This brings us to another, very significant observation; namely, the match between the DSE-computed level ordering and that of experiment, something which has historically been difficult for models to obtain (see, e.g., the discussion in Ref. 99) and is not achieved in contemporary numerical simulations of lattice-regularized QCD (see, e.g., Ref. 88). In particular, the DSE calculations produce a parity-partner for each ground-state that is always more massive than its first radial excitation so that, in the nucleon channel, e.g., the first $J^P = \frac{1}{2}^-$ state lies above the second $J^P = \frac{1}{2}^+$ state.

A veracious expression of DCSB in the meson spectrum is critical to this success. One might ask why and how? It is DCSB that both ensures the dressed quark-cores of pseudoscalar and vector mesons are far lighter than those of their parity partners and produces strong quark + antiquark − meson couplings, which are expressed in large values for the canonically normalized Bethe–Salpeter amplitudes (Table 3 in Ref. 38). The remnants of Pauli–Gürsey symmetry described previously entail that these features are carried into the diquark sector: as evident in Fig. 3 and Table 5 of Ref. 38 and their comparison with Fig. 2 and Table 3 therein. The inflated masses

Table 3. Diquark content of the baryons' dressed quark cores, computed with a symmetry-preserving regularization of a vector × vector contact interaction.[163]

	N	N(1440)	N(1535)	N(1650)	Δ(1232)	Δ(1600)	Δ(1700)	Δ(1940)
0^+	77%							
1^+	23%	100%			100%	100%		
0^-			51%	43%				
1^-			49%	57%			100%	100%

but, more importantly, the suppressed values of the Bethe–Salpeter amplitudes for negative-parity diquarks, in comparison with those of positive-parity diquarks, guarantee the computed level ordering: attraction in a given channel diminishes with the square of the Bethe–Salpeter amplitude (see Appendix C in Ref. 38). Hence, an approach within which DCSB cannot be realized or a simulation whose parameters are such that the importance of DCSB is suppressed will both necessarily have difficulty reproducing the experimental ordering of levels.

The computation of spectra is an important and necessary prerequisite to the calculation of nucleon transition form-factors, the importance of which is difficult to overestimate given the potential of such form-factors to assist in charting the long-range behavior of QCD's running coupling. To place this in context, Refs. 139, 146, 152 and 153 explored the sensitivity of a range of hadron properties to the running of the dressed quark mass-function. These studies established conclusively that static properties are not a sensitive probe of the behavior in Figs. 8 and 27; viz., regularized via a symmetry-preserving procedure, a vector × vector contact-interaction predicts masses, magnetic and quadrupole moments, and radii that are practically indistinguishable from results obtained with the most sophisticated QCD-based interactions currently available.[128,164]

4.5. *Nucleon to resonance transition form-factors*

The story is completely different, however, with the momentum-dependence of form-factors; e.g., in the case of the pion, the difference between the form-factor obtained with $M(p) =$ constant and that derived from $M(p^2)$ in Fig. 8 is dramatically apparent for $Q^2 > M^2(p = 0)$.[152] The study of diquark form-factors in Ref. 139 has enabled another reference computation to be undertaken; namely, nucleon elastic and nucleon-to-Roper transition form-factors.[71] It shows that axial-vector-diquark dominance of the Roper, Table 3, has a material impact on the nucleon-to-Roper transition form-factor.

We choose to illustrate the analysis of Ref. 71 via Fig. 30. The figure displays results obtained using a LF constituent-quark model,[27] which employed a constituent-quark mass of 0.22 GeV and identical momentum-space harmonic oscillator wave functions for both the nucleon and Roper (width = 0.38 GeV) but with a zero introduced for the Roper, whose location was fixed by an orthogonality condition. The quark mass is smaller than that which is typical of DCSB in QCD but a more

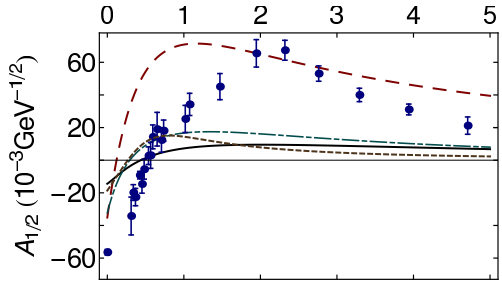

(a)

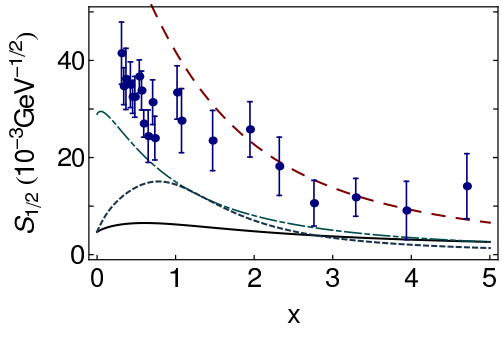

(b)

Fig. 30. (Color online) Helicity amplitudes for the $\gamma^* p \to P_{11}(1440)$ transition, with $x = Q^2/m_N^2$: $A_{1/2}$ (a); and $S_{1/2}$ (b). Solid curves: DSE computation of Ref. 71, obtained using a contact interaction but amended here via an estimate of the impact of the dressed quark mass in Fig. 8, which softens the $x > 1$ behavior without affecting $x < 1$; dashed curves: the LF constituent quark model results from Ref. 27; long-dash-dot curves: the LF constituent quark model results from Ref. 165; short-dashed curves: a smooth fit to the bare form-factors inferred in Refs. 23, 65 and 166; and data; Refs. 19, 26 and 20.

significant difference is the choice of spin-flavor wave functions for the nucleon and Roper. In Ref. 27 they are simple SU(6) × $O(3)$ S-wave states in the three-quark center-of-mass system, in contrast to the markedly different spin-flavor structure produced by Faddeev equation analyses of these states.

Owing to this, in Fig. 30 we also display the LF quark model results from Ref. 165. It is stated therein that large effects accrue from "configuration mixing;" i.e., the inclusion of SU(6)-breaking terms and high-momentum components in the wave functions of the nucleon and Roper. In particular, that configuration mixing yields a marked suppression of the calculated helicity amplitudes in comparison with both relativistic and nonrelativistic results based on a simple harmonic oscillator *ansatz* for the baryon wave functions, as used in Ref. 27.

There is also another difference; namely, Ref. 165 employs Dirac and Pauli form-factors to describe the interaction between a photon and a constituent-quark.[167] As apparent in Fig. 2 of Ref. 165, they also have a noticeable impact, providing roughly

half the suppression on $0.5 \lesssim Q^2/\ \mathrm{GeV}^2 \lesssim 1.5$. The same figure also highlights the impact on the form-factors of high-momentum tails in the nucleon and Roper wave functions.

In reflecting upon constituent-quark form-factors, we note that the interaction between a photon and a dressed quark in QCD is not simply that of a Dirac fermion.[155,168–173] Moreover, the interaction of a dressed quark with the photon in Ref. 71 is also modulated by form-factors, see Appendices A3 and C6 therein. On the other hand, the purely phenomenological form-factors in Refs. 165 and 167 are inconsistent with a number of constraints that apply to the dressed quark-photon vertex in quantum field theory; e.g., the dressed quark's Dirac form-factor should approach unity with increasing Q^2 and neither its Dirac nor Pauli form-factors may possess a zero. Notwithstanding these observations, the results from Ref. 165 are more similar to the DSE curves than those in Ref. 27.

In an interesting new development, the study of Ref. 27 has been updated.[174] The new version models the impact of a running dressed quark mass within the LF formulation of quantum mechanics and yields results that are also closer to those produced by the DSE analysis.

Helicity amplitudes can also be computed using the Argonne-Osaka collaboration's DCC framework.[62] In this approach, one imagines that a Hamiltonian is defined in terms of bare baryon states and bare meson–baryon couplings; the physical amplitudes are computed by solving coupled-channels equations derived therefrom; and the parameters characterizing the bare states are determined by requiring a good fit to data. In connection with the $\gamma^* p \to P_{11}(1440)$ transition, results are available for both helicity amplitudes.[23,65,166] The associated bare form-factors are reproduced in Fig. 30: for $Q^2 < 1.5\ \mathrm{GeV}^2$ we depict a smooth interpolation; and for larger Q^2 an extrapolation based on pQCD power laws ($A_{\frac{1}{2}} \sim 1/Q^3 \sim S_{\frac{1}{2}}$).

The bare form-factors are evidently similar to the results obtained in Refs. 71 and 165: both in magnitude and Q^2-evolution. Regarding the transverse amplitude, Ref. 23 argues that the bare component plays an important role in changing the sign of the real part of the complete amplitude in the vicinity of $Q^2 = 0$. In this case, the similarity between the bare form-factor and the DSE results is perhaps most remarkable — e.g., the appearance of the zero in $A_{\frac{1}{2}}$, and the $Q^2 = 0$ magnitude of the amplitude (in units of $10^{-3}\ \mathrm{GeV}^{-1/2}$)

$$\begin{array}{cccccc} & \text{Ref. 27} & \text{Ref. 165} & \text{Refs. 23, 65, 166} & \text{Ref. 71} \\ A_{\frac{1}{2}}(0) & -35.1 & -32.3 & -18.6 & -16.3 \end{array} . \tag{5}$$

These similarities strengthen support for an interpretation of the bare-masses, -couplings, etc., inferred via coupled-channels analyses, as those quantities comparable with hadron structure calculations that exclude the meson–baryon coupled-channel effects which are determined by multichannel unitarity conditions.

An additional remark is valuable here. The Argonne-Osaka collaboration computes electroproduction form-factors at the resonance pole in the complex plane

and hence they are complex-valued functions. Whilst this is consistent with the standard theory of scattering,[175] it differs markedly from phenomenological approaches that use a Breit–Wigner parametrization of resonant amplitudes in fitting data. As concerns the $\gamma^* p \to P_{11}(1440)$ transition, the real parts of the Argonne-Osaka collaboration's complete amplitudes are qualitatively similar to the results in Refs. 19, 20 and 26 but the Argonne-Osaka collaboration's amplitudes also have sizeable imaginary parts. This complicates a direct comparison between theory and extant data.

4.6. *Prospects*

A compelling goal of the international theory effort that works in concert with the N^*-program is to understand how the interactions between dressed quarks and -gluons create nucleon ground- and excited-states, and how these interactions emerge from QCD. This compilation shows no single approach is yet able to provide a unified description of all N^* phenomena; and that intelligent reaction theory will long be necessary as a bridge between experiment and QCD-based theory. Nonetheless, material progress has been made since the release of the White Paper on "Theory Support for the Excited Baryon Program at the JLab 12-GeV Upgrade",[16] in developing strategies, methods and approaches to the physics of nucleon resonances. Some of that achieved via the Dyson–Schwinger equations is indicated above. Additional contributions relevant to the N^* program are: verification of the accuracy of the diquark truncation of the quark–quark scattering matrix within the Faddeev equation[151]; and a computation of the $\Delta \to \pi N$ transition form-factor.[176]

A continued international effort is necessary if the goal of turning experiment into a probe of the dressed quark mass function and related quantities is to be achieved. In our view, precision data on nucleon-resonance transition form-factors provides a realistic means by which to constrain empirically the momentum evolution of the dressed quark mass function and therefrom the IR behavior of QCD's β-function; in particular, to locate unambiguously the transition boundary between the constituent- and current-quark domains that is signalled by the sharp drop apparent in Fig. 8. That drop can be related to an inflexion point in QCD's β-function. Contemporary theory indicates that this transition boundary lies at $p^2 \sim 0.6\ \mathrm{GeV}^2$. Since a probe's input momentum Q is principally shared equally amongst the dressed quarks in a transition process, then each can be considered as absorbing a momentum fraction $Q/3$. Thus in order to cover the domain $p^2 \in [0.5, 1.0]\ \mathrm{GeV}^2$ one requires $Q^2 \in [5, 10]\ \mathrm{GeV}^2$; i.e., the upgraded JLab facility.

In concrete terms, a DSE study of the $N \to N(1535)$ transition is underway, using the contact-interaction, for comparison with data[9,19] and other computations[177]; and an analysis of the $N \to \Delta$ transition has begun, with the aim of revealing the origin of the unexpectedly rapid Q^2-evolution of the magnetic form-factor in this process.

At the same time, the Faddeev equation framework of Ref. 149, is being applied to the $N \to N(1440)$ transition. The strong momentum dependence of the dressed

quark mass function is an integral part of this framework. Therefore, in this study it will be possible, e.g., to vary artificially the position of the marked drop in the dressed quark mass function and thereby identify experimental signatures for its presence and location. In addition, it will provide a crucial check on the results in Table 3. It is notable that DCSB produces an anomalous EM moment for the dressed quark. This is known to produce a significant modification of the proton's Pauli form-factor at $Q^2 \lesssim 2$ GeV^2.[178] It is also likely to be important for a reliable description of F_2^* in the nucleon-to-Roper transition.

The Faddeev equation framework of Ref. 149 involves parametrizations of the dressed quark propagators that are not directly determined via the gap equation. An important complement would be to employ the *ab initio* rainbow-ladder truncation approach of Refs. 150 and 151 in the computation of properties of excited-state baryons, especially the Roper resonance. Even a result for the Roper's mass and its Faddeev amplitude would be useful, given the results in Table 3. In order to achieve this, however, technical difficulties must be faced and overcome. Here there is incipient progress, made possible through the use of generalized spectral representations of propagators and vertices.

In parallel with the program outlined herein, an effort is beginning with the aim of providing the reaction theory necessary to make reliable contact between experiment and predictions based on the dressed quark core. While rudimentary estimates can and will be made of the contribution from pseudoscalar meson loops to the dressed quark core of the nucleon and its excited states, a detailed comparison with experiment will only follow when the DSE-based results are used to constrain the input for DCC calculations.

5. Light-Cone Sum Rules: A Bridge between Electrocouplings and Distribution Amplitides of Nucleon Resonances

We expect that at photon virtualities from 5 GeV^2 to 10 GeV^2 of CLAS12 the electroproduction cross-sections of nuclear resonances will become amenable to the QCD description in terms of quark partons, whereas the description in terms of meson–baryon degrees of freedom becomes much less suitable than at smaller momentum transfers. The major challenge for theory is that quantitative description of form-factors in this transition region must include nonperturbative contributions. In Ref. 177, we have suggested to use a combination of LCSRs and lattice calculations. To our opinion this approach presents a reasonable compromise between theoretical rigour and the necessity to make phenomenologically relevant predictions.

5.1. *Light-front wave functions and distribution amplitudes*

The quantum-mechanical picture of a nucleon as a superposition of states with different number of partons assumes the infinite momentum frame or light-cone quantization. Although *a priori* there is no reason to expect that the states with, say, 100 partons (quarks and gluons) are suppressed as compared those with the

three valence quarks, the phenomenological success of the quark model allows one to hope that only a first few Fock components are really necessary. In hard exclusive reactions which involve a large momentum transfer to the nucleon, the dominance of valence states is widely expected and can be proven, at least within QCD perturbation theory.[179,180]

The most general parametrization of the three-quark sector involves six scalar LF wave functions[181,182] which correspond to different possibilities to couple the quark helicities λ_i and orbital angular momentum L_z to produce the helicity-1/2 nucleon state: $\lambda_1 + \lambda_2 + \lambda_3 + L_z = 1/2$. In particular, if the quark helicities λ_i sum up to 1/2, then zero angular momentum is allowed, $L = 0$. The corresponding contribution can be written as[179–181]:

$$|N(p)^{\uparrow}\rangle^{L=0} = \frac{\epsilon^{abc}}{\sqrt{6}} \int \frac{[dx][d^2\mathbf{k}]}{\sqrt{x_1 x_2 x_3}} \Psi_N(x_i, \mathbf{k}_i) |u_a^{\uparrow}(x_1, \mathbf{k}_1)\rangle \times [|u_b^{\downarrow}(x_2, \mathbf{k}_2)\rangle |d_c^{\uparrow}(x_3, \mathbf{k}_3)\rangle - |d_b^{\downarrow}(x_2, \mathbf{k}_2)\rangle |u_c^{\uparrow}(x_3, \mathbf{k}_3)\rangle] \,. \quad (6)$$

Here $\Psi_N(x_i, \mathbf{k}_i)$ is the LF wave function that depends on the momentum fractions x_i and transverse momenta $\mathbf{k}_i$ of the quarks, $|u_a^{\uparrow}(x_i, \mathbf{k}_i)\rangle$ is a quark state with the indicated momenta and color index a, and ϵ^{abc} is the fully antisymmetric tensor; arrows indicate helicities. The integration measure is defined as:

$$\int [dx] = \int_0^1 dx_1 dx_2 dx_3 \, \delta\left(\sum x_i - 1\right) ,$$
$$\int [d^2\mathbf{k}] = (16\pi^3)^{-2} \int d\mathbf{k}_1 d\mathbf{k}_2 d\mathbf{k}_3 \delta\left(\sum \mathbf{k}_i\right) . \quad (7)$$

In hard processes the contribution of $\Psi(x_i, \mathbf{k}_i)$ is dominant whereas the other existing three-quark wave functions give rise to a power-suppressed correction, i.e., a correction of higher twist.

The LF description of a nucleon is very attractive for model building. The calculation of LF wave functions from QCD can in principle be done using LF Hamiltonian methods. A first approximation to the QCD LF equation of motion and corresponding model solutions for the LF wave functions of mesons and baryons has recently been obtained using LF holography. This is discussed in Sec. 7. In particular, there are subtle issues with renormalization and gauge dependence. An alternative approach has been to describe nucleon structure in terms of DA corresponding to matrix elements of nonlocal gauge-invariant light-ray operators. The classification of DAs goes in twist rather than number of constituents as for the wave functions. For example, the leading-twist-three nucleon (proton) DA is defined by the matrix element[183]:

$$\langle 0|\epsilon^{ijk}(u_i^{\uparrow}(a_1 n) C \not{n} u_j^{\downarrow}(a_2 n)) \not{n} d_k^{\uparrow}(a_3 n)|N(p)\rangle = -\frac{1}{2} f_N \, p\cdot n \not{n} u_N^{\uparrow}(p) \int [dx] e^{-ip\cdot n \sum x_i a_i} \varphi_N(x_i) \,, \quad (8)$$

where $q^{\uparrow(\downarrow)} = (1/2)(1 \pm \gamma_5)q$ are quark fields of given helicity, p_μ, $p^2 = m_N^2$, is the proton momentum, $u_N(p)$ the usual Dirac spinor in relativistic normalization, n_μ an auxiliary light-like vector $n^2 = 0$ and C the charge-conjugation matrix. The Wilson lines that ensure gauge invariance are inserted between the quarks; they are not shown for brevity. The normalization constant f_N is defined in such a way that

$$\int [dx] \varphi_N(x_i) = 1\,. \tag{9}$$

In principle, the complete set of nucleon DAs carries full information on the nucleon structure, same as the complete basis of LF wave functions. In practice, however, both expansions have to be truncated and usefulness of a truncated version, taking into account either a first few Fock states or a few lowest twists, depends on the physics application.

Using the wave function in Eq. (6) to calculate the matrix element in Eq. (8) it is easy to show that the DA $\varphi_N(x_i)$ is related to the integral of the wave function $\Psi_N(x_i, \mathbf{k}_i)$ over transverse momenta, which corresponds to the limit of zero transverse separation between the quarks in the position space[179]:

$$f_N(\mu)\varphi_N(x_i, \mu) \sim \int_{|\mathbf{k}|<\mu} [d^2\mathbf{k}] \Psi_N(x_i, \mathbf{k}_i)\,. \tag{10}$$

Thus, the normalization constant f_N can be interpreted as the nucleon wave function at the origin (in position space).

Higher-twist three-quark DAs are related, in a loose sense, with similar integrals of the wave functions including extra powers of the transverse momentum, and with contributions of the other existing wave functions which correspond to nonzero quark orbital angular momentum.

As always in a field theory, extraction of the asymptotic behavior produces divergences that have to be regulated. As a result, the DAs become scheme- and scale-dependent. In the calculation of physical observables, this dependence is cancelled by the corresponding dependence of the coefficient functions. The DA $\varphi_N(x_i, \mu)$ can be expanded in the set of orthogonal polynomials $\mathcal{P}_{nk}(x_i)$ defined as eigenfunctions of the corresponding one-loop evolution equation:

$$\varphi_N(x_i, \mu) = 120 x_1 x_2 x_3 \sum_{n=0}^{\infty} \sum_{k=0}^{N} c_{nk}^N(\mu) \mathcal{P}_{nk}(x_i)\,, \tag{11}$$

where

$$\int [dx]\, x_1 x_2 x_3 \mathcal{P}_{nk}(x_i) \mathcal{P}_{n'k'} = \mathcal{N}_{nk} \delta_{nn'} \delta_{kk'} \tag{12}$$

and

$$c_{nk}^N(\mu) = c_{nk}^N(\mu_0) \left(\frac{\alpha_s(\mu)}{\alpha_s(\mu_0)} \right)^{\gamma_{nk}/\beta_0} . \tag{13}$$

Here $\mathcal{N}_{nk}$ are convention-dependent normalization factors, $\beta_0 = 11 - \frac{2}{3} n_f$ and γ_{nk} the corresponding anomalous dimensions. The double sum in Eq. (11) goes over all

existing orthogonal polynomials $\mathcal{P}_{nk}(x_i)$, $k = 0, \ldots, n$, of degree n. Explicit expressions for the polynomials $\mathcal{P}_{nk}(x_i)$ for $n = 0, 1, 2$ and the corresponding anomalous dimensions can be found in Ref. 184.

In what follows, we will refer to the coefficients $c_{nk}(\mu_0)$ as shape parameters. The set of these coefficients together with the normalization constant $f_N(\mu_0)$ at a reference scale μ_0 specifies the momentum fraction distribution of valence quarks on the nucleon. They are nonperturbative quantities that can be related to matrix elements of local gauge-invariant three-quark operators (see below).

In the last twenty years, there had been mounting evidence that the simple-minded picture of a proton with the three valence quarks in an S-wave is insufficient, so that for example the proton spin is definitely not constructed from the quark spins alone. If the orbital angular momenta of quarks and gluons are nonzero, the nucleon is intrinsically deformed. The general classification of three-quark LF wave functions with nonvanishing angular momentum has been worked out in Refs. 181 and 182. In particular, the wave functions with $L_z = \pm 1$ play a decisive role in hard processes involving a helicity flip, e.g., the Pauli EM form-factor $F_2(Q^2)$ of the proton.[185] These wave functions are related, in the limit of small transverse separation, to the twist-four nucleon DAs introduced in Ref. 183:

$$
\begin{aligned}
&\langle 0|\epsilon^{ijk}(u_i^{\uparrow}(a_1 n) C \not{n} u_j^{\downarrow}(a_2 n))\, \not{p} d_k^{\uparrow}(a_3 n)|N(p)\rangle \\
&\qquad = -\frac{1}{4} p\cdot n \not{p} u_{N^*}^{\uparrow}(p) \int [dx] e^{-ip\cdot n \sum x_i a_i} \big[f_N \Phi_4^{N,\mathrm{WW}}(x_i) + \lambda_1^N \Phi_4^N(x_i)\big], \\
&\langle 0|\epsilon^{ijk}\big(u_i^{\uparrow}(a_1 n) C \not{n} \gamma_\perp \not{p} u_j^{\downarrow}(a_2 n)\big)\gamma^\perp \not{n} d_k^{\uparrow}(a_3 n)|N(p)\rangle \\
&\qquad = -\frac{1}{2} p\cdot n \not{n} m_N u_N^{\uparrow}(p) \int [dx] e^{-ip\cdot n \sum x_i a_i} \big[f_N \Psi_4^{N,\mathrm{WW}}(x_i) - \lambda_1^N \Psi_4^N(x_i)\big], \\
&\langle 0|\epsilon^{ijk}\big(u_i^{\uparrow}(a_1 n) C \not{p} \not{n} u_j^{\uparrow}(a_2 n)\big) \not{n} d_k^{\uparrow}(a_3 n)|N(p)\rangle \\
&\qquad = \frac{\lambda_2^N}{12} p\cdot n \not{n}\, m_N u_N^{\uparrow}(p) \int [dx] e^{-ip\cdot n \sum x_i a_i} \Xi_4^N(x_i)\,,
\end{aligned}
\tag{14}
$$

where $\Phi_4^{N,\mathrm{WW}}(x_i)$ and $\Psi_4^{N,\mathrm{WW}}(x_i)$ are the so-called Wandzura–Wilczek contributions, which can be expressed in terms of the leading-twist DA $\varphi_N(x_i)$.[184] The two new constants λ_1^N and λ_2^N are defined in such a way that the integrals of the "genuine" twist-four DAs Φ_4, Ψ_4, Ξ_4 are normalized to unity, similar to Eq. (9). They are related to certain normalization integrals of the LF wave functions for the three-quark states with $L_z = \pm 1$, see Ref. 185 for details.

LF wave functions and DAs of all baryons, including the nucleon resonances, can be constructed in a similar manner, taking into account spin and flavor symmetries. They can be constructed for all baryons of arbitrary spin without any conceptual complications, although it will become messy. The problem is only that "construct" means basically that one can enumerate different independent components and find their symmetries. To calculate them nonperturbatively is becoming increasingly

difficult, however. This extension is especially simple for the parity doublets of the usual $J^P = \frac{1}{2}^+$ octet since the nonlocal operators entering the definitions of nucleon DAs do not have a definite parity. Thus the same operators couple also to $N^*(1535)$ and one can define the corresponding leading-twist DA by the same expression as for the nucleon:

$$\langle 0|\epsilon^{ijk}(u_i^{\uparrow}(a_1 n)C\not{n}u_j^{\downarrow}(a_2 n))\not{n}d_k^{\uparrow}(a_3 n)|N^*(p)\rangle$$
$$= \frac{1}{2} f_{N^*} p\cdot n \not{n} u_{N^*}^{\uparrow}(p) \int [dx] e^{-ip\cdot n \sum x_i a_i} \varphi_{N^*}(x_i)\,, \tag{15}$$

where, of course, $p^2 = m_{N^*}^2$. The constant f_{N^*} has a physical meaning of the wave function of $N^*(1535)$ at the origin. The DA $\phi_{N^*}(x_i)$ is normalized to unity (9) and has an expansion identical to (11):

$$\varphi_{N^*}(x_i,\mu) = 120 x_1 x_2 x_3 \sum_{n=0}^{\infty}\sum_{k=0}^{N} c_{nk}^{N^*}(\mu)\mathcal{P}_{nk}(x_i)\,, \tag{16}$$

albeit with different shape parameters $c_{nk}^{N^*}$.

Similar as for the nucleon, there exist three independent subleading twist-four distribution amplitudes for the $N^*(1535)$ resonance: $\Phi_4^{N^*}$, $\Psi_4^{N^*}$ and $\Xi_4^{N^*}$. Explicit expressions are given in Ref. 177.

5.2. *Moments of distribution amplitudes from lattice QCD*

The normalization constants f, λ_1, λ_2 and the shape parameters c_{nk} are related to matrix elements of local three-quark operators between vacuum and the baryon state of interest, and can be calculated using LQCD. Investigations of excited hadrons using this method are generally much more difficult compared to the ground states. On the other hand, the states of opposite parity can be separated rather reliably as propagating forwards and backwards in euclidian time. For this reason, for the time being we concentrate on the study of the ground state baryon octet $J^P = \frac{1}{2}^+$, and the lowest mass octet with negative parity, $J^P = \frac{1}{2}^-$, $N^*(1535)$ being the prime example.

Following the exploratory studies reported in Refs. 177, 186 and 187, QCDSF Collaboration is investing significant effort to make such calculations fully quantitative. The calculation is rather involved and requires the following steps: (1) Find lattice (discretized) operators that transform according to irreducible representations of spinorial group $\overline{H(4)}$; (2) Calculate nonperturbative renormalization constants for these operators; (3) Compute matrix elements of these operators on the lattice from suitable correlation functions; and (4) Extrapolate $m_\pi \to m_\pi^{\rm phys}$, lattice volume $V \to \infty$ and lattice spacing $a \to 0$.

Irreducibly transforming $\overline{H(4)}$ multiplets for three-quark operators have been constructed in Ref. 188. Nonperturbative renormalization and one-loop scheme conversion factors RI-MOM$\to \overline{\rm MS}$ have been calculated in Ref. 189. A consistent perturbative renormalization scheme for the three-quarks operators in dimensional

regularization has been found[190] and the calculation of two-loop conversion factors using this scheme is in progress.

The matrix elements of interest are calculated from correlation functions of the form $\langle \mathcal{O}_{\alpha\beta\gamma}(x)\bar{\mathcal{N}}(y)_\tau \rangle$, where $\mathcal{N}$ is a smeared nucleon interpolator and $\mathcal{O}$ is a local three-quark operator with up to two derivatives, and applying the parity "projection" operator $(1/2)(1 \pm m\gamma_4/E)$.[191] In this way we get access to the normalization constants, the first and the second moments of the distribution amplitudes. Calculation of yet higher moments is considerably more difficult because one cannot avoid mixing with operators of lower dimension.

The correlation functions were evaluated using $N_f = 2$ dynamic Wilson (clover) fermions on several lattices and a range of pion masses $m_\pi \geq 180$ MeV. Our preliminary results for the wave functions the nucleon and $N^*(1535)$ at the origin are summarized in Fig. 31.[192] The extrapolation of the results for the nucleon to the physical pion mass and infinite volume as well as the analysis of the related systematic errors are in progress. An example of such an analysis is shown in Fig. 32.

This analysis will be done using one-loop chiral perturbation theory. The necessary expressions have been worked out in Ref. 194. Whereas the pion mass dependence of nucleon couplings is generally in agreement with expectations, we observe a large difference (up to a factor of three) in $N^*(1535)$ couplings calculated with heavy and light pions: All couplings drop significantly in the transition region

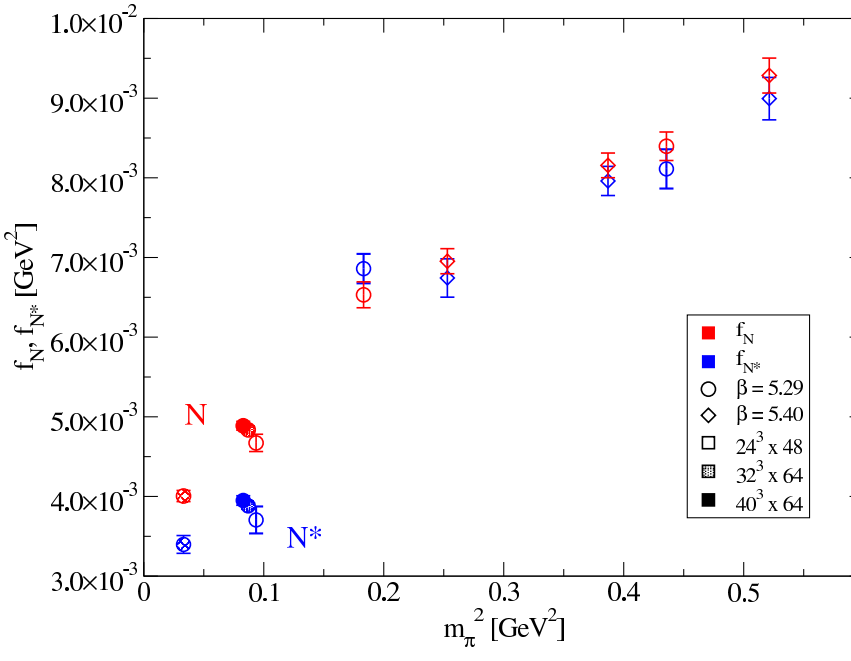

Fig. 31. (Color online) Probability amplitude f_N, f_{N^*} to find the three valence quarks in the nucleon and $N^*(1535)$ at the same space-time point (wave function at the origin).

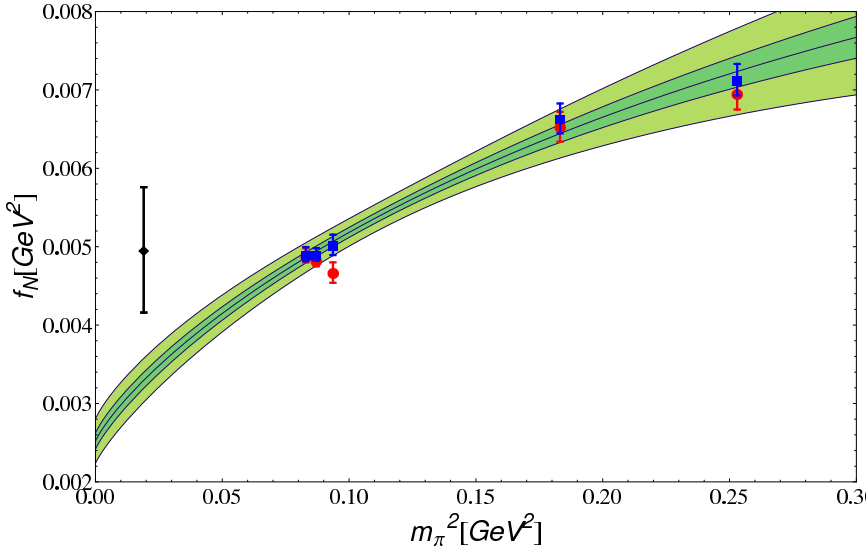

Fig. 32. (Color online) The chiral extrapolation of f_N to the physical (light) quark masses. The red points are lattice data and the blue points are corrected for finite volume effects. The green bands are the 1- and 2-σ errors, respectively. The left-most black "data point" at the physical mass shows the recently updated estimate from QCD sum rule calculations.[193]

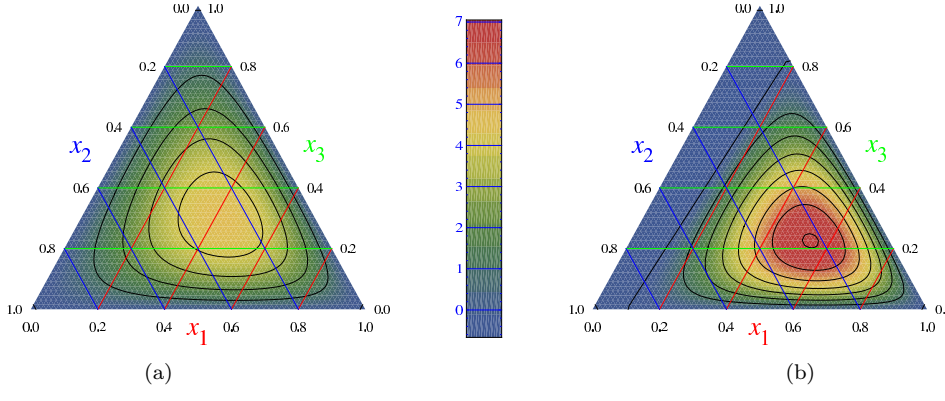

Fig. 33. (Color online) Leading-twist distribution amplitudes of the nucleon (a) and $N^*(1535)$ (b) in barycentric coordinates $x_1 + x_2 + x_3 = 1$.

where the decay $N^* \to N\pi$ opens up. This effect can be due to the change in the structure of the wave function, but also to contamination of our $N^*(1535)$ results by the contribution of the πN scattering state, or some other lattice artefact. This is one of the issues that have to be clarified in future.

We also find that the wave function of the $N^*(1535)$ resonance is much more asymmetric compared to the nucleon: nearly 50% of the total momentum is carried by the u-quark with the same helicity. This shape is illustrated in Fig. 33 where

the leading-twist distribution amplitudes of the nucleon (a) and $N^*(1535)$ (b) are shown in barycentric coordinates $x_1 + x_2 + x_3 = 1$; x_i are the momentum fractions carried by the three valence quarks.

Our plans for the coming 2–3 years are as follows. The final analysis of the QCDSF lattice data using two flavors of dynamic fermions is nearly completed and in future we will go over to $N_f = 2+1$ studies, i.e., include dynamic strange quarks. The generation of the corresponding gauge configurations is in progress and first results are expected in one year from now. We will continue the studies of the lowest mass states in the $J^P = 1/2^+$ and $J^P = 1/2^-$ baryon octets. In particular, the distribution amplitudes of the Λ and Σ baryons will be studied for the first time. At a later stage, we hope to be able to do similar calculations for the $J^P = 3/2^\pm$ decuplets. We are working on the calculation of two-loop conversion factors RI-MOM $\to \overline{\text{MS}}$ using the renormalization scheme suggested in Ref. 190 and plan to employ them in the future studies. Main attention will be payed to the analysis of various sources of systematic uncertainties. With the recent advances in the algorithms and computer hardware the quark mass and finite volume extrapolations of lattice data have become less of a problem, which allows us to concentrate on more subtle issues. Our latest simulations for small pion masses make possible, for the first time, to study the transition region where decays of resonances, e.g., $N^* \to N\pi$, become kinematically allowed. We have to understand the influence of finite resonance width on the calculation of operator matrix elements and to this end plan to consider ρ-meson distribution amplitudes as a simpler example. We will also make detailed studies of meson (pion) distribution amplutides in order to understand better the lattice discretization errors and work out a concrete procedure to minimize their effect. The full program is expected to last five years and is part of the research proposal for the Transregional Collaborative Research Center (SFB Transregio 55 Hadron physics with LQCD) funded by the German Research Council (DFG).

5.3. *Light-cone distribution amplitudes and form-factors*

The QCD approach to hard reactions is based on the concept of factorization: one tries to identify the short distance subprocess which is calculable in perturbation theory and take into account the contributions of large distances in terms of nonprerturbative parton distributions.

The problem is that in the case of the baryon form-factors the hard pQCD contribution is only the third term of the factorization expansion. Schematically, one can envisage the expansion of, say, the Dirac EM nucleon form-factor $F_1(Q^2)$ of the form

$$F_1(Q^2) \sim A(Q^2) + \left(\frac{\alpha_s(Q^2)}{\pi}\right) \frac{B(Q^2)}{Q^2} + \left(\frac{\alpha_s(Q^2)}{\pi}\right)^2 \frac{C}{Q^4} + \cdots , \qquad (17)$$

where C is a constant determined by the nucleon DAs, while $A(Q^2)$ and $B(Q^2)$ are form-factor-type functions generated by contributions of low virtualities, see

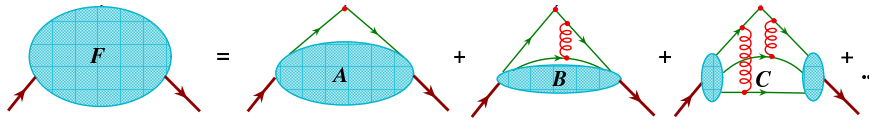

Fig. 34. (Color online) Structure of QCD factorization for baryon form-factors.

Fig. 34. The soft functions $A(Q^2)$ and $B(Q^2)$ are purely nonperturbative and cannot be further simplified e.g., factorized in terms of DAs. In the light-cone formalism, they are determined by overlap integrals of the soft parts of hadronic wave functions corresponding to large transverse separations. Various estimates suggest that $A(Q^2) \lesssim 1/Q^6$, $B(Q^2) \lesssim 1/Q^4$ and at very large Q^2 they are further suppressed by the Sudakov form-factor. To be precise, in higher orders in $\alpha_s(Q)$ there exist double-logarithmic contributions $\sim 1/Q^4$ (Ref. 195) that are not factorized in the standard manner; however, they are also suppressed by the Sudakov mechanism.[195,196] Thus, the third term in (17) is formally the leading one at large Q^2 to power accuracy.

The main problem of the pQCD approach[179,180] is a numerical suppression of each hard gluon exchange by the α_s/π factor which is a standard perturbation theory penalty for each extra loop. If, say, $\alpha_s/\pi \sim 0.1$, the pQCD contribution to baryon form-factors is suppressed by a factor of 100 compared to the purely soft term. As the result, the onset of the perturbative regime is postponed to very large momentum transfers since the factorizable pQCD contribution $O(1/Q^4)$ has to win over nonperturbative effects that are suppressed by extra powers of $1/Q^2$, but do not involve small coefficients. There is an (almost) overall consensus that "soft" contributions play the dominant role at present energies. Indeed, it is known for a long time that the use of QCD-motivated models for the wave functions allows one to obtain, without much effort, soft contributions comparable in size to experimentally observed values. Also models of GPDs usually are chosen such that the experimental data on form-factors are described by the soft contributions alone. A subtle point for these semi-phenomenological approaches is to avoid double counting of hard rescattering contributions "hidden" in the model-dependent hadron wave functions or GPD parametrizations.

One expects that the rapid development of LQCD will allow one to calculate several benchmark baryon form, factors to sufficient precision from first principles. Such calculations are necessary and interesting in its own right, but do not add to our understanding of how QCD actually "works" to transfer the large momentum along the nucleon constituents, the quarks and gluons. The main motivation to study "hard"processes has always been to understand hadron properties in terms of quark and gluon degrees of freedom; for example, the rationale for the continuing measurements of the total inclusive cross-section in deep inelastic scattering is to extract quark and gluon parton distributions. Similar, experimental measurements of the electroproduction of nucleon resonances at large momentum transfers should

eventually allow one to get insight in their structure on parton level, in particular momentum fraction distributions of the valence quarks and their orbital angular momentum encoded in DAs, and this task is obscured by the presence of large "soft" contributions which have to be subtracted.

Starting in Ref. 197 and in subsequent publications we have been developing an approach to hard exclusive processes with baryons based on LCSR.[198,199] This technique is attractive because in LCSRs "soft" contributions to the form-factors are calculated in terms of the same DAs that enter the pQCD calculation and there is no double counting. Thus, the LCSRs provide one with the most direct relation of the hadron form-factors and distribution amplitudes for realistic momentum transfers of the order of 2–10 GeV^2 that is available at present, with no other nonperturbative parameters. It is also sufficiently general and can be applied to many hard reactions.

The basic object of the LCSR approach is the correlation function

$$\int dx e^{iqx} \langle N^*(P)|T\{\eta(0)j(x)\}|0\rangle \tag{18}$$

in which j represents the EM (or weak) probe and η is a suitable operator with nucleon quantum numbers. The nucleon resonance in the final state is explicitly represented by its state vector $|N^*(P)\rangle$, see a schematic representation in Fig. 35. When both the momentum transfer $q^2 = -Q^2$ and the momentum $(P')^2 = (P+q)^2$ flowing in the η vertex are large and negative, the asymptotic of the correlation function is governed by the light-cone kinematics $x^2 \to 0$ and can be studied using the operator product expansion (OPE) $T\{\eta(0)j(x)\} \sim \sum C_i(x)\mathcal{O}_i(0)$ on the light-cone $x^2 = 0$. The x^2-singularity of a particular perturbatively calculable short-distance factor $C_i(x)$ is determined by the twist of the relevant composite operator $\mathcal{O}_i$, whose matrix element $\langle N^*|\mathcal{O}_i(0)|0\rangle$ is given by an appropriate moment of the N^* DA. Next, one can represent the answer in form of the dispersion integral in $(P')^2$ and define the nucleon contribution by the cutoff in the quark–antiquark invariant mass, the so-called interval of duality s_0 (or continuum threshold). The main role of the interval of duality is that it does not allow large momenta $|k^2| > s_0$ to flow through the η-vertex; to the lowest order $O(\alpha_s^0)$ one obtains a purely soft

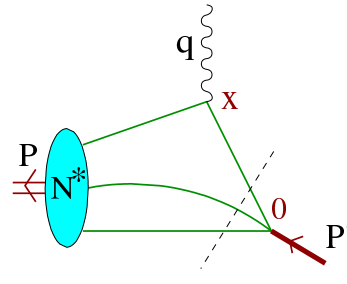

Fig. 35. (Color online) Schematic structure of the LCSR for electroproduction of nucleon resonances.

contribution to the form-factor as a sum of terms ordered by twist of the relevant operators and hence including both the leading- and the higher-twist nucleon DAs. Note that, in difference to the hard mechanism, the contribution of higher-twist DAs is only suppressed by powers of the interval of duality $s_0 \sim 2$ GeV^2 (or by powers of the Borel parameter if one applies some standard QCD sum rule machinery), but not by powers of Q^2. This feature is in agreement with the common wisdom that soft contributions are not constrained to small transverse separations.

We stress that LCSRs are not based on any nonperturbative model of the nucleon structure, but rather present a relation between the physical observables (form-factors) and baryon wave functions at small transverse separation (distribution amplitudes).

Historically, LCSRs were developed in Refs. 198 and 199 in an attempt to overcome difficulties of the Shifman–Vainstein–Zakharov QCD sum rule approach[202] for exclusive processes dominated by the light-cone kinematics. In the last 20 years, LCSRs have been applied extensively to the exclusive B-decays and remain to be the only nonperturbative technique that allows one to calculate the corresponding form-factors directly at large recoil. In fact the value of the CKM matrix element V_{ub} quoted by the Particle Data Group as the one extracted from exclusive semileptonic decay $B \to \pi \ell \nu_\ell$ is largely based on the recently updated LCSR calculations of the form-factor $f_+^{B\to\pi}(0)$[203,204] (although the LQCD calculations have become competitive). Another important application of LCSRs was for calculation of the EM pion form-factor. More references and further details can be found in the review articles.[205,206]

LCSRs for meson form-factors have achieved a certain degree of maturity. One lesson is that they are fully consistent with pQCD and factorization theorems. In particular, the LCSRs also contain terms generating the asymptotic pQCD contributions. In the pion case, it was explicitly demonstrated that the contribution of hard rescattering is correctly reproduced in the LCSR approach as a part of the $O(\alpha_s)$ correction. It should be noted that the diagrams of LCSR that contain the "hard" pQCD contributions also possess "soft" parts, i.e., one should perform a separation of "hard" and "soft" terms inside each diagram. As a result, the distinction between "hard" and "soft" contributions appears to be scale- and scheme-dependent. Most of the LCSRs for meson decays have been derived to the NLO accuracy in the strong coupling. The first NLO LCSR calculations were done in 1997–1998 and since then the NLO accuracy has become standard in this field. The size of NLO corrections depends on the form-factor in question but typically is of the order of 20%, for the momentum transfers of interest.

Derivation of LCSRs for exclusive reactions involving baryons is, conceptually, a straightforward generalization of the LCSRs for mesons. On the other hand, there are a few new technical issues that had to be resolved, and also the calculations become much more challenging. The development so far was mainly to explore the existing possibilities and identify potential applications. Following the first application to the EM and axial form-factors of the nucleon in Refs. 197 and 200, LCSRs

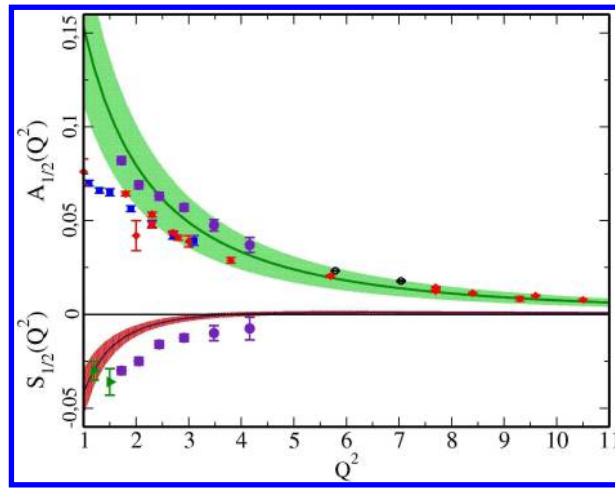

Fig. 36. (Color online) The LCSR calculation for the helicity amplitudes $A_{1/2}(Q^2)$ and $S_{1/2}(Q^2)$ for the electroproduction of the $N^*(1535)$ resonance using the lattice results for the lowest moments of the $N^*(1535)$ DAs. The curves are obtained using the central values of the lattice parameters, and the shaded areas show the corresponding uncertainty. Figure taken from Ref. 177.

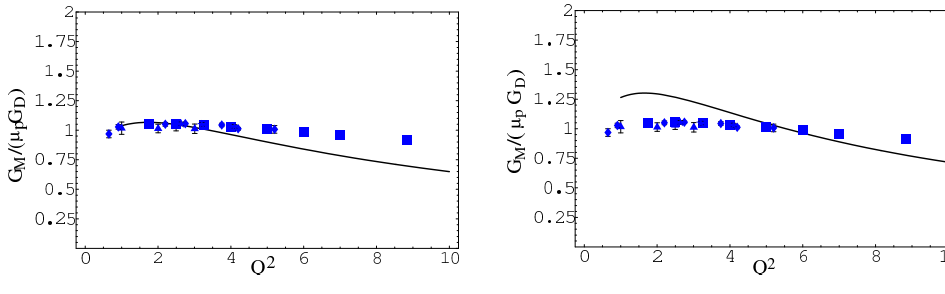

Fig. 37. (Color online) LCSR results for the magnetic proton form-factor (normalized to the dipole formula) for a realistic model of nucleon distribution amplitudes.[200] (a) Leading order (LO); (b) next-to-leading order (NLO) for twist-three contributions. Figure adapted from Ref. 201.

have been considered for the $\gamma^* N \to \Delta$ transition,[207] heavy baryon decays (see Ref. 208 and references therein) and various transitions between baryons in the octet and the decuplet (e.g., Ref. 209). In Ref. 177 we have suggested to use the same approach to the study of electroproduction of resonances at large momentum transfers and in particular $N^*(1535)$. Since the structure of sum rules for the nucleon elastic form-factors and electroproduction of $N^*(1535)$ is very similar, the difference in form-factors should expose directly the difference in the wave functions, which is of prime interest. The results for the helicity amplitudes $A_{1/2}(Q^2)$ and $S_{1/2}(Q^2)$ using the lattice results for the lowest moments of the $N^*(1535)$ DAs appear to be in a good agreement with the existing data, see Fig. 36.

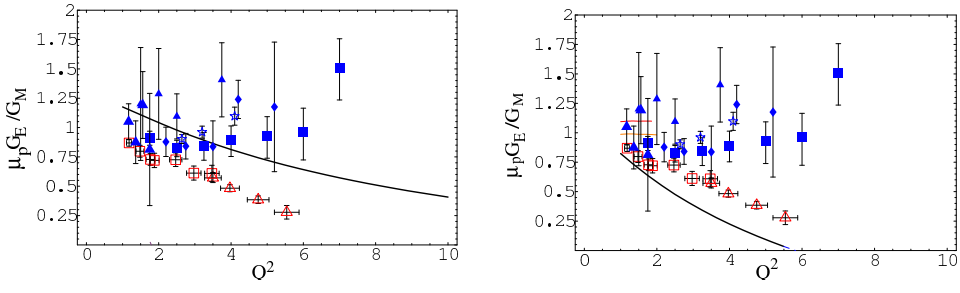

Fig. 38. (Color online) LCSR results for the electric to magnetic proton form-factor ratio for a realistic model of nucleon distribution amplitudes.[200] (a) LO; (b) NLO for twist-three contributions. Figure adapted from Ref. 201.

All existing LCSRs for baryons are written to the LO in the strong coupling which corresponds, roughly speaking, to the parton model level description of deep-inelastic scattering. Combined with realistic models of DAs the existing sum rules yield a reasonable description of the existing data to the expected 30–50% accuracy. In order to match the accuracy of the future experimental data and also of the next generation of lattice results, the LCSRs will have to be advanced to include NLO radiative corrections, as it has become standard for meson decays.

The first step towards LCSRs to the NLO accuracy was done in Ref. 201 where the $\mathcal{O}(\alpha_s)$ corrections are calculated for the (leading) twist-three contributions to the sum rules for EM (elastic) nucleon form-factors derived in Refs. 197 and 200. The results are shown in Figs. 37 and 38.

The NLO corrections are large and their effect *increases* with Q^2 which may be counterintuitive. This behavior is, however, expected on general grounds because the leading regions for large momentum transfers corresponding to the (Efremov–Radyushkin–Brodsky–Lepage ERBL) collinear factorization appear at the NNLO level only, i.e., $\mathcal{O}(\alpha_s^2)$. The corrections for the G_E/G_M ratio are larger than for the magnetic form-factor G_M itself, which is again expected since the electric form-factor suffers from cancellations between chirality-conserving and chirality-violating contributions.

Large NLO corrections can be compensated by the change in the nucleon DA, similar as it happens with parton distributions — e.g., the small-x behavior of the LO and NLO gluon distribution is very different — but such an analysis would so far be premature since NLO corrections have not been calculated so far for the contributions of twist-four DAs that take into account the effects of orbital angular momentum.

In addition, it is necesary to develop a technique for the resummation of "kinematic" corrections to the sum rules that are due to nonvanishing masses of the resonances. The corresponding corrections to the total cross-section of the deep-inelastic scattering are known as Wandzura–Wilczek corrections and can be

resummed to all orders in terms of the Nachtmann variable; we are looking for a generalization of this method to nonforward kinematics which is also important in a broader context.[210]

With these improvements, we expect that the LCSR approach can be used to constrain light-cone DAs of the nucleon and its resonances from the comparison with the electroproduction data. These constraints can then be compared with the LQCD calculations. In order to facilitate this comparison, a work is in progress to derive general expressions for the necessary LCSRs to the NLO accuracy. The project is to have the LCSRs available as a computer code allowing one to calculate elastic EM and axial form-factors and also a range of transition form-factors involving nucleon resonances from a given set of distribution amplitudes. Although gross features of the wave functions of resonances can definitely be extracted from such an analysis, the level of details "seen" in sum rule calculations will have to be tested on case by case basis. For this reason we are also working on similar calculations for the "gold-plated" decays like $\gamma^* \to \pi\gamma$, $\gamma^* \to \eta\gamma$, see Ref. 211, where the theoretical uncertainties are expected to be small.

6. Quark–Hadron Duality and Transition Form-Factors

6.1. *Historical perspective*

Understanding the structure and interactions of hadrons at intermediate energies is one of the most challenging outstanding problems in nuclear physics. While many hadronic observables can be described in terms of effective meson and baryon degrees of freedom at low energies, at energies $\gg$ the nucleon mass M pQCD has been very successful in describing processes in terms of fundamental quark and gluon (parton) constituents.

A connection between the low and high energy realms is realized through the remarkable phenomenon of quark–hadron duality, where one often finds dual descriptions of observables in terms of either explicit partonic degrees of freedom, or as averages over hadronic variables. In principle, with access to complete sets of either hadronic or partonic states, the realization of duality would be essentially trivial, effectively through a simple transformation from one complete set of basis states to another. In practice, however, at finite energies one is typically restricted to a limited set of basis states, so that the experimental observation of duality raises the question of not *why* duality exists, but rather *how* it arises *where* it exists, and how we can make use of it.

Historically, duality in the strong interaction physics represented the relationship between the description of hadronic scattering amplitudes in terms of s-channel resonances at low energies, and t-channel Regge poles at high energies.[222] The merger of these dual descriptions at intermediate energies remained a prized goal of physicists in the decade or so before the advent of QCD. Progress towards synthesizing the two descriptions was made with the development of finite energy sum

rules (FESRs),[223,224]

$$\int_0^{\nu_{\max}} d\nu \nu^n \Im m\, \mathcal{A}(\nu, t) = \int_0^{\nu_{\max}} d\nu \nu^n \Im m\, \mathcal{A}_{\rm asy}(\nu, t) \quad \text{[FESR]} \tag{19}$$

relating the imaginary part of the amplitude $\mathcal{A}$ at finite energy to the asymptotic high energy amplitude $\mathcal{A}_{\rm asy}$, where s, t and u are the usual Mandelstam variables and $\nu \equiv (s-u)/4$. The asymptotic amplitude $\mathcal{A}_{\rm asy}$ is then extrapolated into the $\nu < \nu_{\max}$ region and compared with the measured amplitude $\mathcal{A}$ through Eq. (19). The assumption made here is that beyond some maximum energy $\nu > \nu_{\max}$ the scattering amplitude can be represented by its asymptotic form, calculated within Regge theory.

The FESRs are generalizations of superconvergence relations in Regge theory relating dispersion integrals over the amplitudes at low energies to high-energy parameters. They constitute a powerful tool allowing one to use experimental information on the low energy cross-sections for the analysis of high energy scattering data. Conversely, they can be used to connect low energy parameters (such as resonance widths and couplings) to parameters describing the behavior of cross-sections at high energy. It was in the context of FESRs, in fact, that the early expressions of Bloom–Gilman duality were made in the early 1970s,[225,226] suitably extended to lepton scattering kinematics.

6.2. *Duality in nucleon structure functions*

One of the most dramatic realizations of duality in nature is in inclusive electron–nucleon scattering, usually referred to as "Bloom–Gilman" duality, where structure functions averaged over the resonance region are found to be remarkably similar to the leading twist structure functions describing the deep-inelastic scattering (DIS) continuum.[212,219,225–229] As Fig. 39 illustrates, the resonance data are seen to oscillate around the scaling curve and slide along it with increasing Q^2.

An intriguing feature of the lepton scattering data is that the duality appears to be realized not just over the entire resonance region as a whole, $W \lesssim 2$ GeV, where $W^2 = M^2 + Q^2(1-x)/x$, but also in individual resonance regions. This is illustrated in Fig. 40 for the ratios of structure functions integrated over specific intervals of W at fixed Q^2, with the first, second, third and fourth resonance regions defined by $1.3 \le W^2 \le 1.9$ GeV^2, $1.9 \le W^2 \le 2.5$ GeV^2, $2.5 \le W^2 \le 3.1$ GeV^2, and $3.1 \le W^2 \le 3.9$ GeV^2, respectively. The "DIS" region in Fig. 40 is defined to be $3.9 \le W^2 \le 4.5$ GeV^2. In all cases, the duality is realized at the $\lesssim 10$–15% level, suggesting that Bloom–Gilman duality exists *locally* as well as globally.

Understanding the microscopic origin of quark–hadron duality has proved to be a major challenge in QCD. Until recently the only rigorous connection with QCD has been within the OPE, in which moments (or x-integrals) of structure functions are expanded as a series in inverse powers of Q^2. The leading, $\mathcal{O}(1)$ term is given by matrix elements of (leading twist) quark–gluon bilocal operators associated with free quark scattering, while the $\mathcal{O}(1/Q^2)$ and higher terms correspond to

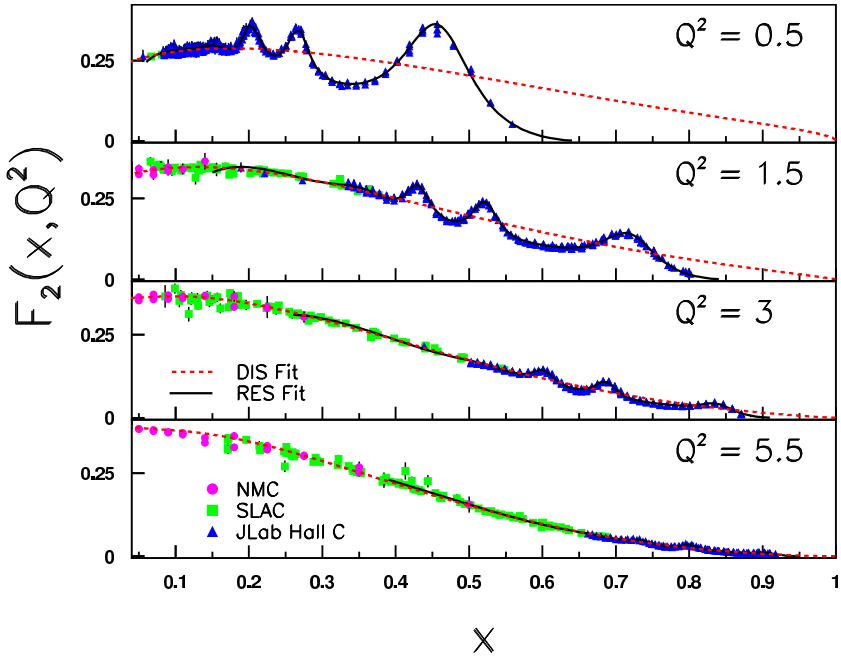

Fig. 39. (Color online) Proton F_2 structure function data from JLab Hall C,[212–214] SLAC,[215,216] and NMC[217] at $Q^2 = 0.5$, 1.5, 3 and 5.5 GeV^2, compared with an empirical fit[218] to the transverse and longitudinal resonance cross-sections (solid), and a global fit to DIS data (dashed). Figure from Ref. 219.

nonperturbative (higher twist) quark–gluon interactions. In the language of the OPE, duality is then synonymous with the suppression of higher twist contributions to the moments.[230]

This close relationship between the leading twist cross-sections and the resonance-averaged cross-sections suggests that the total higher twist contributions are small at scales $Q^2 \sim 1$ GeV^2. This implies that, on average, nonperturbative interactions between quarks and gluons are not dominant at these scales, and that a highly nontrivial pattern of interferences emerges between the resonances (and the nonresonant background) to effect the cancellation of the higher twist contributions. The physics of parton distributions and nucleon resonances is therefore intimately connected. In fact, in the limit of a large number of colors, the spectrum of hadrons in QCD is one of infinitely narrow resonances,[231] which graphically illustrates the fact that resonances are an integral part of scaling structure functions.

The phenomenological results raise the question of how can a scaling structure function be built up entirely from resonances, each of whose contribution falls rapidly with Q^2 (Ref. 232)? A number of studies using various nonperturbative models have demonstrated how sums over resonances can indeed yield a Q^2 independent function (see Ref. 229 for a review). The key observation is that while the contribution from each individual resonance diminishes with Q^2, with increasing

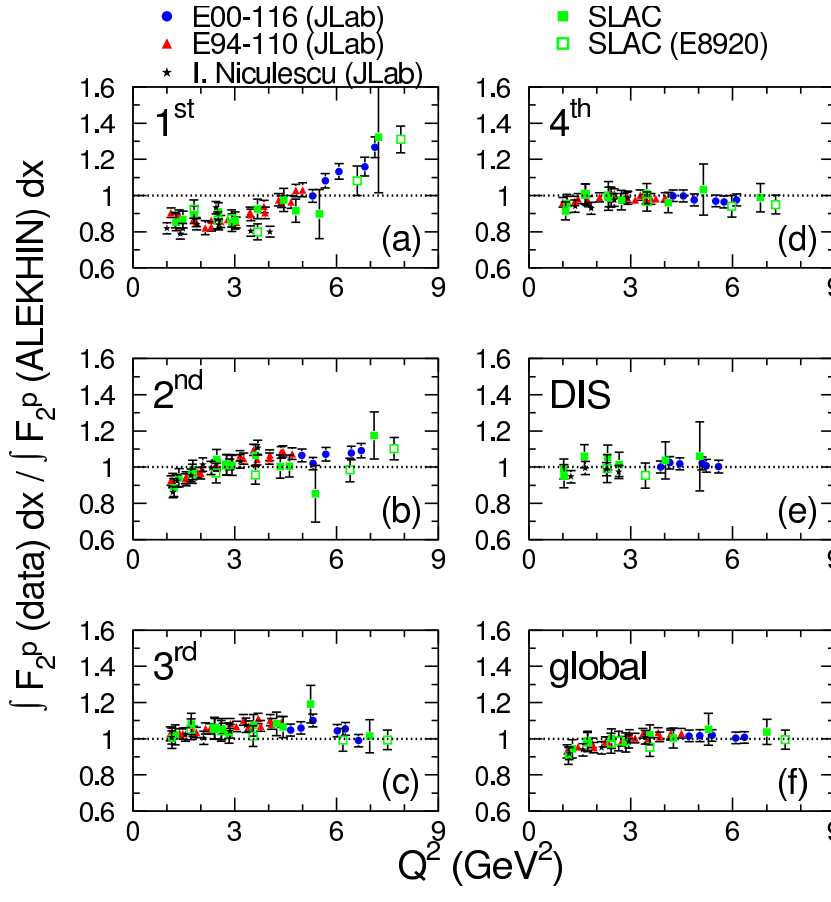

Fig. 40. (Color online) Ratio of proton F_2^p structure functions integrated over specific resonance regions, relative to the global fit of parton distributions from Alekhin *et al.*[220,221] Figure from Ref. 212.

energy new states become accessible whose contributions compensate in such a way as to maintain an approximately constant strength overall. At a more microscopic level, the critical aspect of realizing the suppression of the higher twists is that at least one complete set of even and odd parity resonances must be summed over for duality to hold.[233] Explicit demonstration of how this cancellation takes place was made in the SU(6) quark model and its extensions.[233–235]

One of the ultimate goals of duality studies is to determine the extent to which resonance region data can be used to learn about leading twist structure functions. At present, most global analyses of parton distribution functions impose strong cuts on Q^2 and W^2 for lepton scattering data in order to exclude the region where higher twists and other subleading effects are important. By relaxing the cuts to just inside the traditional resonance region, $W \gtrsim 1.7$ GeV, the CTEQ-JLab (CJ) collaboration could increase the statistics of the DIS data by a factor ~ 2![236,237]

Not only were the fits found to be stable with the weaker cuts, the larger database led to significantly reduced errors, up to 40–60% at large x, where data are scarce. Future plans include extending these cuts to even lower values of W, which demands better understanding of the resonance region and the procedures for systematically averaging over the resonance structure functions.

The determination of parton distributions at large x is vital not just for understanding the dynamics of valence quarks in the nucleon,[238,239] which are currently obscured by nuclear corrections in deuterium DIS data needed to extract the structure function of the free neutron. It is also critical in applications to experiments at high energy coaslliders, where uncertainties at large x in the d quark distribution in particular feeds down to lower x at higher Q^2 (Ref. 240) and can have important consequences for searches for new particles, such as W' and Z' bosons.[241] Thus in an indirect way, better knowledge of the nucleon resonance region can have a profound impact on physics at the LHC!

6.3. *Duality in inclusive meson production*

Extending the concept of duality to less inclusive reactions, we can ask whether the semi-inclusive production of mesons displays a similar relation between partonic and resonance-based descriptions. Such studies have only recently been performed, for ratios of semi-inclusive π^+ to π^- cross-sections measured at JLab as a function of $z = E_\pi/\nu$, where E_π is the pion energy and ν is the energy transfer to the target.[244]

The data displayed a smooth behavior in z, consistent with earlier observations at higher energies at CERN,[245] prompting suggestions that factorization of semi-inclusive cross-sections into scattering and fragmentation sub-processes may hold to relatively low energies. Such factorization was found in fact in simple quark models by explicitly summing over N^* resonances in the s-channel of $\gamma^* N \to \pi N$ scattering.[235]

At the quark level, the (normalized) semi-inclusive cross-section for the production of pions from a nucleon target can be factorized (at leading order in α_s) into a product of a parton distribution function describing the hard scattering from a parton in the target, and the probability of the struck parton fragmenting into a specific hadron,

$$\frac{d\sigma}{dxdz} \propto \sum_q e_q^2 q^N(x) D_q^\pi(z)\,, \tag{20}$$

where e_q is the quark charge, and D_q^π is the fragmentation function for quark q to produce a pion with energy fraction z. As pointed out by Close and Isgur,[233] duality between structure functions represented by (incoherent) parton distributions and by a (coherent) sum of squares of form-factors can be achieved by summing over neighboring odd and even parity states. In the SU(6) model, this is realized by summing over states in the 56^+ ($L = 0$, even parity) and 70^- ($L = 1$, odd parity) multiplets, with each representation weighted equally.

The pion production cross-sections at the hadronic level are constructed by summing coherently over excited nucleon resonances (N_1^*) in the s-channel intermediate state and in the final state (N_2^*) of $\gamma N \to N_1^* \to \pi N_2^*$, where both N_1^* and N_2^* belong to the 56^+ and 70^- multiplets. Within this framework, the probabilities of the $\gamma N \to \pi N_2^*$ transitions can be obtained by summing over the intermediate states N_1^* spanning the 56^+ and 70^- multiplets, with the differential cross-section

$$\frac{d\sigma}{dxdz} \propto \sum_{N_2^*} \left| \sum_{N_1^*} F_{\gamma N \to N_1^*}(Q^2, M_1^*) \mathcal{D}_{N_1^* \to N_2^* \pi}(M_1^*, M_2^*) \right|^2 . \tag{21}$$

Here $F_{\gamma N \to N^*}$ is the $\gamma N \to N^*$ transition form-factor, which depends on the masses of the virtual photon and excited nucleon (M_1^*), and $\mathcal{D}_{N_1^* \to N_2^* \pi}$ is a function representing the decay $N_1^* \to \pi N_2^*$, where M_2^* is the invariant mass of the final state N_2^*.

Summing over the N_2^* states in the 56^+ and 70^- multiplets, one finds ratios of unpolarized π^- to π^+ semi-inclusive cross-sections consistent with the parton model results for ratios of parton distributions satisfying SU(6) symmetry.[233–235] Duality was also found to be realized in more realistic scenarios with broken SU(6) symmetry, with sums over resonances able to reproduce parton model semi-inclusive cross-section ratios.[235] The absence of strong resonant enhancement on top of the smooth background is indeed one of the notable features of the JLab Hall C data,[244] in accord with expectations from duality.

6.4. *Exclusive–inclusive connection*

The general folklore in hadronic physics is that duality works more effectively for inclusive observables than for exclusive, due to the presence in the latter of fewer hadronic states over which to average. For exclusive processes, such as the production of a meson M in coincidence with and a baryon B, $eN \to eMB$, duality may be more speculative. Nevertheless, there are correspondence arguments formulated long ago which relate the exclusive cross-sections at low energy to inclusive production rates at high energy. The exclusive–inclusive connection dates back to the early dates of DIS and the discussion of scaling laws in high energy processes. Bjorken and Kogut[242] proposed the correspondence relations by demanding the continuity of the dynamics as one goes from one (known) region of kinematics to another (which is unknown or poorly known).

For processes such as $\gamma^* N \to MB$, the correspondence principle relates properties of exclusive (resonant) final states with inclusive particle spectra for the corresponding reaction $\gamma^* N \to MX$. This is illustrated in Fig. 41 for a typical inclusive momentum spectrum $Ed^3\sigma/dp^3$, where E and p are the energy and momentum of the observed final state particle M. As p increases, the inclusive continuum gives way to to the region dominated by resonances. The correspondence argument postulates that the resonance contribution to the cross-section should be comparable to the continuum contribution extrapolated from high energy into the

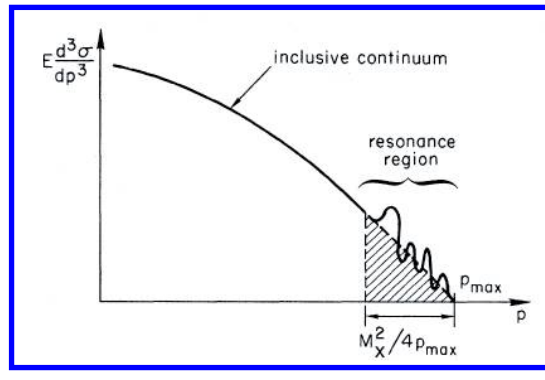

Fig. 41. Momentum spectrum of produced hadrons in the inclusive hadron production reaction $\gamma^* N \to MX$. From Ref. 242.

resonance region,

$$\int_{p_{\min}}^{p_{\max}} dp\, E \frac{d^3\sigma}{dp^3}\bigg|_{\text{incl}} \sim \sum_{\text{res}} E \frac{d\sigma}{dp_T^2}\bigg|_{\text{excl}} , \tag{22}$$

where the integration region over the inclusive cross-section includes contributions up to a missing mass M_X, with $p_{\min} = p_{\max} - M_X^2/4p_{\max}$. The correspondence relation (22) is another manifestation of the FESR in Eq. (19), in which the cross-section in the resonance region for $p_{\min} < p < p_{\max}$ is dual to the high-energy cross-section extrapolated down to the same region.

The inclusive cross-section $d^3\sigma/dp^3$ is generally a function of the longitudinal momentum fraction x, the transverse momentum p_T, and the invariant mass squared s,

$$\frac{E}{\sigma}\frac{d^3\sigma}{dp^3} \equiv f(x, p_T^2, sQ^2) . \tag{23}$$

At large s or large Q^2 this effectively reduces to a function of only x and p_T^2,

$$f(x, p_T^2, sQ^2) \to f(x, p_T^2), \quad s \to \infty . \tag{24}$$

The continuity relation (22) implies that there should be no systematic variation of either side of the equation with external parameters.

Applications of the exclusive–inclusive correspondence have also been made to real Compton scattering cross-sections from the proton at large center of mass frame angles,[246] as well as to hard exclusive pion photoproduction,[247–249] and more recently to deeply virtual Compton scattering, $ep \to e\gamma p$.[243] The latter in particular used a simple model with scalar constituents confined by a harmonic oscillator potential to show how sums over intermediate state resonances, Fig. 42, lead to destructive interference between all but the elastic contribution, and the emergence of scaling behavior for the associated GPDs.

Future work will build on these exploratory studies, generalizing the calculations to include spin-1/2 quarks and nondegenerate multiplets, as well as incorporating

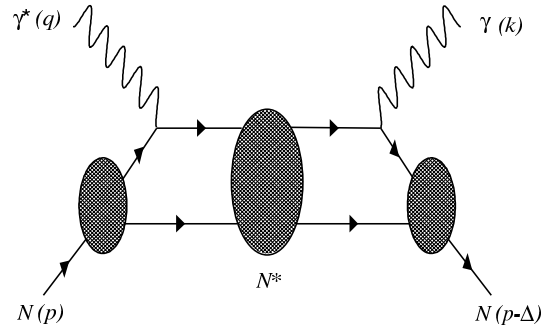

Fig. 42. Deeply virtual (nonforward) Compton scattering at the hadronic level, with excitation of nucleon resonances N^* in the intermediate state. (Adapted from Ref. 243.)

nonresonant background within same framework.[250,251] Extension to flavor nondiagonal transitions will also establish a direct link between transition form-factors and the GPDs, with duality providing a crucial link between the hadronic and partonic descriptions.

7. Light-Front Holographic QCD

The relation between the hadronic short-distance constituent quark and gluon particle limit and the long-range confining domain is yet one of the most challenging aspects of particle physics due to the strong coupling nature of QCD, the fundamental theory of the strong interactions. The central question is how one can compute hadronic properties from first principles; i.e., directly from the QCD Lagrangian. The most successful theoretical approach thus far has been to quantize QCD on discrete lattices in Euclidean space-time.[253] Lattice numerical results follow from computation of frame-dependent moments of distributions in Euclidean space and dynamical observables in Minkowski space-time, such as the time-like hadronic form-factors, are not amenable to Euclidean lattice computations. The Dyson–Schwinger methods have led to many important insights, such as the IR fixed point behavior of the strong coupling constant,[254] but in practice, the analyses are limited to ladder approximation in Landau gauge. Baryon spectroscopy and the excitation dynamics of nucleon resonances encoded in the nucleon transition form-factors can provide fundamental insight into the strong-coupling dynamics of QCD. New theoretical tools are thus of primary interest for the interpretation of the results expected at the new mass scale and kinematic regions accessible to the JLab 12-GeV Upgrade Project.

The AdS/CFT correspondence between gravity or string theory on a higher-dimensional AdS space and conformal field theories in physical space-time[255] has led to a semi-classical approximation for strongly-coupled QCD, which provides physical insights into its nonperturbative dynamics. The correspondence is holographic in the sense that it determines a duality between theories in different

number of space-time dimensions. This geometric approach leads in fact to a simple analytical and phenomenologically compelling nonperturbative approximation to the full LF QCD Hamiltonian — "LF holography".[256] LF holography is in fact one of the most remarkable features of the AdS/CFT correspondence.[255] The Hamiltonian equation of motion in the LF is frame independent and has a structure similar to eigenmode equations in AdS space. This makes a direct connection of QCD with AdS/CFT methods possible.[256] Remarkably, the AdS equations correspond to the kinetic energy terms of the partons inside a hadron, whereas the interaction terms build confinement and correspond to the truncation of AdS space in an effective dual gravity approximation.[256]

One can also study the gauge/gravity duality starting from the bound-state structure of hadrons in QCD quantized in the LF. The LF Lorentz-invariant Hamiltonian equation for the relativistic bound-state system is

$$P_\mu P^\mu |\psi(P)\rangle = (P^+P^- - \mathbf{P}_\perp^2)|\psi(P)\rangle = M^2|\psi(P)\rangle, \qquad P^\pm = P^0 \pm P^3\,, \qquad (25)$$

where the LF time evolution operator P^- is determined canonically from the QCD Lagrangian.[257] To a first semi-classical approximation, where quantum loops and quark masses are not included, this leads to a LF Hamiltonian equation which describes the bound-state dynamics of light hadrons in terms of an invariant impact variable ζ[256] which measures the separation of the partons within the hadron at equal LF time $\tau = x^0 + x^3$.[258] This allows us to identify the holographic variable z in AdS space with an impact variable ζ.[256] The resulting Lorentz-invariant Schrödinger equation for general spin incorporates color confinement and is systematically improvable.

LF holographic methods were originally introduced[259,260] by matching the EM current matrix elements in AdS space[261] with the corresponding expression using LF theory in physical space-time. It was also shown that one obtains identical holographic mapping using the matrix elements of the energy–momentum tensor[262] by perturbing the AdS metric around its static solution.[263]

A gravity dual to QCD is not known, but the mechanisms of confinement can be incorporated in the gauge/gravity correspondence by modifying the AdS geometry in the large IR domain $q \sim 1/\Lambda_{\rm QCD}$, which also sets the scale of the strong interactions.[264] In this simplified approach, we consider the propagation of hadronic modes in a fixed effective gravitational background asymptotic to AdS space, which encodes salient properties of the QCD dual theory, such as the UV conformal limit at the AdS boundary, as well as modifications of the background geometry in the large z IR region to describe confinement. The modified theory generates the point-like hard behavior expected from QCD,[265,266] instead of the soft behavior characteristic of extended objects.[264]

7.1. *Nucleon form-factors*

In the higher-dimensional gravity theory, hadronic amplitudes for the transition $A \to B$ correspond to the coupling of an external EM field $A^M(x,z)$ propagating

in AdS space with a fermionic mode $\Psi_P(x,z)$ given by the left-hand side of the equation below

$$\int d^4x dz \sqrt{g} \bar{\Psi}_{B,P'}(x,z) e_M^A \Gamma_A A_q^M(x,z) \Psi_{A,P}(x,z) \sim (2\pi)^4 \delta^4(P'-P-q) \epsilon_\mu \langle \psi_B(P'), \sigma' | J^\mu | \psi_A(P), \sigma \rangle ,$$

where the coordinates of AdS_5 are the Minkowski coordinates x^μ and z labeled $x^M = (x^\mu, z)$, with M, $N = 1, \ldots, 5$, g is the determinant of the metric tensor and e_M^A is the vielbein with tangent indices $A, B = 1, \ldots, 5$. The expression on the right-hand side represents the QCD EM transition amplitude in physical space-time. It is the EM matrix element of the quark current $J^\mu = e_q \bar{q} \gamma^\mu q$, and represents a local coupling to point-like constituents. Can the transition amplitudes be related for arbitrary values of the momentum transfer q? How can we recover hard pointlike scattering at large q from the soft collision of extended objects?[261] Although the expressions for the transition amplitudes look very different, one can show that a precise mapping of the J^+ elements can be carried out at fixed LF time, providing an exact correspondence between the holographic variable z and the LF impact variable ζ in ordinary space-time.[259]

A particularly interesting model is the "soft wall" model of Ref. 267, since it leads to linear Regge trajectories consistent with the light-quark hadron spectroscopy and avoids the ambiguities in the choice of boundary conditions at the IR wall. In this case, the effective potential takes the form of a harmonic oscillator confining potential $\kappa^4 z^2$. For a hadronic state with twist $\tau = N + L$ (N is the number of components and L the internal orbital angular momentum) the elastic form-factor is expressed as a $\tau - 1$ product of poles along the vector meson Regge radial trajectory ($Q^2 = -q^2 > 0$)[260]

$$F(Q^2) = \frac{1}{\left(1 + \frac{Q^2}{M_\rho^2}\right)\left(1 + \frac{Q^2}{M_{\rho'}^2}\right) \cdots \left(1 + \frac{Q^2}{M_{\rho^{\tau-2}}^2}\right)}, \tag{26}$$

where $M_{\rho_n}^2 \to 4\kappa^2(n + 1/2)$. For a pion, for example, the lowest Fock state — the valence state — is a twist-two state, and thus the form-factor is the well-known monopole form. The remarkable analytical form of Eq. (26), expressed in terms of the ρ vector meson mass and its radial excitations, incorporates the correct scaling behavior from the constituent's hard scattering with the photon[265,266] and the mass gap from confinement.

7.2. *Computing nucleon form-factors in light-front holographic QCD*

As an illustrative example, we consider in this section the spin nonflip elastic proton form-factor and the form-factor for the $\gamma^* p \to N(1440)P_{11}$ transition measured recently at JLab. In order to compute the separate features of the proton an neutron

form-factors one needs to incorporate the spin-flavor structure of the nucleons, properties which are absent in the usual models of the gauge/gravity correspondence. This can be readily included in AdS/QCD by weighting the different Fock-state components by the charges and spin-projections of the quark constituents; e.g., as given by the SU(6) spin-flavor symmetry.

Using the SU(6) spin-flavor symmetry the expression for the spin nonflip proton form-factors for the transition $n, L \to n'L$ is[268]

$$F^p_{1n,L\to n',L}(Q^2) = R^4 \int \frac{dz}{z^4} \Psi_+^{n',L}(z) V(Q,z) \Psi_+^{n,L}(z)\,, \tag{27}$$

where we have factored out the plane wave dependence of the AdS fields

$$\Psi_+(z) = \frac{\kappa^{2+L}}{R^2} \sqrt{\frac{2n!}{(n+L+1)!}} z^{7/2+L} L_n^{L+1}(\kappa^2 z^2) e^{-\kappa^2 z^2/2}\,. \tag{28}$$

The bulk-to-boundary propagator $V(Q,z)$ has the integral representation[269]

$$V(Q,z) = \kappa^2 z^2 \int_0^1 \frac{dx}{(1-x)^2} x^{\frac{Q^2}{4\kappa^2}} e^{-\kappa^2 z^2 x/(1-x)}\,, \tag{29}$$

with $V(Q=0,z) = V(Q,z=0) = 1$. The orthonormality of the Laguerre polynomials in (28) implies that the nucleon form-factor at $Q^2 = 0$ is one if $n = n'$ and zero otherwise. Using (29) in (27) we find

$$F_1^p(Q^2) = \frac{1}{\left(1 + \dfrac{Q^2}{M_\rho^2}\right)\left(1 + \dfrac{Q^2}{M_{\rho'}^2}\right)}\,, \tag{30}$$

for the elastic proton Dirac form-factor and

$$F_{1\,N\to N^*}^p(Q^2) = \frac{\sqrt{2}}{3} \frac{\dfrac{Q^2}{M_\rho^2}}{\left(1 + \dfrac{Q^2}{M_\rho^2}\right)\left(1 + \dfrac{Q^2}{M_{\rho'}^2}\right)\left(1 + \dfrac{Q^2}{M_{\rho''}^2}\right)}\,, \tag{31}$$

for the EM spin nonflip proton to Roper transition form-factor. The results (30) and (31), compared with available data in Fig. 43, correspond to the valence approximation. The transition form-factor (31) is expressed in terms of the mass of the ρ vector meson and its first two radial excited states, with no additional parameters. The results in Fig. 43 are in good agreement with experimental data. The transition form-factor to the $N(1440)P_{11}$ state shown in Fig. 43 corresponds to the first radial excitation of the three-quark ground state of the nucleon. In fact, the Roper resonance $N(1440)P_{11}$ and the $N(1710)P_{11}$ are well accounted in the LF holographic framework as the first and second radial states of the nucleon family, likewise the $\Delta(1600)P_{33}$ corresponds to the first radial excitation of the Δ family as shown in Fig. 44 for the positive-parity light-baryons.[270] In the case of massless quarks, the nucleon eigenstates have Fock components with different orbital angular

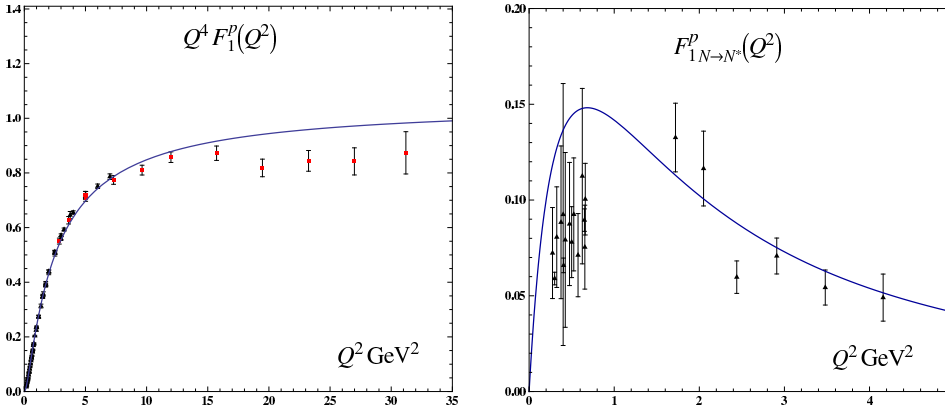

(a) (b)

Fig. 43. (Color online) Dirac proton form-factors in LF holographic QCD. (a) Scaling of proton elastic form-factor $Q^4 F_1^p(Q^2)$. (b) Proton transition form-factor $F_{1\,N\to N^*}^p(Q^2)$ for the $\gamma^* p \to N(1440)P_{11}$ transition. Data compilation from Diehl[300] (a) and CLAS π and 2π electroproduction data[19,41,301,302] (b).

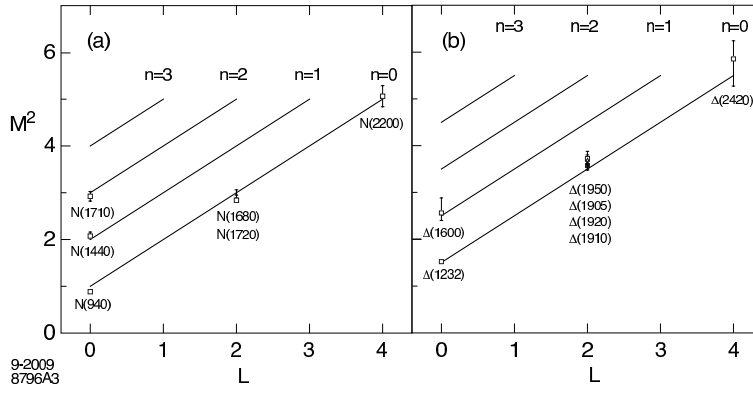

Fig. 44. Positive parity Regge trajectories for the N and Δ baryon families for $\kappa = 0.5$ GeV. Only confirmed PDG[303] states are shown.

momentum, $L = 0$ and $L = 1$, but with equal probability. In effect, in AdS/QCD the nucleons angular momentum is carried by quark orbital angular momentum since soft gluons do not appear as quanta in the proton.

LF holographic QCD methods have also been used to obtain GPDs in Ref. 271, and a study of the EM nucleon to Δ transition form-factors and nucleon to the $S_{11}(1535)$ negative parity nucleon state has been carried out in the framework of the Sakai and Sugimoto model in Refs. 272 and 273, respectively. It is certainly worth to extend the simple computations described here and perform a systematic study of the different transition form-factors measured at JLab. This study will help to discriminate among models and compare with the new results expected from the

JLab 12-GeV Upgrade Project, in particular at photon virtualities $Q^2 > 5$ GeV^2, which correspond to the experimental coverage of the CLAS12 detector.

8. The N^* Electrocoupling Interpretation within the Framework of Constituent Quark Models

8.1. *Introduction*

The study of the EM excitation of the nucleon resonances is expected to provide a good test for our knowledge concerning the internal structure of baryons. From a fundamental point of view, the description of the resonance spectrum and excitation should be performed within a QCD approach, which, however, does not allow up to now to extract all the hadron properties in a systematic way. Therefore, one has to rely on models, such as the constituent quark models (CQM). In CQMs, quarks are considered as effective internal degrees of freedom and can acquire a mass and a finite size. Phenomenological results of these models provide useful constraints based on experimental data for the development of QCD-based approaches such as LQCD and DSEQCD. For instance the choice of basis configurations in the recent LQCD studies of N^* spectrum[14] was motived by quark model results.

In the following, we report some results of recent approaches using the constituent quark idea in the framework of various LF formulations of the quark wave function (Secs. 7, 8.2 and 8.3) and a discussion on the use of CQM for the interpretation of resonance electrocouplings at high Q^2 with particular attention to some future perspectives (Sec. 8.4).

8.2. *Covariant quark–diquark model for the N and N^* electromagnetic transition form-factors*

The study of hadron structure using the fundamental theory, QCD, can in practise be done only in the large Q^2 regime or, by means of lattice simulations, in the unphysical quark masses regime.[16] For this reason, one has to rely on effective descriptions either with the degrees of freedom of QCD (quarks and gluons) within the Dyson–Schwinger framework,[16] or in terms of the degrees of freedom observed at low Q^2, the meson cloud and the light baryon core, using a DCCs reaction (dynamical models or DM) framework.[16,304] The DSEQCD helps to understand the transition between the perturbative regime of QCD and the low Q^2 regime, where the quarks acquire masses and structure dynamically due to the gluon dressing, although the meson degrees of freedom are not included till the moment.[16] Dynamical models, on the other hand, help to explain the transition between the low Q^2 picture, in terms of a finite size baryon and the surrounding meson cloud, and the intermediate region when $Q^2 > 2$ GeV^2, where the baryon core effects become increasingly important.[304] To complete the picture, a parametrization of the structure of the baryon core is required, and a possibility is to use the meson–baryon dressing model to extract from the data the contributions of the core, that can be interpreted as a three-valence quark system.[65,73]

Alternative descriptions comprise effective chiral perturbation theory, that can be used to interpolate LQCD results but is restricted to the low Q^2 regime, pQCD that works only at very large Q^2 with a threshold that is still under discussion, QCD sum rules and constituent quark models that can include also chiral symmetry and/or unquenched effects.[16]

CQMs include the gluon and quark–antiquark polarization in the quark substructure (that also generates the constituent quark mass) with effective inter-quark interactions.[16] There are different versions according to the inter-quark interaction potential and the kinematic considered (nonrelativistic or relativistic). Among the relativistic descriptions, there are, in particular, different implementations of relativity based on the Poincare invariance.[16]

We discuss now with some detail the covariant quark–diquark model, also known as the spectator quark model, and present some of its results. Contrarily to other CQMs, this model is not based on a wave equation determined by some complex and nonlinear potential. For that reason, the model is not used to predict the baryonic spectrum. Instead, the wave functions are built from the baryon internal symmetries only, with the shape of the wave functions determined directly by the experimental data, or lattice data for some ground state systems.[305]

In the CST[306] the three-body baryon systems are described in terms of a vertex function Γ where two quarks are on-mass-shell.[252,307,308] In this approach, confinement ensures that the vertex Γ vanishes when the three quarks are simultaneously on-mass-shell, and the singularities associated with the propagator of the off-mass-shell quark are canceled by the vertex Γ.[307,308] The baryon state can then be described by a wave function $\Psi(P,k) = (m_q - \not{k} - i\varepsilon)^{-1}\Gamma(P,k)$, where P is the baryon momentum, m_q the quark mass and k the quark four-momentum.[252,308]

The CST formulation is motivated by the fact that in impulse approximation only one quark interacts with the photon, while the two other quarks are spectators. Therefore, by integrating over the relative momentum of these two quarks, one can reduce the three-quark system to a quark–diquark system, where the effective diquark has an averaged mass m_D.[252,308] In these conditions, the baryon is described by a wave function for the quark–diquark, with individual states associated with the internal symmetries (color, flavor, spin, momentum, etc.). The EM interaction current is given in impulse approximation by the coupling of the photon with the off-mass-shell quark, while the diquark acts as a spectator on-mass-shell particle.[252,305,309]

The photon–quark interaction is parametrized by using the vector meson dominance (VMD) mechanism, based on a combination of two poles associated with vector mesons: a light vector meson (mass $m_v = m_\rho \simeq m_\omega$) and an effective heavy meson with mass $M_h = 2M$, where M is the nucleon mass, which modulates the short range structure.[252,305,309] The free parameters of the current were calibrated for the SU(3) sector by nucleon EM form-factor data[252] and with LQCD simulations associated with the baryon decuplet.[309] A parametrization based on VMD has the advantage in the generalization to the LQCD regime[309–312] and also for the time-like region ($Q^2 < 0$).[313]

The covariant spectator quark model was applied to the description of the nucleon elastic form-factors using a simple model where the quark–diquark motion is taken in the S-state approximation.[252] The nucleon data were used to fix the quark current as well as the radial wave function.[252] A specific model with no explicit pion cloud effects, except the effects included in the VMD parametrization is presented in Fig. 45. This parametrization, based only on the valence quark degrees of freedom, was extended successfully for the nucleon on the lattice regime.[77]

The model was also applied to the first nucleon resonance the $\Delta(1232)$, in particular to the $\gamma N \to \Delta(1232)$ transition. Within a minimal model where the Δ is described as an S-state of three-quarks with the total spin and isospin-3/2, one obtains, for dominant transition form-factor $G_M^*(0) \leq 2.07\ \mathcal{I} \leq 2.07$, where $\mathcal{I} \leq 1$,

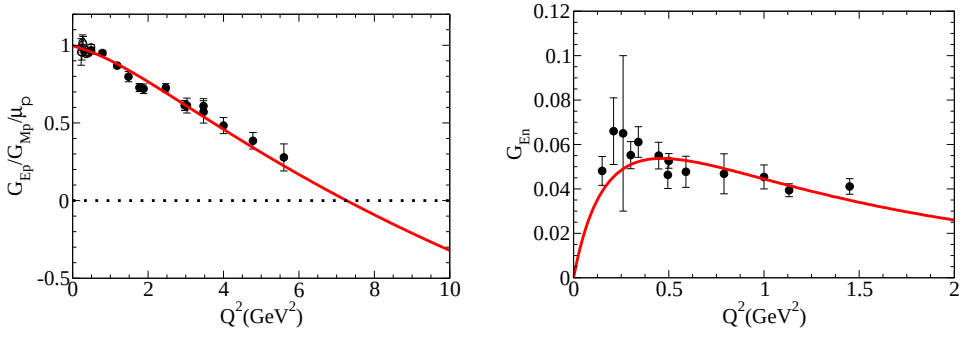

(a) (b)

Fig. 45. (Color online) Nucleon form-factors. Model II of Ref. 252. (a) $\mu_p\, G_{Ep}/G_{Mp}$ ratio, including the JLab data. (b) Neutron electric form-factor.

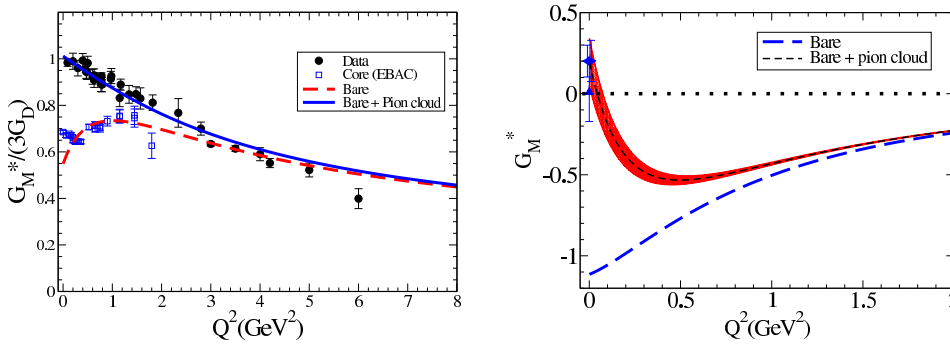

(a) (b)

Fig. 46. (Color online) Nucleon electromagnetic–transition for spin-3/2 resonances. (a) $G_M^*/(3G_D)$ (G_D is the nucleon dipole form-factor) for the $\gamma N \to \Delta(1232)$ reaction.[274] (b) G_M^* for the $\gamma N \to \Delta(1600)$ reaction.[275] In both cases the dashed line gives the valence quark contribution and the solid line the full result.

is the overlap integral between the nucleon and Δ radial wave functions (both are S-states) in the limit $Q^2 = 0$.[314] This simple relation, which is a consequence of the normalization of the nucleon and Δ quark wave functions, illustrates the incapability in describing the $\gamma N \to \Delta(1232)$, with quark degrees of freedom only, since the experimental result is $G_M^*(0) \simeq 3$. The discrepancy, is common to all constituent quark models, and is also a manifestation of the importance of the pion excitation which contributes with about 30–40% of the strength of the reaction.[16,73,304] The model can however explain the quark core contribution in the transition, as extracted from the data using the EBAC model,[73] when the meson–baryon cloud is subtracted.[314] The comparison of the model with the EBAC estimate is presented in [Fig. 46(a), dashed line], and also with the G_M^* data, when meson–baryon cloud is included (solid line). The model was also extended successfully to the reaction in the lattice regime.[310,311] The description of the quadrupole form-factors G_E^* (electric) and G_C^* (Coulomb) is also possible once small D-state components are included.[274,311] In that case, the LQCD data can be well described by an extension of the model with an admixture of D-states less than 1%,[311] but the experimental data are fairly explained only when the meson–baryon cloud and valence quark degrees of freedom are combined.[311] Finally, the model was also applied to the first radial excitation of the $\Delta(1232)$, the $\Delta(1600)$ resonance.[275] In this case, no extra parameters are necessary and the meson–baryon cloud effects are largely dominant at low Q^2. The results for G_M^* are presented in Fig. 46(b). In both systems, the valence quark effects are dominant for $Q^2 > 2$ GeV^2.

The model was also extended to the spin-1/2 state $N(1440)$ (Roper), interpreted as the first radial excitation of the nucleon.[276] The $N(1440)$ shared with the nucleon the spin and isospin structure, differing in the radial wave function. Under that assumption we calculated the transition form-factors for the $\gamma N \to N(1440)$ reaction based exclusively on the valence quark degrees of freedom.[276] As an example, we present the Dirac-type form-factor F_1^* in Fig. 47(a). The model is also consistent

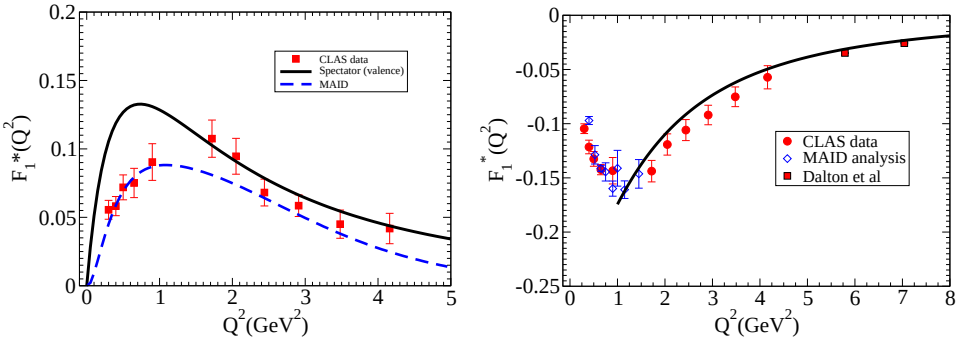

(a) (b)

Fig. 47. (Color online) Dirac-type form-factors F_1^* for $\gamma N \to N^*$ transitions. (a) $\gamma N \to P_{11}(1440)$ reaction.[276] (b) $\gamma N \to S_{11}(1535)$ reaction.[277]

with the lattice data.[276] The covariant spectator quark model was also applied to the chiral partner of the nucleon $N(1535)$ (negative parity) under two approximations: a point-like diquark and a quark core restricted to spin-1/2 states.[277] Under these approximations, the $\gamma N \to N(1535)$ transition form-factors were calculated for the region $Q^2 \gg 0.23$ GeV^2.[277] The result for F_1^* is presented in Fig. 47(b). In both reactions, the results are consistent with the data for $Q^2 > 1.5$ GeV^2,[276,277] except for F_2^* for the reaction with $N(1535)$. Our results support the idea that the valence quark dominance for the intermediate and high Q^2 region, but also the necessity of the meson excitations for the lower Q^2 region ($Q^2 < 2$ GeV^2). The form-factor F_2^* for the $\gamma N \to N(1535)$ reaction is particularly interesting from the perspective of a quark model, since the data indicate that $F_2^* \approx 0$ for $Q^2 > 2$ GeV^2, contrarily to the result of the spectator quark model. These facts suggest that the valence quark and meson cloud contributions have opposite signs and cancel in the sum.[277,316] The direct consequence of the result for $F_2^* \approx 0$ is the proportionality between the amplitudes $A_{1/2}$ and $S_{1/2}$ for $Q^2 > 2$ GeV^2.[317]

Other applications of the covariant spectator quark model are the elastic EM form-factors of the baryon octet (spin-1/2),[312,318] and the baryon decuplet (spin-3/2),[309,319–321] as well as the EM transition between octet and decuplet baryons, similarly to the $\gamma N \to \Delta(1232)$ reaction.[322] The study of the octet EM structure in the nuclear medium is also in progress.[323]

Future work will establish how higher angular momentum states in the wave function, namely P and D states, may contribute to the nucleon form-factors. This work will be facilitated by the results in Refs. 324 and 325, where it was already possible to constrain those terms of the wave function by existing deep inelastic scattering data.

Extensions for higher resonances are underway for $P_{11}(1710)$, $D_{13}(1520)$ and $S_{11}(1650)$. The last two cases depend on the inclusion of an isospin-1/2, spin-3/2 core in a state of the total angular momentum 1/2. These states are expected to be the same as that in the part of the nucleon structure.[324]

In future developments, the quality and quantity of the future LQCD studies will be crucial to constrain the parametrization of the wave functions, and clarify the effect of the valence quarks and meson cloud, following the successful applications to the LQCD regime for the nucleon,[312,324] $\gamma N \to \Delta(1232)$ transition[311] and Roper.[276]

In parallel, the comparison with the estimate of the quark core contributions performed by the EBAC group preferentially for $Q^2 > 2$ GeV^2,[65,73] will be also very useful in the next two years. To complement the quark models, the use of dynamical models and/or effective chiral models[326] to estimate the meson cloud effects are also very important. This is particularly relevant for the $\gamma N \to N(1535)$ reaction. From the experimental side, new accurate measurements in the low Q^2 region as well as the high Q^2 region, as will be measured in the future after the JLab 12-GeV Upgrade, will be crucial, for the purposes of either to test the present parametrizations at high Q^2, or to calibrate the models for new calculations at

even larger Q^2. The clarifications between the different analysis of the data such as EBAC, CLAS, SAID, MAID, Jülich and Bonn-Gatchina, will also have an important role.[16,19,42,43,327–329]

8.3. *Nucleon electromagnetic form-factors and electroexcitation of low lying nucleon resonances up to $Q^2 = 12$ GeV^2 in a light-front relativistic quark model*

8.3.1. *Introduction*

In recent decade, with the advent of the new generation of electron beam facilities, there is a dramatic progress in the investigation of the electroexcitation of nucleon resonances with significant extension of the range of Q^2. The most accurate and complete information has been obtained for the electroexcitation amplitudes of the four lowest excited states, which have been measured in a range of Q^2 up to 8 GeV^2 and 4.5 GeV^2 for the $\Delta(1232)P_{33}$, $N(1535)S_{11}$ and $N(1440)P_{11}$, $N(1520)D_{13}$, respectively (see Refs. 16 and 25), and the recent update.[20,174] At relatively small Q^2, nearly massless Goldstone bosons (pions) can produce significant pion-loop contributions. However, it is expected that the corresponding hadronic component, including meson–cloud contributions, will be losing strength with increasing Q^2. The JLab 12-GeV Upgrade will open up a new era in the exploration of excited nucleons when the ground state and excited nucleon's quark core will be fully exposed to the EM probe.

Our goal is to predict $3q$ core contribution to the electroexcitation amplitudes of the resonances $\Delta(1232)P_{33}$, $N(1440)P_{11}$, $N(1520)D_{13}$, and $N(1535)S_{11}$. The approach we use is based on LF dynamics which realizes Poincaré invariance and the description of the vertices $N(N^*) \to 3q, N\pi$ in terms of wave functions. The corresponding LF relativistic model for bound states is formulated in Refs. 330–333. The parameters of the model for the $3q$ contribution have been specified via description of the nucleon EM form-factors in the approach that combines $3q$ and pion-cloud contributions. The pion-loop contributions to nucleon EM form-factors have been described according to the LF approach of Ref. 278.

8.3.2. *Quark core contribution to transition amplitudes*

The $3q$ contribution to the $\gamma^* N \to N(N^*)$ transitions has been evaluated within the approach of Refs. 332 and 333 where the LF relativistic quark model is formulated in infinite momentum frame (IMF). The IMF is chosen in such a way, that the initial hadron moves along the z-axis with the momentum $P \to \infty$, the virtual photon momentum is

$$k^\mu = \left(\frac{m_{\rm out}^2 - m_{\rm in}^2 - \mathbf{Q}_\perp^2}{4P}, \mathbf{Q}_\perp, -\frac{m_{\rm out}^2 - m_{\rm in}^2 - \mathbf{Q}_\perp^2}{4P} \right),$$

the final hadron momentum is $P' = P + k$, and $Q^2 \equiv -k^2 = \mathbf{Q}_\perp^2$; $m_{\rm in}$ and $m_{\rm out}$ are masses of the initial and final hadrons, respectively. The matrix elements of the

EM current are related to the $3q$-wave functions in the following way:

$$\frac{1}{2P} < N(N^*), S'_z|J^{0,3}_{\rm em}|N, S_z\rangle|_{P\to\infty} = e\Sigma_i \int \Psi'^{+} Q_i \Psi d\Gamma \,, \tag{32}$$

where S_z and S'_z are the projections of the hadron spins on the z-direction, Q_i $(i = a, b, c)$ are the charges of the quarks in units of e, $e^2/4\pi = \alpha$, Ψ and Ψ' are wave functions in the vertices $N(N^*) \to 3q$, and $d\Gamma$ is the phase space volume:

$$d\Gamma = (2\pi)^{-6} \frac{d\mathbf{q}_{b\perp} d\mathbf{q}_{c\perp} dx_b dx_c}{4x_a x_b x_c} \,. \tag{33}$$

The quark momenta in the initial and final hadrons are parametrized via:

$$\mathbf{p}_i = x_i \mathbf{P} + \mathbf{q}_{i\perp}, \qquad \mathbf{p}'_i = x_i \mathbf{P}' + \mathbf{q}'_{i\perp} \,, \tag{34}$$

$$\mathbf{P}\mathbf{q}_{i\perp} = \mathbf{P}'\mathbf{q}'_{i\perp} = 0, \qquad \Sigma\mathbf{q}_{i\perp} = \Sigma\mathbf{q}'_{i\perp} = 0, \qquad \mathbf{q}'_{i\perp} = \mathbf{q}_{i\perp} - y_i \mathbf{Q}_\perp \,, \tag{35}$$

$$\Sigma x_i = 1, \quad y_a = x_a - 1, \quad y_b = x_b, \quad y_c = x_c \,. \tag{36}$$

Here we have supposed that quark a is an active quark.

The wave function Ψ is related to the wave function in the c.m.s. of the system of three quarks through Melosh matrices[334]:

$$\Psi = U^+(p_a) U^+(p_b) U^+(p_c) \Psi_{fss} \Phi(\mathbf{q}_a, \mathbf{q}_b, \mathbf{q}_c) \,, \tag{37}$$

where we have separated the flavor–spin–space part of the wave function Ψ_{fss} in the c.m.s. of the quarks and its spatial part $\Phi(\mathbf{q}_a, \mathbf{q}_b, \mathbf{q}_c)$. The Melosh matrices are defined by

$$U(p_i) = \frac{m_q + M_0 x_i + i\epsilon_{lm}\sigma_l q_{im}}{\sqrt{(m_q + M_0 x_i)^2 + \mathbf{q}^2_{i\perp}}}, \tag{38}$$

where m_q is the quark mass. The flavor–spin–space parts of the wave functions are constructed according to commonly used rules.[28,335] To construct these parts, we need also the z-components of quark momenta in the c.m.s. of quarks. They are defined by

$$q_{iz} = \frac{1}{2}\left(x_i M_0 - \frac{m_q^2 + \mathbf{q}^2_{i\perp}}{x_i M_0} \right), \quad q'_{iz} = \frac{1}{2}\left(x_i M'_0 - \frac{m_q^2 + \mathbf{q}'^2_{i\perp}}{x_i M'_0} \right) \,, \tag{39}$$

where M_0 and M'_0 are invariant masses of the systems of initial and final quarks:

$$M_0^2 = \Sigma \frac{\mathbf{q}^2_{i\perp} + m_q^2}{x_i}, \quad M'^2_0 = \Sigma \frac{\mathbf{q}'^2_{i\perp} + m_q^2}{x_i} \,. \tag{40}$$

To study sensitivity to the form of the quark wave function, we employ two widely used forms of the spatial parts of wave functions:

$$\Phi_1 \sim \exp(-M_0^2/6\alpha_1^2), \quad \Phi_2 \sim \exp[-(\mathbf{q}_1^2 + \mathbf{q}_2^2 + \mathbf{q}_3^2)/2\alpha_2^2] \,, \tag{41}$$

used, respectively, in Refs. 330–333 and 96.

8.3.3. *Nucleon*

The nucleon EM form-factors were described by combining the $3q$-core and pion-cloud contributions to the nucleon wave function. With the pion loops evaluated according to Ref. 278, the nucleon wave function has the form:

$$|N\rangle = 0.95|3q\rangle + 0.313|N\pi\rangle\,, \tag{42}$$

where the portions of different contributions were found from the condition the charge of the proton be unity: $F_{1p}(Q^2 = 0) = 1$. The value of the quark mass at $Q^2 = 0$ has been taken equal to $m_q(0) = 0.22$ GeV from the description of baryon and meson masses in the relativized quark model.[96,336] Therefore, the only unknown parameters in the description of the $3q$ contribution to nucleon form-factors were the quantities α_1 and α_2 in Eqs. (41). These parameters were found equal to

$$\alpha_1 = 0.37 \text{ GeV}, \quad \alpha_2 = 0.405 \text{ GeV} \tag{43}$$

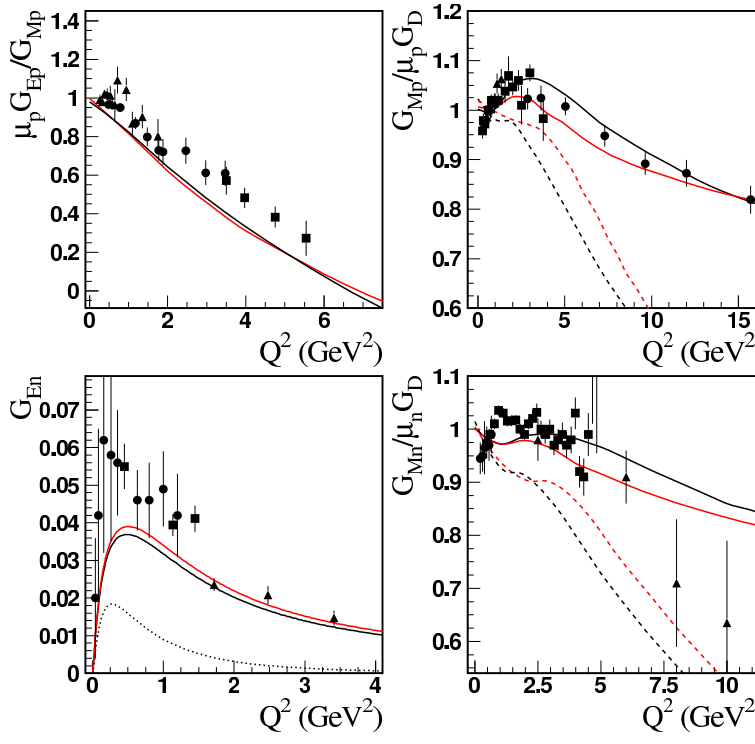

Fig. 48. (Color online) Nucleon EM form-factors. The solid curves correspond to the results obtained taking into account two contributions to the nucleon (Eq. (42)): the pion-cloud[278] and the $3q$ core with the running quark masses (44) for the wave functions Φ_1 (black curves) and Φ_2 (red curves) in Eq. (41). The black and red dashed curves are the results obtained for the nucleon taken as a pure $3q$ state with the parameters (43) and constant quark mass. Dotted curve for $G_{En}(Q^2)$ is the pion cloud contribution.[278] Data are from Refs. 279–287.

from the description of the magnetic moments at $Q^2 = 0$ (see Fig. 48). The parameters (43) give very close magnitudes for the mean values of invariant masses and momenta of quarks at $Q^2 = 0$: $\langle M_0^2 \rangle \approx 1.35$ GeV^2 and $\langle \mathbf{q}_i^2 \rangle \approx 0.1$ GeV^2, $i = a, b.c.$

The constant value of the quark mass gives rapidly decreasing form, factors $G_{Ep}(Q^2)$, $G_{Mp}(Q^2)$, and $G_{Mn}(Q^2)$ (see Fig. 48). The wave functions (41) increase as m_q decreases. Therefore, to describe the experimental data we have assumed the Q^2-dependent quark mass that decreases with increasing Q^2:

$$m_q^{(1)}(Q^2) = \frac{0.22 \text{ GeV}}{1 + Q^2/60 \text{ GeV}^2}, \quad m_q^{(2)}(Q^2) = \frac{0.22 \text{ GeV}}{1 + Q^2/10 \text{ GeV}^2} \tag{44}$$

for the wave functions Φ_1 and Φ_2, respectively. Momentum dependent quark mass allowed us to obtain good description of the nucleon EM form-factors up to $Q^2 = 16$ GeV^2. From Fig. 49, it can be seen that at $Q^2 > 2$ GeV^2, these form-factors are dominated by the $3q$-core contribution.

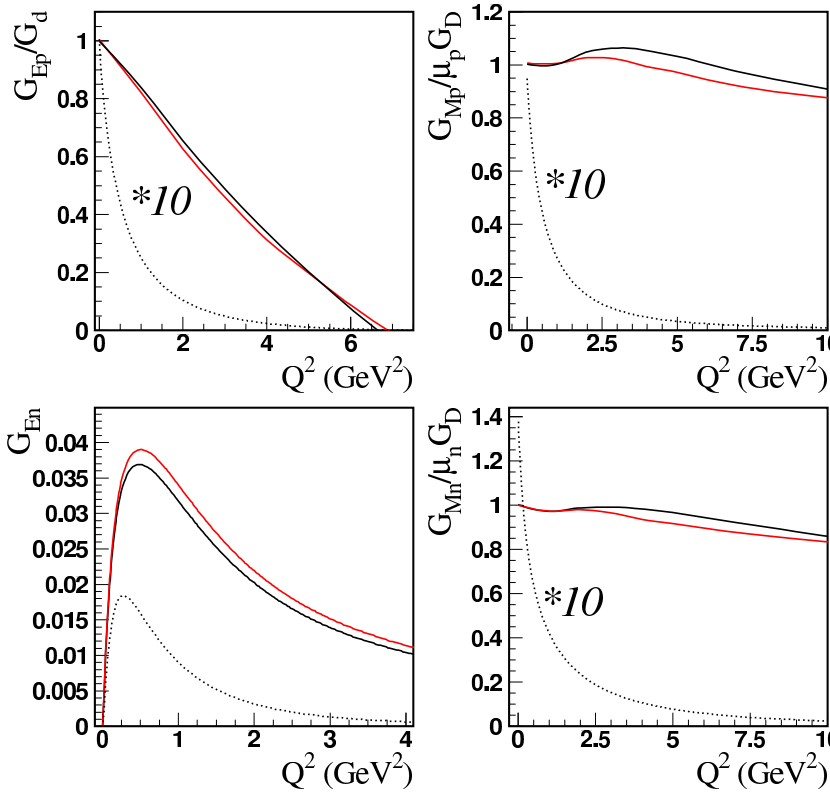

Fig. 49. (Color online) Nucleon EM form-factors. The legend for the black and red solid curves is as for Fig. 48. Dotted curves are the pion cloud contributions.[278]

8.3.4. *Nucleon resonances* $\Delta(1232)P_{33}$, $N(1440)P_{11}$, $N(1520)D_{13}$, *and* $N(1535)S_{11}$

No calculations are available that allow for the separation of the $3q$ and $N\pi$ (or nucleon–meson) contributions to nucleon resonances. Therefore, the weights c^* ($c^* < 1$) of the $3q$ contributions to the resonances: $|N^*\rangle = c^*|3q\rangle + \cdots$, are unknown. We determine these weights by fitting to experimental amplitudes at $Q^2 = 2$–3 GeV^2, assuming that at these Q^2 the transition amplitudes are dominated by the $3q$-core contributoin, as is the case for the nucleon. Then we predict the transition amplitudes at higher Q^2 (see Figs. 50–53).

As it is shown in Refs. 337 and 338, there are difficulties in the utilization of the LF approaches[28,330,331,339,340] for the hadrons with spins $J \geq 1$. These difficulties can be avoided if Eq. (32) is used to calculate only those matrix elements that correspond to $S'_z = J$.[337] This restricts the number of transition form-factors that can be calculated for the resonances $\Delta(1232)P_{33}$ and $N(1520)D_{13}$, and only two transition form-factors can be investigated for these resonances: $G_1(Q^2)$ and $G_2(Q^2)$ (the definitions can be found in review[6]). For these resonances we can not present the results for the transition helicity amplitudes. The results for the resonances with $J = \frac{1}{2}$: $N(1440)P_{11}$ and $N(1535)S_{11}$, are presented in terms of the transition helicity amplitudes.

8.3.5. *Discussion*

The important feature of the obtained predictions for the resonances is the fact that at $Q^2 > 2$–3 GeV^2 both investigated amplitudes for each resonance are

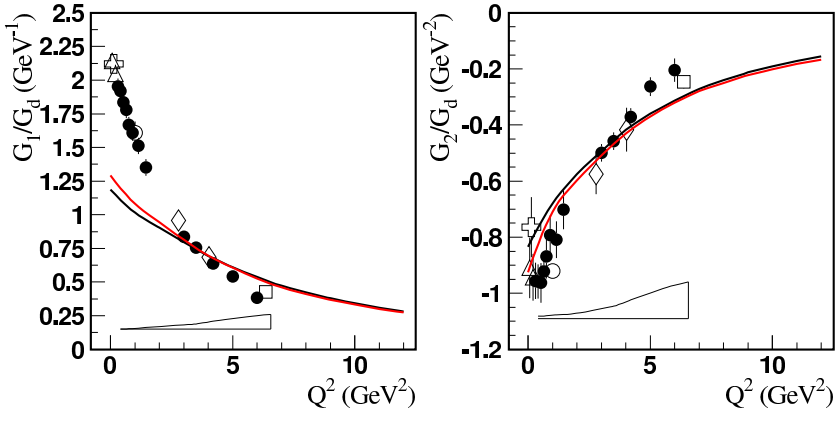

Fig. 50. (Color online) The $\gamma^* p \to \Delta(1232)\mathrm{P}_{33}$ transition form-factors; $G_1(Q^2) \sim G_M - G_E$. Weight factors are $c^{(1)}_{N^*} = 0.67 \pm 0.04$ and $c^{(2)}_{N^*} = 0.72 \pm 0.04$ for the wave functions Φ_1 (black curves) and Φ_2 (red curves) in Eq. (41). Solid circles correspond to the amplitudes extracted from the CLAS data by JLab group,[19] bands represent model uncertainties of these results. The results from other experiments are: open triangles;[288–290] open crosses;[291–293] open rhombuses;[294] open boxes;[295] and open circles.[296,297]

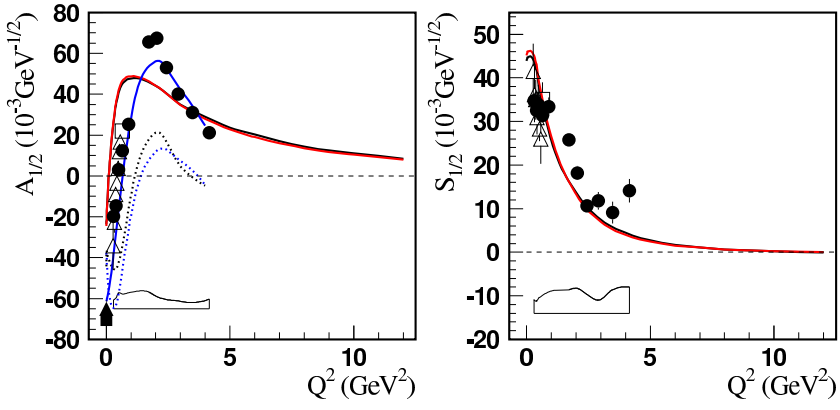

Fig. 51. (Color online) The $\gamma^* p \to N(1440)\mathrm{P}_{11}$ transition amplitudes. Blue lines correspond to the MAID results.[298,299] Dotted curves are estimated pion-cloud contributions. $c^{(1)}_{N^*} = 0.73 \pm 0.05$, $c^{(2)}_{N^*} = 0.77 \pm 0.05$. The open triangles correspond to the amplitudes extracted from CLAS 2π electroproduction data.[41] Other legend is as for Fig. 50.

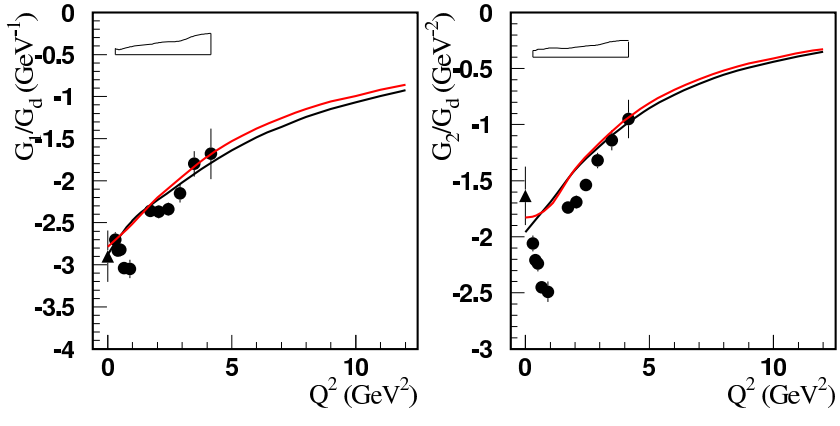

Fig. 52. (Color online) The $\gamma^* p \to N(1520)\mathrm{D}_{13}$ transition form-factors; $G_1(Q^2) \sim A_{1/2} - A_{3/2}/\sqrt{3}$. $c^{(1)}_{N^*} = 0.78 \pm 0.06$, $c^{(2)}_{N^*} = 0.82 \pm 0.06$. Other legend is as for Fig. 50.

described well by the $3q$ contribution by fitting the only parameter, that is the weight of this contribution to the resonance. These predictions need to be checked at higher Q^2.

The results for the resonances allow us also to make conclusions on the size and form of expected pion-cloud and/or meson–baryon contributions to the amplitudes. According to our predictions for the $3q$ contributions, one can expect that pion-cloud contributions to the form-factor $G_2(Q^2)$ for the $\Delta(1232)P_{33}$, to $S_{1/2}$ amplitude for the $N(1440)P_{11}$, and to the form-factor $G_1(Q^2)$ for the $N(1520)D_{13}$ are small. Large contributions are expected to the longitudinal amplitude for the $N(1535)S_{11}$ and to the form-factor $G_2(Q^2)$ for the $N(1520)D_{13}$. The expected pion-

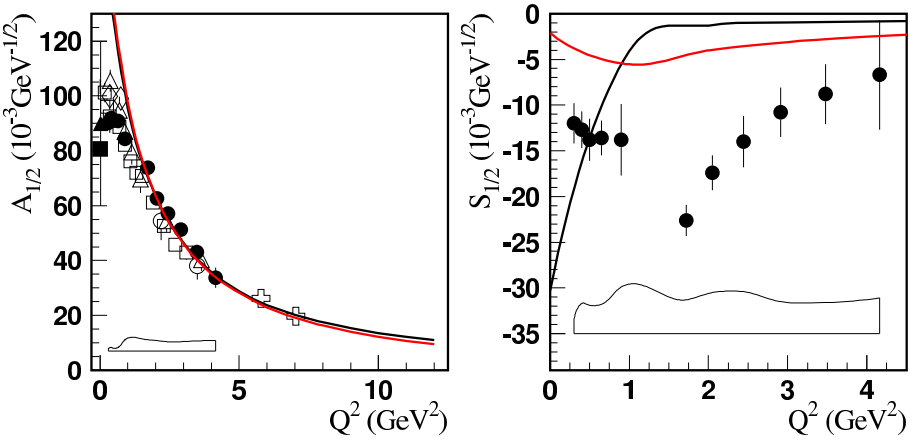

Fig. 53. (Color online) The $\gamma^* p \to N(1535)S_{11}$ transition amplitudes. The amplitudes extracted from the CLAS and JLab/Hall C data on $ep \to e\eta p$ are: the stars,[55] the open boxes,[9] the open circles,[56] the crosses,[57] and the rhombuses.[19,40] $c^{(1)}_{N^*} = 0.88 \pm 0.03$, $c^{(2)}_{N^*} = 0.94 \pm 0.03$. Other legend is as for Fig. 50.

cloud contributions to the form-factor $G_1(Q^2)$ for the $\Delta(1232)P_{33}$ and to $A_{1/2}$ amplitude for the $N(1535)S_{11}$ have Q^2 behavior similar to that in the nucleon form-factors $G_{Mp(n)}(Q^2)$. In Fig. 51, by dotted curves, we show estimated pion-cloud contribution to $A_{1/2}$ amplitude for the Roper resonance. It can be seen that nontrivial Q^2-dependence of this contribution can be expected.

The remarkable feature that follow from the description of the nucleon EM form-factors in our approach is the decreasing quark mass with increasing Q^2. This is in qualitative agreement with the QCD lattice calculations and with Dyson–Schwinger equations[35,36,341] where the running quark mass is generated dynamically. The mechanism that generates the running quark mass can generate also the quark anomalous magnetic moments and form-factors. This should be incorporated in model calculations. Introducing quark form-factors will cause a faster Q^2 fall-off of EM form-factors in quark models. This will force $m_q(Q^2)$ to drop faster with Q^2 to describe the data.

8.4. *Constituent quark models and the interpretation of the nucleon form-factors*

Various CQMs have been proposed in the past decades after the pioneering work of Isgur and Karl (IK).[95] Among them, let us quote the relativized Capstick–Isgur (CI) model,[96] the algebraic approach (BIL),[342] the hypercentral CQM (hCQM),[343] the chiral Goldstone Boson Exchange model[98] (χCQM) and the Bonn instanton (BN) model.[344,345] They are all able to fairly reproduce the baryon spectrum, which is the first test to be performed before applying any model to the description of other baryon properties. The models, although different, have a simple general structure,

Table 4. Illustration of the features of various CQMs.

CQM	Kin. Energy	$V_{\rm inv}$	$V_{\rm sf}$	Ref.
Isgur–Karl	Nonrel.	h.o. + shift	OGE	95
Capstick–Isgur	Rel.	string +coul-like	OGE	96
$U(7)$ BIL	Rel. M^2	vibr + L	Gürsey-Rad	342
Hypercentral G.S.	Nonrel./rel.	$O(6)$: lin + hyp.coul	OGE	343
Glozman–Riska	Rel.	h.o./linear	GBE	98
Bonn	Rel.	linear + 3 body	instanton	344

since, according to the prescription provided by the early LQCD calculations,[346] the three-quark interaction V_{3q} is split into a spin-flavor independent part $V_{\rm inv}$, which is SU(6)-invariant and contains the confinement interaction, and a SU(6)-dependent part $V_{\rm sf}$, which contains spin and eventually flavor dependent interactions

$$V_{3q} = V_{\rm inv} + V_{\rm sf}\,. \tag{45}$$

In Table 4, a summary of the main features of various CQMs reported.

After having checked that these models provide a reasonable description of the baryon spectrum, they have been applied to the calculation of many baryon properties, including electrocouplings. One should however not forget that in many cases the calculations referred to as CQM calculations are actually performed using a simple h.o. wave function for the internal quark motion either in the nonrelativistic (HO) or relativistic (relHO) framework. The former (HO) applies to the calculations of Refs. 347 and 335, while the latter (relHO) is valid for Ref. 28. The relativized CI model of Ref. 96 is used for a systematic calculation of the transition amplitudes in Ref. 348 and, within a LF approach in Refs. 349 and 165 for the transitions to the Δ and Roper resonances respectively. In the algebraic approach,[342] a particular form of the charge distribution along the string is assumed and used for both the elastic and transition form-factors; the elastic form-factors are fairly well reproduced, but there are problems with the transition amplitudes, specially at low Q^2. There is no helicity amplitude calculation with the GBE model, whereas the BN model has been also used for the helicity amplitudes,[350] with particular attention to the strange baryons.[351] Finally, the hCQM has produced predictions for the transverse excitation of the negative parity resonances[30] and also for the main resonances, both for the longitudinal and transverse excitation.[352]

In some recent approaches, the CQ idea is used to derive relations between the various EM form-factors, relations which, after having fitted one selected quantity, say the elastic proton form-factor (Sec. 8.3.2) or the helicity amplitude at intermediate Q^2 (Sec. 8.3.3), are used to predict the other quantities of interest. A remarkable prediction of both the proton elastic form-factor and the proton transition to the Roper resonance is provided by the LF holographic approach (Sec. 8.3.4).

The works briefly illustrated above have shown that the three-quark idea is able to fairly reproduce a large variety of observables, in particular the helicity amplitudes at medium Q^2, however, a detailed comparison with data shows that,

besides the fundamental valence quarks, other issues are or presumably will be of relevant importance for the interpretation of the transition amplitudes. These issues are: relativity, meson–cloud and quark–antiquark pair effects, and quark form-factors.

A consistent relativistic treatment is certainly important for the description of the elastic nucleon form-factors. In fact, in the nonrelativistic hCQM,[343] the proton radius compatible with the spectrum is too low, about 0.5 fm, and the resulting form-factors[353] are higher than data. However, the introduction of the Lorentz boosts improves the description of the elastic form-factors[353] and determines a ratio $\mu_p G_e^p/G_M^p$ lower than 1.[354] Using a relativistic formulation of the hCQM in the point form approach, in which again the unknown parameters are fitted to the spectrum, the predicted elastic nucleon form-factors are nicely close to data.[315] Furthermore, if one introduces quark form-factors, an accurate description of data is achieved.[315] Since such form-factors are fitted, this means that they contain, in an uncontrolled manner, all the missing contributions.

Applying hCQM to the excitation of higher resonances demonstrated that the inclusion of relativity is less crucial, since the Lorentz boosts affect only slightly the helicity amplitudes.[355] A quite different situation occurs for the excitation to the Δ, which is a spin–isospin excitation of the nucleon and as such it shares with the nucleon the spatial structure. In this case, relativity is certainly important, however it does not seem to be sufficient even within LF approaches. In fact, the good results of the Rome group[349] are obtained introducing quark form-factors, while in Sec. 8.3.2 the quark wave function fitted to the elastic nucleon form-factor leads to a lack of strength at low Q^2 in the Δ excitation. In Sec. 8.3.3, a pion-cloud term is present from the beginning in the nucleon form-factor, nevertheless the transition to the Δ is too low at low Q^2.

Of course, the future data at high Q^2 will force, at least for consistency reasons, to use a relativistic approach also for the other resonances.

At medium-low Q^2 the behavior of the helicity amplitudes is often described quite well, also in a nonrelativistic approach.[352] An example is provided in Fig. 54, where the hCQM results are compared with the more recent JLab data. In Fig. 54, there are also the h.o. results, which do not seem to be able to reproduce the data. The good agreement achieved by the hCQM has a dynamical origin. Let us remind that in hCQM the SU(6)-invariant part of the quark potential of Eq. (45) is

$$V_{\rm inv}^{\rm hCQM} = -\frac{\tau}{x} + \alpha x\,. \tag{46}$$

($x = \sqrt{\rho^2 + \lambda^2}$ is the hyperradius) however the main responsible of the medium–high Q^2 behavior of the helicity amplitudes is the hypercoulomb interaction $-\frac{\tau}{x}$. In fact, in the analytical version of hCQM presented in Ref. 356, it is shown that the helicity amplitudes provided by the $-\frac{\tau}{x}$ term are quite similar to the ones calculated with the full hCQM.

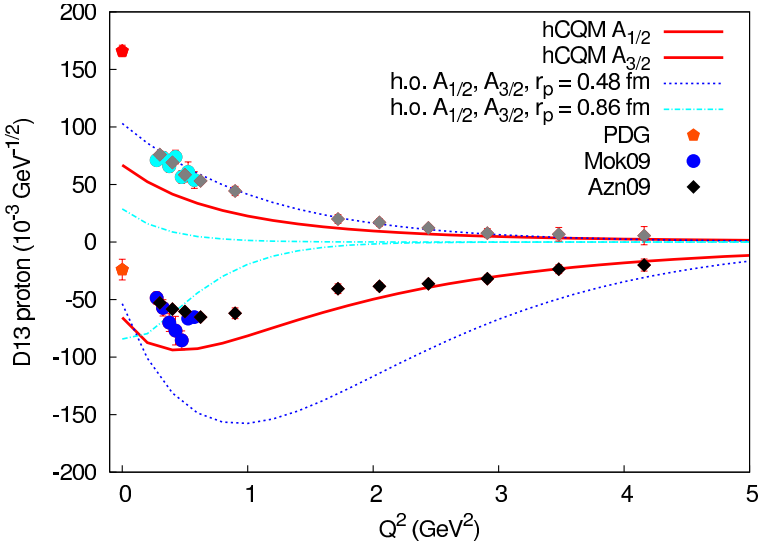

Fig. 54. (Color online) The $D_{13}(1520)$ helicity amplitudes $A_{3/2}$ (upper part) and $A_{1/2}$ (lower part) predicted by the hCQM (full curves), in comparison with the data of Refs. 19, 20 and 41 and the PDG values[4] at the photon point. The h.o. results for two different values of the proton r.m.s. radius (0.5 fm and 0.86 fm) are also shown.

The main problem with the description provided by CQM (nonrelativistic or relativistic) is the lack of strength at low Q^2, which is attributed, with general consensus, to the missing meson–cloud or quark–antiquark pair effects.[25,30,60,65] In fact, it has been shown within a dynamical model[25,60,65] that the meson–cloud contributions are relevant at low Q^2 and tend to compensate the lack of strength of quenched three-quark models.[357]

To conclude, a fully relativistic and unquenched hCQM is not yet available and work is now in progress in this direction, but certainly it will be a valuable tool for the interpretation of the helicity amplitudes at high Q^2.

However, also taking into account the one pion contribution there seems to be some problem. In Sec. 8.3.2, the quark wave function is chosen in order to reproduce the proton form-factor, in this way all possible extra contributions (meson–cloud, quark form-factors, ...) are implicitly included, but the description of the $N - \Delta$ transition needs an extra pion term. On the other hand, in Sec. 8.3.3 it is shown that the pion term explicitly included in the fit to the proton is not sufficient for the description of the $N - \Delta$ transition. In fact, the inclusion of a pion-cloud term, either fitted or calculated (e.g., as in Ref. 358) seems to be too restrictive, since it is equivalent to only one quark–antiquark configuration. If one wants to include consistently all quark–antiquark effects, one has to proceed to unquenching the CQM, as it has been done in Ref. 359. Such an unquenching is achieved by summing over all quark loops, that is over all intermediate meson–baryon states; the sum is in particular necessary in order to preserve the OZI rule.

This unquenching has been recently performed also for the baryon sector.[360] The state for a baryon A is written as

$$|\Psi_A\rangle = N\left[|A\rangle + \sum_{BClj}\int d\mathbf{k}|BC|\mathbf{k}lJ\rangle\frac{\langle BC\mathbf{k}lJ||T^\dagger|A\rangle}{M_A - E_B - E_C}\right], \tag{47}$$

where $B(C)$ is any intermediate baryon (meson), $E_B(E_C)$ are the corresponding energies, M_A is the baryon mass, $T^\dagger$ is the $^3P_0$ pair creation operator and $\mathbf{k}$, $\mathbf{l}$ and $\mathbf{J}$ are the relative momentum, the orbital and total angular momentum, respectively. Such unquenched model, with the inclusion of the quark–antiquark pair creation mechanism, will allow to build up a consistent description of all the baryon properties (spectrum, form-factors, etc.). There are already some applications,[360–362] in particular it has been checked that, thanks to the summation over all the intermediate states described in Eq. (47), the good reproduction of the baryon magnetic moments provided by the CQM is preserved after renormalization.[360] Using an interaction containing the quark–antiquark production the resonances acquire a finite width, at variance with what happens in all CQMs, allowing a consistent description of both EM and strong vertices.

The structure of the state in Eq. (47) is more general than the one containing a single pion contribution. The influence of the quark–antiquark cloud will be certainly important at low Q^2, but one can also expect that the multiquark components, which are mixed with the standard $3q$ states as in Eq. (47), may have a quite different behavior[363–365] in the medium–high Q^2 region, leading therefore to some new and interesting behavior also at short distances. Actually, there are some clues that this may really happen. First, it has been shown in Ref. 19 that the quantity $Q^3A^p_{1/2}$ seems to become flat in the range around 4 GeV^2 (see Fig. 5), while the CQM calculations do not show any structure.

A second important issue is the ratio $R_p = \mu_p G^p_e/G^p_M$ between the proton form-factors. A convenient way of understanding its behavior is to consider the ratio $Q^2F^p_2/F^P_1$, which is expected to saturate at high Q^2,[366,367] while it should pass through the value $4M^2_p/\kappa_p$ in correspondence of a zero for R_p.[368] The predictions of the hCQM[315] are compared with the JLab data[279,280,369–372] in Fig. 55. For a pure three-quark state, even in presence of quark form-factors as in Ref. 315 the occurrence of a zero seems to be difficult, while an interference between three- and multi-quark configurations may be a possible candidate for the generation of a dip in the electric form-factors.[368]

It is interesting to note that the interacting quark–diquark model introduced in Ref. 373 and its relativistic reformulation Ref. 374, both of which do not exhibit missing states in the nonstrange sector under 2 GeV^2, give rise to a ratio $R = \mu_p G^p{}_E/G^p{}_M$ that goes through a zero at around 8 GeV^2 after the introduction of quark form-factors, as calculated in Ref. 375.

Once the quark–antiquark pair creation effects have been included consistently in the CQM, it will be possible to disentangle the quark forms-factors from the

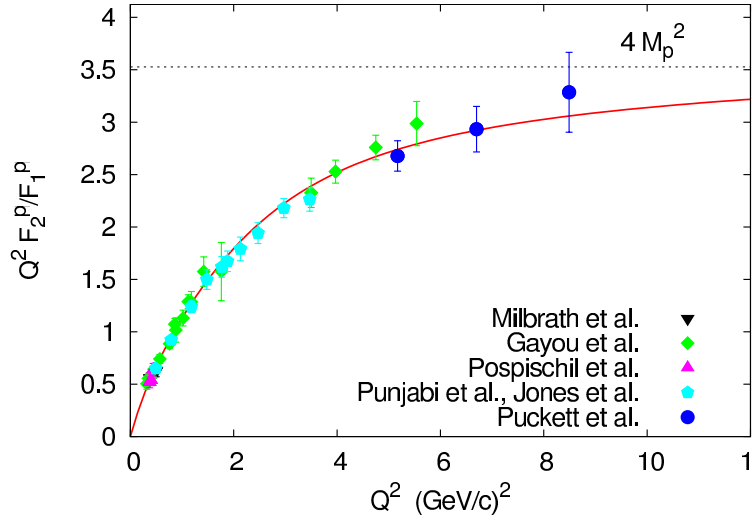

Fig. 55. (Color online) The ratio F_p at high Q^2 calculated using the theoretical form-factors of Ref. 315.

other dynamic mechanisms. The presence of structures with a finite dimension has been shown in a recent analysis of deep inelastic electron–proton scattering.[376]

9. Conclusions and Outlook

Studying $\gamma_v N N^*$ electrocouplings gives insight into the relevant degrees of freedom of the baryon structure and its evolution with distance. The CLAS 6 GeV program has already provided information on the transition in the N^* structure from a superposition of meson–baryon and quark degrees of freedom to a quark-core dominance. The approved experiment, Nucleon resonance studies with CLAS12,[18] will run within the first year following the commissioning of the CLAS12 detector in Hall B of JLab. This experiment seeks to extract all prominent excited state electrocouplings by analyzing all the major exclusive meson electroproduction channels, including $\pi^+ n$, $\pi^0 p$, and $\pi^+\pi^- p$, in the almost unmeasured Q^2 region of 5–12 GeV^2, and, as in the 6-GeV program, we expect high-quality electrocoupling results for all prominent N^*s. As delineated in this paper, there are plans to develop advanced reaction models to reliably extract the $\gamma_v p N^*$ electrocouplings in this unexplored range of photon virtualities. These models will explicitly take into account the contributions from quark–gluon degrees of freedom, and will be extended in scope to incorporate the ηp and KY exclusive channels. The evaluation of the resonance electrocouplings can also ensue from the less constrained semi-inclusive meson electroproduction data, as soon as reliable modeling of nonresonant contributions to πs and ηs in semi-inclusive electroproduction becomes available.

The 12-GeV N^* program, with the highest Q^2 reach worldwide, will allow direct access to quarks decoupled from the meson–baryon cloud and to the evolution of

quark and gluon interactions with distance that are ultimately responsible for the formation of the excited states. These nucleon resonances have larger transverse sizes in comparison with the ground nucleon states. Data on the electrocouplings of excited proton states will enable exploration of the nonperturbative interactions at larger transverse separations between quarks, which are especially sensitive to the nonperturbative contributions to baryon structure. Systematic studies of $\gamma_v NN^*$ electrocouplings at high photon virtualities are key in accessing the very essence of the strong interaction in the nonperturbative regime; that is, the region where the active degrees of freedom in hadron structure, along with their interactions, become very different from those of current quarks, gluons, and their interactions, as described in the perturbative expansion of the QCD Lagrangian. This is the unique feature of the strong interaction evolution with distance that shapes the structure of hadronic matter.

The data expected from the CLAS12 N^* experiment[18] will make possible the study of the kinematic regime of momenta $0.5 < p < 1.1$ GeV running over the dressed quark propagator, where $p = \sqrt{Q^2}/3$. This kinematic region spans the transition from the almost-completely dressed constituent quarks to the almost-completely undressed current quarks. The $\gamma_v pN^*$ electrocouplings will be sensitive to the transition from the confinement regime of strongly bound dressed quarks and gluons at small momenta, $p < 0.5$ GeV, to the pQCD regime for $p > 2$ GeV, where almost-undressed and weakly-interacting current quarks and gluons gradually emerge as the relevant degrees of freedom in resonance structure with increasing Q^2. The momentum dependence of the dressed quark mass should affect all dressed quark propagators and therefore the Q^2 evolution of $\gamma_v NN^*$ electrocouplings. Virtual photon interactions with the dressed quark EM current should thus be sensitive to the dynamical structure of dressed quarks, including spin and helicity-flip dependent parts of the dressed quark EM current that is generated nonperturbatively through DCSB. The dressed quark dynamical structure and its mass function should be practically independent of the excited state quantum numbers. Therefore, the combined physics analyses of the data on electrocouplings of several prominent N^* states will considerably improve our knowledge of the momentum dependence of dressed quark masses and their dynamical structure.

The theoretical interpretation of experimental results on resonance electrocouplings will be a critical component of the successful realization of the CLAS12 N^* program. QCD-based approaches, as well as more model-dependent frameworks, will be important for examining the capability of QCD as the fundamental theory of strong interactions in describing the full complexity of nonperturbative processes, which generate all N^* states from quarks and gluons through the strong interaction.

LQCD results on electrocouplings of prominent N^* states can be directly compared with their values determined from experimental data analyses, offering a unique way to explore the capability of this method in describing the nonperturbative QCD interactions responsible for the generation of N^* states with

different quantum numbers. LQCD methods will be further developed to provide reliable evaluations of $\gamma_v NN^*$ electrocouplings employing a realistic basis of projection operators, approaching the physical pion mass, and carried out in boxes that fully include the physics of the pion cloud. Available analyses from CLAS experimental results on $\gamma_v pN^*$ electrocouplings[19,20] allow one to develop and cross check LQCD simulations in the regime of small and intermediate photon virtualities, $Q^2 < 5$ GeV^2. The extension of LQCD calculations to higher Q^2 (up to $Q^2 = 12$ GeV^2) represents an important additional challenge.

The Dyson–Schwinger equation of QCD allows for mapping out the momentum dependence of the dressed quark running mass, structure, and nonperturbative interaction from the data on excited nucleon electrocouplings, such for the Q^2 evolution of $P_{11}(1440)$ state. Since DSEQCD can currently only describe the quark-core contribution, these predictions will be compared with the experimental data at large photon virtualities, $Q^2 > 5$ GeV^2, where the quark degrees of freedom are expected to dominate resonance structure. Analyses of the future data on $\gamma_v NN^*$ electrocouplings expected from CLAS12 within this approach will provide the first pieces of information on the generation of the dominant part of N^* masses through dynamical chiral symmetry breaking, and will allow one to explore how confinement in baryons emerges from the pQCD regime. Experiments, coupled with theoretical studies, therefore lay out an ambitious program to map out the momentum-dependent dressed quark mass function and thereby seek evidence for how dynamical chiral symmetry breaking generates more than 98% of baryon masses and to explore the nature of confinement in baryons.

In conjunction with LQCD and DSEQCD, the LF sum rule approach opens up prospects for constraining quark distribution amplitudes for various N^* states from the data on $\gamma_v pN^*$ electrocouplings, thereby offering access to the partonic degrees of freedom in excited nucleons for the first time. This approach can be employed and tested in analyses of available CLAS data on $\gamma_v NN^*$ electrocouplings for Q^2 from 2 GeV^2 to 5 GeV^2. After that, it is straightforward to use this approach for accessing the partonic degrees of freedom in the N^* structure at high photon virtualities up to 12 GeV^2 in the analyses of future results from CLAS12. These studies will provide important information for an extension of GPDs to the transition GPDs from ground to excited nucleon states.

Theory and experiment go hand in hand and all these studies of the structure of excited nucleons will further refine the quark models of the N^* structure. The AdS/QCD LF holographic approach is particularly intriguing for nucleon and nucleon resonance physics. This nonperturbative model predicts both hadron dynamics as well as spectroscopy, accounting for elastic and transition form-factors and the overall characteristics of the complete nucleon resonance spectrum, based on one mass scale parameter κ^2. The AdS/QCD LF holographic model is confining, satisfies chiral invariance, and agrees with quark counting rules at high Q^2. It also predicts nonzero quark orbital angular momentum and the frame-independent LF wave functions underlying many hadron observables. The form of the color-confining

potential is uniquely determined by general arguments based on chiral symmetry and conformal invariance.[377] The formalism is extended to hadrons of general spin in Ref. 378. Despite the shortcomings of quark models in not being directly related (according to our currently understanding) to the QCD Lagrangian, they offer very useful phenomenological tools for analyses of the experimental results on the structure of all excited nucleon states predicted by these models. We expect that analyses of resonance electrocouplings within the framework of quark models will provide important information for a QCD-based theory of hadron structure. As an example, the first encouraging attempt to observe the manifestation of the momentum dependence of the dressed quark mass and structure was undertaken in interpreting the low-lying resonance electrocouplings within the framework of the LF quark model.[174] Finally, from a more phenomenological perspective, a better understanding of quark–hadron duality in exclusive reactions holds the prospect of utilizing information on the N^* resonance structure to constrain the behavior of exclusive processes at higher energies, in kinematic regions difficult to access experimentally. Conversely, the details of the quark–hadron transition can be tested by comparing the future CLAS12 N^* data with results of quark–gluon calculations extrapolated into the low-W region.

Understanding the underlying structure of the proton and neutron is of primary importance to the 12 GeV upgrade for JLab. Detailed information on the structure of the ground nucleon states in terms of different partonic structure functions, including access to the structure in three-dimensions expected from results on GPDs and transverse momentum dependent distribution functions is the driving component of the physics program. Nonetheless, all these studies together still mark only the first step in the exploration of nucleon structure as they are limited to studying the ground state of the nucleon. Nonperturbative QCD interactions generate both the ground and excited nucleon states, thereby manifesting themselves differently in the case of excited states with their different quantum numbers. Comprehensive information on the ground state nucleon structure must therefore be extended with the results on transition $\gamma_v NN^*$ electrocouplings. This will provide deeper insights into the essence of the nonperturbative strong interactions responsible for the formation of ground and excited nucleon states from quarks and gluons, and their emergence from QCD. These studies will allow us to finally answer the central and most challenging questions in present-day hadron physics: (a) how more than 98% of hadron masses are generated nonperturbatively; (b) how quark and gluon confinement and dynamical chiral symmetry breaking emerge from QCD; and (c) how the nonperturbative strong interaction generates the ground and excited nucleon states with various quantum numbers from quarks and gluons.

Acknowledgments

The authors thank B. Juliá-Díaz, H. Kamano, A. Matsuyama, S. X. Nakamura, T. Sato, and N. Suzuki for their collaborations at EBAC, and would also like to thank M. Pennington and A. W. Thomas for their strong support and many

constructive discussions. We also acknowledge valuable discussions with S.-X. Qin, H. L. L. Roberts and P. C. Tandy, and thank the University of South Carolina for their support of the most recent EmNN* 2012 Workshop. This work is supported by the U.S. National Science Foundation udner Grants NSF-PHY-0856010, NSF-PHY-0903991, and NSF-PHY-1206082, and U.S. Department of Energy, Office of Nuclear Physics Division, under Contract No. DE-AC02-76SF00515, DE-AC02-06CH11357 and DE-AC05-06OR23177 under which Jefferson Science Associates operates the JLab, European Union under the HadronPhysics3 Grant No. 283286, Fundação para a Ciência e a Tecnologia under Grant No. SFRH/BPD/26886/2006 and PTDC/FIS/113940/2009, *Programa de Cooperación Bilateral México-Estados Unidos* CONACyT Project 46614-F, Coordinación de la Investigación Científica (CIC) Project No. 4.10, Forschungszentrum Jülich GmbH, the University of Adelaide and the Australian Research Council through Grant No. FL0992247, and Fundação de Amparo à Pesquisa do Estado de São Paulo, Grant No. 2009/51296-1 and 2010/05772-3. This research used resources of the National Energy Research Scientific Computing Center, which is supported by the Office of Science of the U.S. Department of Energy under Contract No. DE-AC02-05CH11231, resources provided on "Fusion," a 320-node computing cluster operated by the Laboratory Computing Resource Center at Argonne National Laboratory, and resources of Barcelona Sucpercomputing Center (BSC/CNS).

References

1. V. D. Burkert, *EPJ Web Conf.* **37** (2012) 01017, arXiv:1209.2402 [nucl-ex].
2. E. Klempt, Hadron Spectroscopy, Results and Ideas, arXiv:1207.1601 [hep-ph].
3. A. V. Anisovich *et al.*, *Eur. Phys. J. A* **48** (2012) 15, arXiv:1112.4937 [hep-ph].
4. Particle Data Group (J. Beringer *et al.*), *Phys. Rev. D* **86** (2012) 010001.
5. I. Aznauryan, V. D. Burkert, T.-S. H. Lee and V. I. Mokeev, *J. Phys. Conf. Ser.* **299** (2011) 012008, arXiv:1102.0597 [nucl-ex].
6. I. G. Aznauryan and V. D. Burkert, *Prog. Part. Nucl. Phys.* **67** (2012) 1, arXiv:1109.1720 [hep-ph].
7. CLAS Collaboration (M. Ripani *et al.*), *Phys. Rev. Lett.* **91** (2003) 022002, arXiv:hep-ex/0210054.
8. CLAS Collaboration (G. Fedotov *et al.*), *Phys. Rev. C* **79** (2009) 015204, arXiv:0809.1562 [nucl-ex].
9. CLAS Collaboration (H. Denizli *et al.*), *Phys. Rev. C* **76** (2007) 015204, arXiv:0704.2546 [nucl-ex].
10. CLAS Collaboration (D. Carman *et al.*), *Phys. Rev. C* **79** (2009) 065205, arXiv:0904.3246 [hep-ex].
11. CLAS Collaboration (P. Ambrozewicz *et al.*), *Phys. Rev. C* **75** (2007) 045203, arXiv:hep-ex/0611036.
12. V. Burkert, M. Jones, M. Pennington and D. Richards (eds.), The physics of excited nucleons, *Proc. 8th Int. Workshop NSTAR 2011*, Newport News, USA (May 17–20, 2011).
13. C. Roberts, *AIP Conf. Proc.* **1432** (2012) 19, arXiv:1108.1030 [nucl-th].
14. J. J. Dudek and R. G. Edwards, *Phys. Rev. D* **85** (2012) 054016, arXiv:1201.2349 [hep-ph].

15. R. W. Gothe, *AIP Conf. Proc.* **1432** (2012) 26, arXiv:1108.4703 [nucl-ex].
16. I. Aznauryan *et al.*, Theory Support for the Excited Baryon Program at the Jlab 12 GeV Upgrade, arXiv:0907.1901 [nucl-th].
17. G. F. de Teramond and S. J. Brodsky. Hadronic Form Factor Models and Spectroscopy Within the Gauge/Gravity Correspondence, arXiv:1203.4025 [hep-ph].
18. R. W. Gothe *et al*, Nucleon Resonance Studies with CLAS12, in *JLab Experiment E12-09-003*, www.jlab.org/exp_prog/12GEV_EXP.
19. CLAS Collab. (I. Aznauryan *et al.*), *Phys. Rev. C* **80** (2009) 055203, arXiv:0909.2349 [nucl-ex].
20. CLAS Collab. (V. Mokeev *et al.*), *Phys. Rev. C* **86** (2012) 035203, arXiv:1205.3948 [nucl-ex].
21. I. Aznauryan, V. Burkert and V. Mokeev, *AIP Conf. Proc.* **1432** (2012) 68, arXiv:1108.1125 [nucl-ex].
22. H. Kamano, PoS **QNP2012** (2012) 011, arXiv:1206.3374 [nucl-th].
23. N. Suzuki, T. Sato and T.-S. Lee, *Phys. Rev. C* **82** (2010) 045206, arXiv:1006.2196 [nucl-th].
24. V. D. Burkert, The JLab 12GeV Upgrade and the Initial Science Program, arXiv:1203.2373 [nucl-ex].
25. L. Tiator, D. Drechsel, S. Kamalov and M. Vanderhaeghen, *Eur. Phys. J. ST* **198** (2011) 141, arXiv:1109.6745 [nucl-th].
26. CLAS Collab. (M. Dugger *et al.*), *Phys. Rev. C* **79** (2009) 065206, arXiv:0903.1110 [hep-ex].
27. I. Aznauryan, *Phys. Rev. C* **76** (2007) 025212, arXiv:nucl-th/0701012.
28. S. Capstick and B. Keister, *Phys. Rev. D* **51** (1995) 3598, arXiv:nucl-th/9411016.
29. B. Julia-Diaz, T.-S. Lee, A. Matsuyama, T. Sato and L. Smith, *Phys. Rev. C* **77** (2008) 045205, arXiv:0712.2283 [nucl-th].
30. M. Aiello, M. Giannini and E. Santopinto, *J. Phys. G* **24** (1998) 753, arXiv:nucl-th/9801013.
31. *Electromagnetic N–N^* Transition Form Factors Workshop*, Newport News, USA (October 13–15, 2008), www.jlab.org/conferences/EmNN.
32. *Nucleon Resonance Structure in Exclusive Electroproduction at High Photon Virtualities Workshop*, Newport News, USA (May 16, 2011), www.jlab.org/conferences/electroproduction/index.html.
33. *Nucleon Resonance Structure in Exclusive Electroproduction at High Photon Virtualities Workshop*, University of South Carolina, Columbia, South Carolina, USA (August 13–15, 2012), http://www.jlab.org/conferences/EmNN2012/.
34. H.-W. Lin and S. D. Cohen, *AIP Conf. Proc.* **1432** (2012) 305, arXiv:1108.2528 [hep-lat].
35. P. O. Bowman *et al.*, *Phys. Rev. D* **71** (2005) 054507, arXiv:hep-lat/0501019.
36. M. Bhagwat and P. Tandy, *AIP Conf. Proc.* **842** (2006) 225, arXiv:nucl-th/0601020.
37. C. Roberts, *Prog. Part. Nucl. Phys.* **61** (2008) 50, arXiv:0712.0633 [nucl-th].
38. C. Chen, L. Chang, C. D. Roberts, S. Wan and D. J. Wilson, *Few Body Syst.* **53** (2012) 293, arXiv:1204.2553 [nucl-th].
39. I. Aznauryan, *Phys. Rev. C* **67** (2003) 015209, arXiv:nucl-th/0206033.
40. I. Aznauryan *et al.*, *Phys. Rev. C* **71** (2005) 015201, arXiv:nucl-th/0407021.
41. V. I. Mokeev *et al.*., *Phys. Rev. C* **80** (2009) 045212, arXiv:0809.4158 [hep-ph].
42. R. A. Arndt, J. M. Ford and L. D. Roper, *Phys. Rev. D* **32** (1985) 1085.
43. R. Arndt, W. Briscoe, I. Strakovsky and R. Workman, *Phys. Rev. C* **74** (2006) 045205, arXiv:nucl-th/0605082.
44. R. Walker, *Phys. Rev.* **182** (1969) 1729.

45. M. Guidal, J. Laget and M. Vanderhaeghen, *Nucl. Phys. A* **627** (1997) 645.
46. M. Guidal, J. Laget and M. Vanderhaeghen, *Phys. Lett. B* **400** (1997) 6.
47. CLAS Collaboration (K. Park *et al.*), *Phys. Rev. C* **77** (2008) 015208, arXiv:0709.1946 [nucl-ex].
48. V. I. Mokeev, in *Proc. 11th Workshop on the Physics of Excited Nucleons NSTAR2007*, eds. H.-W. Hammer, V. Kleber, U. Thoma and H. Schmieden (Springer, 2008), p. 76.
49. I. Aitchison, *Nucl. Phys. A* **189** (1972) 417.
50. M. Ripani *et al.*, *Nucl. Phys. A* **672** (2000) 220, arXiv:hep-ph/0001265.
51. V. Burkert *et al.*, *Phys. Atom. Nucl.* **70** (2007) 427.
52. V. Mokeev *et al.*, Phenomenological analysis of the clas data on double charged pion photo and electro-production, in *Proc. of NSTAR2005 Conf.*, Florida (2005), p. 47, arXiv:hep-ph/0512164.
53. I. Aitchison and J. Brehm, *Phys. Rev. D* **17** (1978) 3072.
54. V. I. Mokeev. "N^* electrocouplings and $N\pi\pi$ hadronic decay widths from phenomenological analysis of the CLAS $\pi^+\pi^-p$ electroproduction data," Invited talk at *Sixth International Workshop on Pion-Nucleon Partial-Wave Analysis and the Interpretation of Baryon Resonances*, Washington, DC, USA (May 23–27, 2011), wdac.phys.gwu.edu/pwa2011/PWAhome.htm.
55. CLAS Collab. (R. Thompson *et al.*), *Phys. Rev. Lett.* **86** (2001) 1702, arXiv:hep-ex/0011029.
56. Jefferson Lab E94014 Collab. (C. Armstrong *et al.*), *Phys. Rev. D* **60** (1999) 052004, arXiv:nucl-ex/9811001.
57. M. Dalton *et al.*, *Phys. Rev. C* **80** (2009) 015205, arXiv:0804.3509 [hep-ex].
58. V. Burkert, R. De Vita, M. Battaglieri, M. Ripani and V. Mokeev, *Phys. Rev. C* **67** (2003) 035204, arXiv:hep-ph/0212108.
59. H. Kamano and T.-S. Lee, *AIP Conf. Proc.* **1432** (2012) 74, arXiv:1108.0324 [nucl-th].
60. S. Krewald, *AIP Conf. Proc.* **1432** (2012) 39.
61. T. Sato, *AIP Conf. Proc.* **1432** (2012) 45.
62. A. Matsuyama, T. Sato and T.-S. Lee, *Phys. Rept.* **439** (2007) 193, arXiv:nucl-th/0608051.
63. T. Sato and T. Lee, *Phys. Rev. C* **54** (1996) 2660, arXiv:nucl-th/9606009.
64. B. Julia-Diaz, T.-S. Lee, A. Matsuyama and T. Sato, *Phys. Rev. C* **76** (2007) 065201, arXiv:0704.1615 [nucl-th].
65. B. Julia-Diaz *et al.*, *Phys. Rev. C* **80** (2009) 025207, arXiv:0904.1918 [nucl-th].
66. H. Kamano, B. Julia-Diaz, T.-S. Lee, A. Matsuyama and T. Sato, *Phys. Rev. C* **79** (2009) 025206, arXiv:0807.2273 [nucl-th].
67. H. Kamano, B. Julia-Diaz, T.-S. Lee, A. Matsuyama and T. Sato, *Phys. Rev. C* **80** (2009) 065203, arXiv:0909.1129 [nucl-th].
68. N. Suzuki *et al.*, *Phys. Rev. Lett.* **104** (2010) 042302, arXiv:0909.1356 [nucl-th].
69. N. Suzuki, T. Sato and T.-S. Lee, *Phys. Rev. C* **79** (2009) 025205, arXiv:0806.2043 [nucl-th].
70. H. Kamano, S. Nakamura, T.-S. Lee and T. Sato, *Phys. Rev. C* **81** (2010) 065207, arXiv:1001.5083 [nucl-th].
71. D. Wilson, I. Cloet, L. Chang and C. Roberts, *Phys. Rev. C* **85** (2012) 025205, arXiv:1112.2212 [nucl-th].
72. E. L. Isupov, Two pion cross sections from e1-6 data, Presented at the *CLAS Hadron Spectroscopy Group Meeting*, wwwold.jlab.org/Hall-B/claschair/agendas/clasagenda_march10.html.

73. B. Julia-Diaz, T.-S. Lee, T. Sato and L. Smith, *Phys. Rev. C* **75** (2007) 015205, arXiv:nucl-th/0611033.
74. S. V. Goloskokov and P. Kroll, *Eur. Phys. J. C* **53** (2008) 367, arXiv:0708.3569 [hep-ph].
75. S. V. Goloskokov and P. Kroll, *Eur. Phys. J. C* **65** (2010) 137, arXiv:0906.0460 [hep-ph].
76. S. Goloskokov and P. Kroll, *Eur. Phys. J. A* **47** (2011) 112, arXiv:1106.4897 [hep-ph].
77. LHPC Collaborations (Ph. Hagler *et al.*), *Phys. Rev. D* **77** (2008) 094502, arXiv:0705.4295 [hep-lat].
78. P. Kroll, H. Moutarde and F. Sabatie, From hard exclusive meson electroproduction to deeply virtual Compton scattering, arXiv:1210.6975 [hep-ph].
79. K. Goeke, M. V. Polyakov and M. Vanderhaeghen, *Prog. Part. Nucl. Phys.* **47** (2001) 401, arXiv:hep-ph/0106012.
80. A. Belitsky and A. Radyushkin, *Phys. Rept.* **418** (2005) 1, arXiv:hep-ph/0504030.
81. H.-W. Lin, *Chin. J. Phys.* **49** (2011) 827, arXiv:1106.1608 [hep-lat].
82. M. Mahbub, W. Kamleh, D. B. Leinweber, A. O. Cais and A. G. Williams, *Phys. Lett. B* **693** (2010) 351, arXiv:1007.4871 [hep-lat].
83. M. Mahbub, A. O. Cais, W. Kamleh, D. B. Leinweber and A. G. Williams, *Phys. Rev. D* **82** (2010) 094504, arXiv:1004.5455 [hep-lat].
84. BGR [Bern-Graz-Regensburg] Collab. (G. P. Engel, C. Lang, M. Limmer, D. Mohler and A. Schafer), *Phys. Rev. D* **82** (2010) 034505, arXiv:1005.1748 [hep-lat].
85. N. Mathur *et al.*, *Phys. Lett. B* **605** (2005) 137.
86. R. G. Edwards, B. Joo and H.-W. Lin, *Phys. Rev. D* **78** (2008) 054501, arXiv:0803.3960 [hep-lat].
87. Hadron Spectrum Collab. (H.-W. Lin *et al.*), *Phys. Rev. D* **79** (2009) 034502, arXiv:0810.3588 [hep-lat].
88. R. G. Edwards, J. J. Dudek, D. G. Richards and S. J. Wallace, *Phys. Rev. D* **84** (2011) 074508, arXiv:1104.5152 [hep-ph].
89. Hadron Spectrum Collab. (L. Liu *et al.*), *J. High Energy Phys.* **1207** (2012) 126, arXiv:1204.5425 [hep-ph].
90. J. J. Dudek, R. G. Edwards, M. J. Peardon, D. G. Richards and C. E. Thomas, *Phys. Rev. Lett.* **103** (2009) 262001, arXiv:0909.0200 [hep-ph].
91. J. J. Dudek, R. G. Edwards, M. J. Peardon, D. G. Richards and C. E. Thomas, *Phys. Rev. D* **82** (2010) 034508, arXiv:1004.4930 [hep-ph].
92. J. J. Dudek *et al.*, *Phys. Rev. D* **83** (2011) 111502, arXiv:1102.4299 [hep-lat].
93. J. J. Dudek, *Phys. Rev. D* **84** (2011) 074023, arXiv:1106.5515 [hep-ph].
94. R. G. Edwards, N. Mathur, D. G. Richards and S. J. Wallace, The flavor structure of the excited baryon spectra from lattice QCD, doi: 10.1103/PhysRevD.87.054506, arXiv:1212.5236 [hep-ph].
95. N. Isgur and G. Karl, *Phys. Rev. D* **19** (1979) 2653.
96. S. Capstick and N. Isgur, *Phys. Rev. D* **34** (1986) 2809.
97. M. Anselmino, E. Predazzi, S. Ekelin, S. Fredriksson and D. Lichtenberg, *Rev. Mod. Phys.* **65** (1993) 1199.
98. L. Y. Glozman and D. Riska, *Phys. Rept.* **268** (1996) 263, arXiv:hep-ph/9505422.
99. S. Capstick and W. Roberts, *Prog. Part. Nucl. Phys.* **45** (2000) S241, arXiv:nucl-th/0008028.
100. J. Goity, C. Schat and N. Scoccola, *Phys. Lett. B* **564** (2003) 83, arXiv:hep-ph/0304167.
101. D. Lichtenberg and L. Tassie, *Phys. Rev.* **155** (1967) 1601.
102. L. Y. Glozman, *Phys. Lett. B* **475** (2000) 329, arXiv:hep-ph/9908207.

103. C. E. Thomas, R. G. Edwards and J. J. Dudek, *Phys. Rev. D* **85** (2012) 014507, arXiv:1107.1930 [hep-lat].
104. J. J. Dudek, R. G. Edwards and C. E. Thomas, *Phys. Rev. D* **86** (2012) 034031, arXiv:1203.6041 [hep-ph].
105. M. Luscher, *Nucl. Phys. B* **364** (1991) 237.
106. M. Lage, U.-G. Meissner and A. Rusetsky, *Phys. Lett. B* **681** (2009) 439, arXiv:0905.0069 [hep-lat].
107. J. J. Dudek, R. G. Edwards and C. E. Thomas, *Phys. Rev. D* **87** (2013) 034505, arXiv:1212.0830 [hep-ph].
108. C. Kim, C. Sachrajda and S. R. Sharpe, *Nucl. Phys. B* **727** (2005) 218, arXiv:hep-lat/0507006.
109. J. J. Dudek, R. G. Edwards, N. Mathur and D. G. Richards, *Phys. Rev. D* **77** (2008) 034501, arXiv:0707.4162 [hep-lat].
110. J. J. Dudek, R. Edwards and C. E. Thomas, *Phys. Rev. D* **79** (2009) 094504, arXiv:0902.2241 [hep-ph].
111. H.-W. Lin, S. D. Cohen, R. G. Edwards and D. G. Richards, *Phys. Rev. D* **78** (2008) 114508, arXiv:0803.3020 [hep-lat].
112. H.-W. Lin and S. D. Cohen, Nucleon and pion form factors from $N_f = 2 + 1$ anisotropic lattices, arXiv:1104.4319 [hep-lat].
113. H.-W. Lin, S. D. Cohen, R. G. Edwards, K. Orginos and D. G. Richards, PoS **LATTICE2008** (2008) 140, arXiv:0810.5141 [hep-lat].
114. S. Caracciolo, R. G. Edwards, A. Pelissetto and A. D. Sokal, *Phys. Rev. Lett.* **75** (1995) 1891, arXiv:hep-lat/9411009.
115. M. Guagnelli, F. Palombi, R. Petronzio and N. Tantalo, *Phys. Lett. B* **546** (2002) 237, arXiv:hep-lat/0206023.
116. D. Guazzini, R. Sommer and N. Tantalo, *J. High Energy Phys.* **0801** (2008) 076, arXiv:0710.2229 [hep-lat].
117. D. Renner, uSQCD proposal, 2011.
118. SESAM Collaboration (G. S. Bali, H. Neff, T. Duessel, T. Lippert and K. Schilling), *Phys. Rev. D* **71** (2005) 114513, arXiv:hep-lat/0505012.
119. L. Chang, I. C. Cloet, B. El-Bennich, T. Klahn and C. D. Roberts, *Chin. Phys. C* **33** (2009) 1189, arXiv:0906.4304 [nucl-th].
120. P. Boucaud *et al.*, *Few Body Syst.* **53** (2012) 387, arXiv:1109.1936 [hep-ph].
121. G. Krein, C. D. Roberts and A. G. Williams, *Int. J. Mod. Phys. A* **7** (1992) 5607.
122. V. Gribov, *Eur. Phys. J. C* **10** (1999) 91, arXiv:hep-ph/9902279.
123. H. Munczek and A. Nemirovsky, *Phys. Rev. D* **28** (1983) 181.
124. M. Stingl, *Phys. Rev. D* **29** (1984) 2105.
125. R. Cahill, *Austral. J. Phys.* **42** (1989) 171.
126. R. Streater and A. Wightman, *PCT, Spin and Statistics, and All That* (Addison-Wesley Publishing Co., Inc., USA, 1989).
127. J. Glimm and A. Jaffee, *Quantum Physics*: *A Functional Point of View* (Springer-Verlag, New York, 1981).
128. S.-X. Qin, L. Chang, Y.-X. Liu, C. D. Roberts and D. J. Wilson, *Phys. Rev. C* **84** (2011) 042202, arXiv:1108.0603 [nucl-th].
129. S. J. Brodsky, G. F. de Teramond and A. Deur, *Phys. Rev. D* **81** (2010) 096010, arXiv:1002.3948 [hep-ph].
130. A. Aguilar, D. Binosi and J. Papavassiliou, *J. High Energy Phys.* **1007** (2010) 002, arXiv:1004.1105 [hep-ph].
131. A. Bender, C. D. Roberts and L. Von Smekal, *Phys. Lett. B* **380** (1996) 7, arXiv:nucl-th/9602012.

132. P. O. Bowman, U. M. Heller, D. B. Leinweber, M. B. Parappilly and A. G. Williams, *Phys. Rev. D* **70** (2004) 034509, arXiv:hep-lat/0402032.
133. A. Aguilar, D. Binosi, J. Papavassiliou and J. Rodriguez-Quintero, *Phys. Rev. D* **80** (2009) 085018, arXiv:0906.2633 [hep-ph].
134. J. I. Skullerud, P. O. Bowman, A. Kizilersu, D. B. Leinweber and A. G. Williams, *J. High Energy Phys.* **0304** (2003) 047, arXiv:hep-ph/0303176.
135. M. Bhagwat and P. Tandy, *Phys. Rev. D* **70** (2004) 094039, arXiv:hep-ph/0407163.
136. C. D. Roberts and B. H. McKellar, *Phys. Rev. D* **41** (1990) 672.
137. J. C. Bloch, *Phys. Rev. D* **66** (2002) 034032, arXiv:hep-ph/0202073.
138. A. Bashir and M. Pennington, *Phys. Rev. D* **50** (1994) 7679, arXiv:hep-ph/9407350.
139. H. Roberts, A. Bashir, L. Gutierrez-Guerrero, C. Roberts and D. Wilson, *Phys. Rev. C* **83** (2011) 065206, arXiv:1102.4376 [nucl-th].
140. L. Chang and C. D. Roberts, *Phys. Rev. Lett.* **103** (2009) 081601, arXiv:0903.5461 [nucl-th].
141. L. Chang and C. D. Roberts, *Phys. Rev. C* **85** (2012) 052201, arXiv:1104.4821 [nucl-th].
142. S.-X. Qin, L. Chang, Y.-X. Liu, C. D. Roberts and D. J. Wilson, *Phys. Rev. C* **85** (2012) 035202, arXiv:1109.3459 [nucl-th].
143. V. Flambaum, A. Holl, P. Jaikumar, C. Roberts and S. Wright, *Few Body Syst.* **38** (2006) 31, arXiv:nucl-th/0510075.
144. R. Young and A. Thomas, *Phys. Rev. D* **81** (2010) 014503, arXiv:0901.3310 [hep-lat].
145. Y. Nambu and G. Jona-Lasinio, *Phys. Rev.* **122** (1961) 345.
146. H. L. Roberts, L. Chang, I. C. Cloet and C. D. Roberts, *Few Body Syst.* **51** (2011) 1, arXiv:1101.4244 [nucl-th].
147. P. Maris and P. C. Tandy, *Phys. Rev. C* **62** (2000) 055204, arXiv:nucl-th/0005015.
148. M. Bhagwat and P. Maris, *Phys. Rev. C* **77** (2008) 025203, arXiv:nucl-th/0612069.
149. I. Cloet, G. Eichmann, B. El-Bennich, T. Klahn and C. Roberts, *Few Body Syst.* **46** (2009) 1, arXiv:0812.0416 [nucl-th].
150. G. Eichmann, I. Cloet, R. Alkofer, A. Krassnigg and C. Roberts, *Phys. Rev. C* **79** (2009) 012202, arXiv:0810.1222 [nucl-th].
151. G. Eichmann, *Phys. Rev. D* **84** (2011) 014014, arXiv:1104.4505 [hep-ph].
152. L. Gutierrez-Guerrero, A. Bashir, I. Cloet and C. Roberts, *Phys. Rev. C* **81** (2010) 065202, arXiv:1002.1968 [nucl-th].
153. H. Roberts, C. Roberts, A. Bashir, L. Gutierrez-Guerrero and P. Tandy, *Phys. Rev. C* **82** (2010) 065202, arXiv:1009.0067 [nucl-th].
154. A. Holl, A. Krassnigg, P. Maris, C. Roberts and S. Wright, *Phys. Rev. C* **71** (2005) 065204, arXiv:nucl-th/0503043.
155. L. Chang, Y.-X. Liu and C. D. Roberts, *Phys. Rev. Lett.* **106** (2011) 072001, arXiv:1009.3458 [nucl-th].
156. A. Gasparyan, J. Haidenbauer, C. Hanhart and J. Speth, *Phys. Rev. C* **68** (2003) 045207, arXiv:nucl-th/0307072.
157. R. Cahill, C. D. Roberts and J. Praschifka, *Austral. J. Phys.* **42** (1989) 129.
158. R. Cahill, C. D. Roberts and J. Praschifka, *Phys. Rev. D* **36** (1987) 2804.
159. L. Chang, C. D. Roberts and P. C. Tandy, *Chin. J. Phys.* **49** (2011) 955, arXiv:1107.4003 [nucl-th].
160. L. D. Roper and R. M. Wright, Energy-Dependent Pion — Nucleon Phase Shift Analysis 0-MeV-700-MeV, $l(m) = 4$ Solution (1964).
161. C. D. Roberts, Confinement, diquarks and Goldstone's theorem, in *Proc. of Quark Confinement and the Hadron Spectrum Conf.* (World Scientific, 1996), p. 224, arXiv:nucl-th/9609039.

162. J. C. Bloch, C. D. Roberts and S. Schmidt, *Phys. Rev. C* **60** (1999) 065208, arXiv:nucl-th/9907086.
163. C. D. Roberts, I. C. Cloet, L. Chang and H. L. Roberts, *AIP Conf. Proc.* **1432** (2012) 309, arXiv:1108.1327 [nucl-th].
164. P. Maris and P. C. Tandy, *Phys. Rev. C* **60** (1999) 055214, arXiv:nucl-th/9905056.
165. F. Cardarelli, E. Pace, G. Salme and S. Simula, *Phys. Lett. B* **397** (1997) 13, arXiv:nucl-th/9609047.
166. H. Kamano, T.-S. H. Lee and Sato, Private communication.
167. F. Cardarelli, E. Pace, G. Salme and S. Simula, *Phys. Lett. B* **357** (1995) 267, arXiv:nucl-th/9507037.
168. J. S. Ball and T.-W. Chiu, *Phys. Rev. D* **22** (1980) 2542.
169. D. Curtis and M. Pennington, *Phys. Rev. D* **42** (1990) 4165.
170. R. Alkofer, A. Bender and C. D. Roberts, *Int. J. Mod. Phys. A* **10** (1995) 3319, arXiv:hep-ph/9312243.
171. M. Frank, *Phys. Rev. C* **51** (1995) 987, arXiv:nucl-th/9403009.
172. C. D. Roberts, *Nucl. Phys. A* **605** (1996) 475, arXiv:hep-ph/9408233.
173. P. Maris and P. C. Tandy, *Phys. Rev. C* **61** (2000) 045202, arXiv:nucl-th/9910033.
174. I. Aznauryan and V. Burkert, *Phys. Rev. C* **85** (2012) 055202, arXiv:1201.5759 [hep-ph].
175. J. R. Taylor, *Scattering Theory, The Quantum Theory of Nonrelativistic Collisions* (Wiley, New York, 1972).
176. V. Mader, G. Eichmann, M. Blank and A. Krassnigg, *Phys. Rev. D* **84** (2011) 034012, arXiv:1106.3159 [hep-ph].
177. V. Braun *et al.*, *Phys. Rev. Lett.* **103** (2009) 072001, arXiv:0902.3087 [hep-ph].
178. L. Chang, I. Cloet, C. Roberts and H. Roberts, *AIP Conf. Proc.* **1354** (2011) 110, arXiv:1101.3787 [nucl-th].
179. G. P. Lepage and S. J. Brodsky, *Phys. Rev. D* **22** (1980) 2157.
180. V. Chernyak and A. Zhitnitsky, *Phys. Rept.* **112** (1984) 173.
181. X.-D. Ji, J.-P. Ma and F. Yuan, *Nucl. Phys. B* **652** (2003) 383, arXiv:hep-ph/0210430.
182. X.-D. Ji, J.-P. Ma and F. Yuan, *Eur. Phys. J. C* **33** (2004) 75, arXiv:hep-ph/0304107.
183. V. Braun, R. Fries, N. Mahnke and E. Stein, *Nucl. Phys. B* **589** (2000) 381, arXiv:hep-ph/0007279.
184. V. Braun, A. Manashov and J. Rohrwild, *Nucl. Phys. B* **807** (2009) 89, arXiv:0806.2531 [hep-ph].
185. A. V. Belitsky, X.-D. Ji and F. Yuan, *Phys. Rev. Lett.* **91** (2003) 092003, arXiv:hep-ph/0212351.
186. M. Gockeler *et al.*, *Phys. Rev. Lett.* **101** (2008) 112002, arXiv:0804.1877 [hep-lat].
187. QCDSF Collab. (V. M. Braun *et al.*), *Phys. Rev. D* **79** (2009) 034504, arXiv:0811.2712 [hep-lat].
188. T. Kaltenbrunner, M. Gockeler and A. Schafer, *Eur. Phys. J. C* **55** (2008) 387, arXiv:0801.3932 [hep-lat].
189. QCDSF Collaboration, UKQCD Collaboration (M. Gockeler *et al.*), *Nucl. Phys. B* **812** (2009) 205, arXiv:0810.3762 [hep-lat].
190. S. Krankl and A. Manashov, *Phys. Lett. B* **703** (2011) 519, arXiv:1107.3718 [hep-ph].
191. F. X. Lee and D. B. Leinweber, *Nucl. Phys. Proc. Suppl.* **73** (1999) 258, arXiv:hep-lat/9809095.
192. R. Schiel *et al.*, PoS **LATTICE2011** (2011) 175, arXiv:1112.0473 [hep-lat].
193. M. Gruber, *Phys. Lett. B* **699** (2011) 169, arXiv:1011.0758 [hep-ph].
194. P. Wein, P. C. Bruns, T. R. Hemmert and A. Schafer, *Eur. Phys. J. A* **47** (2011) 149, arXiv:1106.3440 [hep-ph].

195. A. Duncan and A. H. Mueller, *Phys. Rev. D* **21** (1980) 1636.
196. N. Kivel and M. Vanderhaeghen, *Phys. Rev. D* **83** (2011) 093005, arXiv:1010.5314 [hep-ph].
197. V. M. Braun, A. Lenz, N. Mahnke and E. Stein, *Phys. Rev. D* **65** (2002) 074011, arXiv:hep-ph/0112085.
198. I. Balitsky, V. M. Braun and A. Kolesnichenko, *Nucl. Phys. B* **312** (1989) 509.
199. V. Chernyak and I. Zhitnitsky, *Nucl. Phys. B* **345** (1990) 137.
200. V. Braun, A. Lenz and M. Wittmann, *Phys. Rev. D* **73** (2006) 094019, arXiv:hep-ph/0604050.
201. K. Passek-Kumericki and G. Peters, *Phys. Rev. D* **78** (2008) 033009, arXiv:0805.1758 [hep-ph].
202. M. A. Shifman, A. Vainshtein and V. I. Zakharov, *Nucl. Phys. B* **147** (1979) 385.
203. P. Ball and R. Zwicky, *Phys. Rev. D* **71** (2005) 014015, arXiv:hep-ph/0406232.
204. G. Duplancic, A. Khodjamirian, T. Mannel, B. Melic and N. Offen, *J. High Energy Phys.* **0804** (2008) 014, arXiv:0801.1796 [hep-ph].
205. V. M. Braun, Light cone sum rules, arXiv:hep-ph/9801222 [hep-ph].
206. P. Colangelo and A. Khodjamirian, QCD sum rules, a modern perspective, arXiv:hep-ph/0010175.
207. V. Braun, A. Lenz, G. Peters and A. Radyushkin, *Phys. Rev. D* **73** (2006) 034020, arXiv:hep-ph/0510237.
208. A. Khodjamirian, C. Klein, T. Mannel and Y.-M. Wang, *J. High Energy Phys.* **1109** (2011) 106, arXiv:1108.2971 [hep-ph].
209. T. Aliev, K. Azizi and M. Savci, *Eur. Phys. J. A* **47** (2011) 125, arXiv:1106.5060 [hep-ph].
210. V. Braun and A. Manashov, *Phys. Rev. Lett.* **107** (2011) 202001, arXiv:1108.2394 [hep-ph].
211. S. Agaev, V. Braun, N. Offen and F. Porkert, *Phys. Rev. D* **83** (2011) 054020, arXiv:1012.4671 [hep-ph].
212. Jefferson Lab E00-115 Collab. (S. Malace *et al.*), *Phys. Rev. C* **80** (2009) 035207, arXiv:0905.2374 [nucl-ex].
213. Jefferson Lab Hall C E94-110 Collab. (Y. Liang *et al.*), Measurement of R = sigma(L)/sigma(T) and the separated longitudinal and transverse structure functions in the nucleon resonance region, arXiv:nucl-ex/0410027.
214. Spokespersons (C. E. Keppel and M. I. Niculescu), F_2^N *at low* Q^2, Jefferson Lab Experiment E00-002.
215. L. Whitlow, Deep inelastic structure functions from electron scattering on hydrogen, deuterium, and iron at 0.6 GeV, Ph.D. thesis, American University, 1990.
216. L. Whitlow, E. Riordan, S. Dasu, S. Rock and A. Bodek, *Phys. Lett. B* **282** (1992) 475.
217. EAS-TOP and MACRO Collabs. (M. Aglietta *et al.*), *Nucl. Phys. Proc. Suppl.* **70** (1999) 483.
218. M. Christy and P. E. Bosted, *Phys. Rev. C* **81** (2010) 055213, arXiv:0712.3731 [hep-ph].
219. M. Christy and W. Melnitchouk, *J. Phys. Conf. Ser.* **299** (2011) 012004, arXiv:1104.0239 [nucl-ex].
220. S. Alekhin, *JETP Lett.* **82** (2005) 628, arXiv:hep-ph/0508248.
221. S. I. Alekhin, *Phys. Rev. D* **63** (2001) 094022, arXiv:hep-ph/0011002.
222. M. Fukugita and K. Igi, *Phys. Rept.* **31** (1977) 237.
223. P. Collins, *An Introduction to Regge Theory and High-Energy Physics* (Cambridge Univ. Press, 1977), 445 pp.

224. S. Donnachie, H. G. Dosch, O. Nachtmann and P. Landshoff, *Camb. Monogr. Part. Phys. Nucl. Phys. Cosmol.* **19** (2002) 1.
225. E. D. Bloom and F. J. Gilman, *Phys. Rev. D* **4** (1971) 2901.
226. E. D. Bloom and F. J. Gilman, *Phys. Rev. Lett.* **25** (1970) 1140.
227. I. Niculescu *et al.*, *Phys. Rev. Lett.* **85** (2000) 1186.
228. I. Niculescu *et al.*, *Phys. Rev. Lett.* **85** (2000) 1182.
229. W. Melnitchouk, R. Ent and C. Keppel, *Phys. Rept.* **406** (2005) 127, arXiv:hep-ph/0501217.
230. A. De Rujula, H. Georgi and H. D. Politzer, *Ann. Phys.* **103** (1977) 315.
231. M. B. Einhorn, *Phys. Rev. D* **14** (1976) 3451.
232. N. Isgur, S. Jeschonnek, W. Melnitchouk and J. Van Orden, *Phys. Rev. D* **64** (2001) 054005, arXiv:hep-ph/0104022.
233. F. E. Close and N. Isgur, *Phys. Lett. B* **509** (2001) 81, arXiv:hep-ph/0102067.
234. F. Close and W. Melnitchouk, *Phys. Rev. C* **68** (2003) 035210, arXiv:hep-ph/0302013.
235. F. Close and W. Melnitchouk, *Phys. Rev. C* **79** (2009) 055202, arXiv:0902.4256. [nucl-th].
236. A. Accardi *et al.*, *Phys. Rev. D* **81** (2010) 034016, arXiv:0911.2254 [hep-ph].
237. A. Accardi *et al.*, *Phys. Rev. D* **84** (2011) 014008, arXiv:1102.3686 [hep-ph].
238. W. Melnitchouk and A. W. Thomas, *Phys. Lett. B* **377** (1996) 11, arXiv:nucl-th/9602038.
239. R. J. Holt and C. D. Roberts, *Rev. Mod. Phys.* **82** (2010) 2991, arXiv:1002.4666 [nucl-th].
240. S. Kuhlmann *et al.*, *Phys. Lett. B* **476** (2000) 291, arXiv:hep-ph/9912283.
241. L. Brady, A. Accardi, W. Melnitchouk and J. Owens, *J. High Energy Phys.* **1206** (2012) 019, arXiv:1110.5398 [hep-ph].
242. J. Bjorken and J. B. Kogut, *Phys. Rev. D* **8** (1973) 1341.
243. F. E. Close and Q. Zhao, *Phys. Rev. D* **66** (2002) 054001, arXiv:hep-ph/0202181.
244. T. Navasardyan *et al.*, *Phys. Rev. Lett.* **98** (2007) 022001, arXiv:hep-ph/0608214.
245. European Muon Collaboration (M. Arneodo *et al.*), *Nucl. Phys. B* **321** (1989) 541.
246. D. Scott, *Phys. Rev. D* **10** (1974) 3117.
247. D. Scott, *Phys. Lett. B* **59** (1975) 171.
248. P. Eden, P. Hoyer and A. Khodjamirian, *J. High Energy Phys.* **0110** (2001) 040, arXiv:hep-ph/0110297.
249. Q. Zhao and F. E. Close, *Phys. Rev. Lett.* **91** (2003) 022004, arXiv:hep-ph/0305017.
250. R. Fiore, A. Flachi, L. L. Jenkovszky, A. Lengyel and V. Magas, *Phys. Rev. D* **69** (2004) 014004, arXiv:hep-ph/0308178.
251. R. Fiore, A. Flachi, L. L. Jenkovszky, A. Lengyel and V. Magas, *Eur. Phys. J. A* **15** (2002) 505, arXiv:hep-ph/0206027.
252. F. Gross, G. Ramalho and M. Peña, *Phys. Rev. C* **77** (2008) 015202, arXiv:nucl-th/0606029.
253. K. G. Wilson, *Phys. Rev. D* **10** (1974) 2445.
254. J. M. Cornwall, *Phys. Rev. D* **26** (1982) 1453.
255. J. M. Maldacena, *Adv. Theor. Math. Phys.* **2** (1998) 231, arXiv:hep-th/9711200.
256. G. F. de Teramond and S. J. Brodsky, *Phys. Rev. Lett.* **102** (2009) 081601, arXiv:0809.4899 [hep-ph].
257. S. J. Brodsky, H.-C. Pauli and S. S. Pinsky, *Phys. Rept.* **301** (1998) 299, arXiv:hep-ph/9705477.
258. P. A. Dirac, *Rev. Mod. Phys.* **21** (1949) 392.
259. S. J. Brodsky and G. F. de Teramond, *Phys. Rev. Lett.* **96** (2006) 201601, arXiv:hep-ph/0602252.

260. S. J. Brodsky and G. F. de Teramond, *Phys. Rev. D* **77** (2008) 056007, arXiv:0707.3859 [hep-ph].
261. J. Polchinski and M. J. Strassler, *J. High Energy Phys.* **0305** (2003) 012, arXiv:hep-th/0209211.
262. S. J. Brodsky and G. F. de Teramond, *Phys. Rev. D* **78** (2008) 025032, arXiv:0804.0452 [hep-ph].
263. Z. Abidin and C. E. Carlson, *Phys. Rev. D* **77** (2008) 095007, arXiv:0801.3839 [hep-ph].
264. J. Polchinski and M. J. Strassler, *Phys. Rev. Lett.* **88** (2002) 031601, arXiv:hep-th/0109174.
265. S. J. Brodsky and G. R. Farrar, *Phys. Rev. Lett.* **31** (1973) 1153.
266. V. Matveev, R. Muradian and A. Tavkhelidze, *Lett. Nuovo Cim.* **7** (1973) 719.
267. A. Karch, E. Katz, D. T. Son and M. A. Stephanov, *Phys. Rev. D* **74** (2006) 015005, arXiv:hep-ph/0602229.
268. S. J. Brodsky and G. F. de Teramond, AdS/CFT and light-front QCD, arXiv:0802.0514 [hep-ph].
269. H. Grigoryan and A. Radyushkin, *Phys. Rev. D* **76** (2007) 095007, arXiv:0706.1543 [hep-ph].
270. G. F. de Teramond and S. J. Brodsky, *Nucl. Phys. Proc. Suppl.* **199** (2010) 89, arXiv:0909.3900 [hep-ph].
271. A. Vega, I. Schmidt, T. Gutsche and V. E. Lyubovitskij, *Phys. Rev. D* **83** (2011) 036001, arXiv:1010.2815 [hep-ph].
272. H. R. Grigoryan, T.-S. Lee and H.-U. Yee, *Phys. Rev. D* **80** (2009) 055006, arXiv:0904.3710 [hep-ph].
273. A. Ballon-Bayona, H. Boschi-Filho, N. R. Braga, M. Ihl and M. A. Torres, Production of negative parity baryons in the holographic Sakai-Sugimoto model, arXiv:1209.6020 [hep-ph].
274. G. Ramalho, M. Peña and F. Gross, *Phys. Rev. D* **78** (2008) 114017, arXiv:0810.4126 [hep-ph].
275. G. Ramalho and K. Tsushima, *Phys. Rev. D* **82** (2010) 073007, arXiv:1008.3822 [hep-ph].
276. G. Ramalho and K. Tsushima, *Phys. Rev. D* **81** (2010) 074020, arXiv:1002.3386 [hep-ph].
277. G. Ramalho and M. Peña, *Phys. Rev. D* **84** (2011) 033007, arXiv:1105.2223 [hep-ph].
278. G. A. Miller, *Phys. Rev. C* **66** (2002) 032201, arXiv:nucl-th/0207007.
279. Jefferson Lab Hall A Collab. (M. Jones *et al.*), *Phys. Rev. Lett.* **84** (2000) 1398, arXiv:nucl-ex/9910005.
280. Jefferson Lab Hall A Collab. (O. Gayou *et al.*), *Phys. Rev. Lett.* **88** (2002) 092301, arXiv:nucl-ex/0111010.
281. A. Sill *et al.*, *Phys. Rev. D* **48** (1993) 29.
282. W. Bartel *et al.*, *Nucl. Phys. B* **58** (1973) 429.
283. E93-038 Collab. (R. Madey *et al.*), *Phys. Rev. Lett.* **91** (2003) 122002, arXiv:nucl-ex/0308007.
284. S. Riordan *et al.*, *Phys. Rev. Lett.* **105** (2010) 262302, arXiv:1008.1738 [nucl-ex].
285. Jefferson Lab E95-001 Collab. (B. Anderson *et al.*), *Phys. Rev. C* **75** (2007) 034003, arXiv:nucl-ex/0605006.
286. CLAS Collab. (J. Lachniet *et al.*), *Phys. Rev. Lett.* **102** (2009) 192001, arXiv:0811.1716 [nucl-ex].
287. S. Rock *et al.*, *Phys. Rev. Lett.* **49** (1982) 1139.
288. S. Stave *et al.*, *Eur. Phys. J. A* **30** (2006) 471, arXiv:nucl-ex/0604013.
289. N. Sparveris *et al.*, *Phys. Lett. B* **651** (2007) 102, arXiv:nucl-ex/0611033.

290. A1 Collab. (S. Stave *et al.*), *Phys. Rev. C* **78** (2008) 025209, arXiv:0803.2476 [hep-ex].
291. C. Mertz *et al.*, *Phys. Rev. Lett.* **86** (2001) 2963, arXiv:nucl-ex/9902012.
292. MIT-Bates OOPS Collab. (C. Kunz *et al.*), *Phys. Lett. B* **564** (2003) 21, arXiv:nucl-ex/0302018.
293. OOPS Collab. (N. Sparveris *et al.*), *Phys. Rev. Lett.* **94** (2005) 022003, arXiv:nucl-ex/0408003.
294. V. Frolov *et al.*, *Phys. Rev. Lett.* **82** (1999) 45, arXiv:hep-ex/9808024.
295. A. Villano *et al.*, *Phys. Rev. C* **80** (2009) 035203, arXiv:0906.2839 [nucl-ex].
296. Jefferson Lab Hall A Collab. (J. J. Kelly *et al.*), *Phys. Rev. Lett.* **95** (2005) 102001, arXiv:nucl-ex/0505024.
297. J. Kelly *et al.*, *Phys. Rev. C* **75** (2007) 025201, arXiv:nucl-ex/0509004.
298. D. Drechsel, O. Hanstein, S. Kamalov and L. Tiator, *Nucl. Phys. A* **645** (1999) 145, arXiv:nucl-th/9807001.
299. S. S. Kamalov, S. N. Yang, D. Drechsel, O. Hanstein and L. Tiator, *Phys. Rev. C* **64** (2001) 032201, arXiv:nucl-th/0006068.
300. M. Diehl, *Nucl. Phys. Proc. Suppl.* **161** (2006) 49, arXiv:hep-ph/0510221.
301. I. Aznauryan, V. Burkert, G. Fedotov, B. Ishkhanov and V. Mokeev, *Phys. Rev. C* **72** (2005) 045201, arXiv:hep-ph/0508057.
302. CLAS Collab. (I. Aznauryan *et al.*), *Phys. Rev. C* **78** (2008) 045209, arXiv:0804.0447 [nucl-ex].
303. Data Group Collab. (C. Amsler *et al.*), *Phys. Lett. B* **667** (2008) 1.
304. V. Burkert and T. Lee, *Int. J. Mod. Phys. E* **13** (2004) 1035, arXiv:nucl-ex/0407020.
305. G. Ramalho, F. Gross, M. Peña and K. Tsushima, A covariant formalism for the N^* electroproduction at high momentum transfer, in *Proc. of the 4th Workshop on Exclusive Reactions at High Momentum Transfer*, ed. A. Radyushkin (World Scientific, Singapore, 2011), p. 287, arXiv:1008.0371 [hep-ph].
306. F. Gross, J. Van Orden and K. Holinde, *Phys. Rev. C* **45** (1992) 2094.
307. A. Stadler, F. Gross and M. Frank, *Phys. Rev. C* **56** (1997) 2396, arXiv:nucl-th/9703043.
308. F. Gross and P. Agbakpe, *Phys. Rev. C* **73** (2006) 015203, arXiv:nucl-th/0411090.
309. G. Ramalho, K. Tsushima and F. Gross, *Phys. Rev. D* **80** (2009) 033004, arXiv:0907.1060 [hep-ph].
310. G. Ramalho and M. Peña, *J. Phys. G* **36** (2009) 115011, arXiv:0812.0187 [hep-ph].
311. G. Ramalho and M. Peña, *Phys. Rev. D* **80** (2009) 013008, arXiv:0901.4310 [hep-ph].
312. G. Ramalho and K. Tsushima, *Phys. Rev. D* **84** (2011) 054014, arXiv:1107.1791 [hep-ph].
313. G. Ramalho and M. Peña, *Phys. Rev. D* **85** (2012) 113014, arXiv:1205.2575 [hep-ph].
314. G. Ramalho, M. Peña and F. Gross, *Eur. Phys. J. A* **36** (2008) 329, arXiv:0803.3034 [hep-ph].
315. M. D. Sanctis, M. Giannini, E. Santopinto and A. Vassallo, *Phys. Rev. C* **76** (2007) 062201.
316. G. Ramalho, D. Jido and K. Tsushima, *Phys. Rev. D* **85** (2012) 093014, arXiv:1202.2299 [hep-ph].
317. G. Ramalho and K. Tsushima, *Phys. Rev. D* **84** (2011) 051301, arXiv:1105.2484 [hep-ph].
318. F. Gross, G. Ramalho and K. Tsushima, *Phys. Lett. B* **690** (2010) 183, arXiv:0910.2171 [hep-ph].
319. G. Ramalho, M. Peña and F. Gross, *Phys. Lett. B* **678** (2009) 355, arXiv:0902.4212 [hep-ph].

320. G. Ramalho, M. Peña and F. Gross, *Phys. Rev. D* **81** (2010) 113011, arXiv:1002.4170 [hep-ph].
321. G. Ramalho and M. Peña, *Phys. Rev. D* **83** (2011) 054011, arXiv:1012.2168 [hep-ph].
322. G. Ramalho and K. Tsushima, *Phys. Rev. D* **87** (2013) 093011, arXiv:1302.6889 [hep-ph].
323. G. Ramalho, K. Tsushima and A. W. Thomas, *J. Phys. G* **40** (2013) 015102, arXiv:1206.2207 [hep-ph].
324. F. Gross, G. Ramalho and M. Peña, *Phys. Rev. D* **85** (2012) 093005, arXiv:1201.6336 [hep-ph].
325. F. Gross, G. Ramalho and M. Peña, *Phys. Rev. D* **85** (2012) 093006, arXiv:1201.6337 [hep-ph].
326. D. Jido, M. Doering and E. Oset, *Phys. Rev. C* **77** (2008) 065207, arXiv:0712.0038 [nucl-th].
327. D. Drechsel, S. Kamalov and L. Tiator, *Eur. Phys. J. A* **34** (2007) 69, arXiv:0710.0306 [nucl-th].
328. M. Doring, C. Hanhart, F. Huang, S. Krewald and U.-G. Meissner, *Phys. Lett. B* **681** (2009) 26, arXiv:0903.1781 [nucl-th].
329. A. Anisovich *et al.*, *Eur. Phys. J. A* **44** (2010) 203, arXiv:0911.5277 [hep-ph].
330. V. Berestetsky and M. Terentev, *Sov. J. Nucl. Phys.* **25** (1977) 347.
331. V. Berestetsky and M. Terentev, *Sov. J. Nucl. Phys.* **24** (1976) 547.
332. I. Aznauryan, A. Bagdasaryan and N. Ter-Isaakian, *Yad. Fiz.* **36** (1982) 1278.
333. I. Aznauryan, *Z. Phys. A* **346** (1993) 297.
334. H. Melosh, *Phys. Rev. D* **9** (1974) 1095.
335. R. Koniuk and N. Isgur, *Phys. Rev. D* **21** (1980) 1868.
336. S. Godfrey and N. Isgur, *Phys. Rev. D* **32** (1985) 189.
337. I. G. Aznauryan and A. S. Bagdasaryan, *Sov. J. Nucl. Phys.* **41** (1985) 158.
338. B. Keister, *Phys. Rev. D* **49** (1994) 1500, arXiv:hep-ph/9303264.
339. I. Aznauryan, A. Bagdasaryan and N. Ter-Isaakian, *Phys. Lett. B* **112** (1982) 393.
340. I. Aznauryan, *Phys. Lett. B* **316** (1993) 391.
341. M. Bhagwat, M. Pichowsky, C. Roberts and P. Tandy, *Phys. Rev. C* **68** (2003) 015203, arXiv:nucl-th/0304003.
342. R. Bijker, F. Iachello and A. Leviatan, *Ann. Phys.* **236** (1994) 69, arXiv:nucl-th/9402012.
343. M. Ferraris, M. Giannini, M. Pizzo, E. Santopinto and L. Tiator, *Phys. Lett. B* **364** (1995) 231.
344. U. Loring, K. Kretzschmar, B. C. Metsch and H. R. Petry, *Eur. Phys. J. A* **10** (2001) 309, arXiv:hep-ph/0103287.
345. U. Loring, B. C. Metsch and H. R. Petry, *Eur. Phys. J. A* **10** (2001) 447, arXiv:hep-ph/0103290.
346. A. De Rujula, H. Georgi and S. Glashow, *Phys. Rev. D* **12** (1975) 147.
347. L. Copley, G. Karl and E. Obryk, *Phys. Lett. B* **29** (1969) 117.
348. S. Capstick, *Phys. Rev. D* **46** (1992) 2864.
349. F. Cardarelli, E. Pace, G. Salme and S. Simula, *Phys. Lett. B* **371** (1996) 7, arXiv:nucl-th/9509033.
350. D. Merten, U. Loring, K. Kretzschmar, B. Metsch and H. R. Petry, *Eur. Phys. J. A* **14** (2002) 477, arXiv:hep-ph/0204024.
351. T. Van Cauteren, J. Ryckebusch, B. Metsch and H.-R. Petry, *Eur. Phys. J. A* **26** (2005) 339, arXiv:nucl-th/0509047.
352. E. Santopinto and M. M. Giannini, *Phys. Rev. C* **86** (2012) 065202.
353. M. De Sanctis, E. Santopinto and M. Giannini, *Eur. Phys. J. A* **1** (1998) 187, arXiv:nucl-th/9801015.

354. M. D. Sanctis, M. M. Giannini, L. Repetto and E. Santopinto, *Phys. Rev. C* **62** (2000) 025208.
355. M. De Sanctis, E. Santopinto and M. Giannini, *Eur. Phys. J. A* **2** (1998) 403.
356. E. Santopinto, F. Iachello and M. Giannini, *Nucl. Phys. A* **623** (1997) 100C.
357. L. Tiator *et al.*, *Eur. Phys. J. A* **19** (2004) 55, arXiv:nucl-th/0310041.
358. D. Chen, Y. Dong, M. Giannini and E. Santopinto, *Nucl. Phys. A* **782** (2007) 62, arXiv:nucl-th/0611016.
359. P. Geiger and N. Isgur, *Phys. Rev. Lett.* **67** (1991) 1066.
360. R. Bijker and E. Santopinto, *AIP Conf. Proc.* **947** (2007) 168.
361. R. Bijker and E. Santopinto, *Phys. Rev. C* **80** (2009) 065210.
362. R. Bijker, J. Ferretti and E. Santopinto, *Phys. Rev. C* **85** (2012) 035204.
363. C. An, Q. Li, D. Riska and B. Zou, *Phys. Rev. C* **74** (2006) 055205, arXiv:nucl-th/0610009.
364. C. An and B. Zou, *Eur. Phys. J. A* **39** (2009) 195, arXiv:0802.3996 [nucl-th].
365. B. Julia-Diaz and D. O. Riska, *Nucl. Phys. A* **780** (2006) 175, arXiv:nucl-th/0609064.
366. S. J. Brodsky and G. R. Farrar, *Phys. Rev. D* **11** (1975) 1309.
367. G. P. Lepage and S. J. Brodsky, *Phys. Rev. Lett.* **43** (1979) 545; Erratum: *ibid.* **43** (1979) 1625.
368. E. Santopinto, A. Vassallo, M. Giannini and M. De Sanctis, *Phys. Rev. C* **82** (2010) 065204.
369. O. Gayou *et al.*, *Phys. Rev. C* **64** (2001) 038202.
370. Bates FPP Collab. (B. Milbrath *et al.*), *Phys. Rev. Lett.* **80** (1998) 452, arXiv:nucl-ex/9712006.
371. V. Punjabi *et al.*, *Phys. Rev. C* **71** (2005) 055202, arXiv:nucl-ex/0501018.
372. A. J. R. Puckett *et al.*, *Phys. Rev. Lett.* **104** (2010) 242301, arXiv:1005.3419 [nucl-ex].
373. E. Santopinto, *Phys. Rev. C* **72** (2005) 022201, arXiv:hep-ph/0412319.
374. J. Ferretti, A. Vassallo and E. Santopinto, *Phys. Rev. C* **83** (2011) 065204.
375. M. De Sanctis, J. Ferretti, E. Santopinto and A. Vassallo, *Phys. Rev. C* **84** (2011) 055201.
376. R. Petronzio, S. Simula and G. Ricco, *Phys. Rev. D* **67** (2003) 094004, arXiv:hep-ph/0301206.
377. S. J. Brodsky, G. F. de Teramond and H. G. Dosch, Threefold complementary approach to holographic QCD, arXiv:1302.4105 [hep-th].
378. G. F. de Teramond, H. G. Dosch and S. J. Brodsky, Kinematical and dynamical aspects of higher-spin bound-state equations in holographic QCD, arXiv:1301.1651 [hep-ph].

This article has been cited by:

1. G. Ramalho, K. Tsushima. 2013. What is the role of the meson cloud in the Σ^{*0}#γΛ and Σ^{*}#γΣ decays?. *Physical Review D* **88**:5. . [CrossRef]
2. H. Kamano, S. X. Nakamura, T.-S. H. Lee, T. Sato. 2013. Nucleon resonances within a dynamical coupled-channels model of πN and γN reactions. *Physical Review C* **88**:3. . [CrossRef]
3. B. Golli, S. Širca. 2013. A chiral quark model for meson electroproduction in the region of D-wave resonances. *The European Physical Journal A* **49**:9. . [CrossRef]
4. T. M. Aliev, Y. Öktem, M. Savcı. 2013. Electromagnetic transitions among octet and decuplet baryons in QCD. *Physical Review D* **88**:3. . [CrossRef]